Mechanisms of Decreased Moisture Uptake in *ortho*- Methylated Di(Cyanate Esters)

Andrew J. Guenthner,[1]* Michael E. Wright,[2,†] Andrew P. Chafin,[2] Josiah T. Reams,[3] Kevin R. Lamison,[3] Michael D. Ford,[3] Shawn P. J. Kirby,[4] Jacob J. Zavala,[3] Joseph M. Mabry[1]

[1] Aerospace Systems Directorate, Air Force Research Laboratory, Edwards AFB, 93524 USA

[2] Naval Air Warfare Center, Weapons Division, China Lake, CA 93555 USA

[3] ERC Incorporated, Air Force Research Laboratory, Edwards AFB, CA 93524 USA

[4] California State University, Long Beach, Long Beach, CA 90840 USA

* andrew.guenthner@us.af.mil

†Present address: Cobalt Technologies, Mountain View, CA 94043 USA

KEYWORDS cyanate ester, cyanurate, moisture uptake, thermosetting networks, structure-property relationships

ABSTRACT

Decreases of up to 50% in the moisture uptake of polycyanurate networks based on 2,2-bis(4-cyanatophenyl)propane (BADCy) and 1,1-bis(4-cyanatophenyl)ethane (LECy) were observed when analogous networks containing a single methyl group *ortho*- to each aryl- cyanurate linkage were prepared by reduction and acid-catalyzed coupling of salicylic acid followed by treatment with cyanogen bromide and subsequent cyclotrimerization. The differences in water uptake were observed despite similar decreases in packing fraction as conversion proceeded in

all networks studied. Conversely, the presence or absence of methyl groups at arylene bridges, remote from the cyanurate oxygen, had no influence on water uptake. Vitrification during cure had little effect on either free volume development or moisture uptake. These results confirm that steric hindrance from *ortho*- methyl groups inhibits absorption of water presumably by decreasing the thermodynamic favorability of sterically permitted interaction with the cyanurate oxygen. A further examination of the effect of two different catalysts, 2 parts per hundred of a 30 : 1 by weight mixture of nonylphenol and copper(II) acetylacetonate and 500 parts per million of dibutyl tin dilaurate (DBTDL), compared to analogous uncatalyzed networks, showed that hydrolytic stability was dramatically affected by catalyst choice, while thermo-chemical stability was also impacted. These results provide important insights into the mechanisms that determine structure-property relationships in polycyanurate networks.

Introduction

Polycyanurate networks derived from the thermal cyclotrimerization of cyanate ester monomers are becoming increasingly important high-performance materials[1-4] in technology areas including: printed circuit boards,[5] rocket and missile structures,[6] spacecraft structures,[7] and thermonuclear fusion reactors[8,9] due to their advantageous stability characteristics in demanding environments involving elevated temperatures,[10] cryogenic temperatures,[11] exposure to vacuum,[12] and high-energy radiation.[13] In wet environments, these networks demonstrate a mixture of highly desirable traits, such as a very low coefficient of hygrothermal expansion during short-term exposure[14] and low moisture permeability,[15] along with undesirable characteristics such as blistering and loss of mechanical properties during long-term exposure to moisture at elevated temperatures.[16-18] Interestingly, many of the desirable traits stem from physical characteristics of the network, such as a high density of cross-links (typically 3 mmol /

cc or greater) and the presence of micro-scale free volume with characteristic hole sizes large enough to accommodate water without swelling,[14] while many of the undesirable traits can be traced to unwanted chemical reactions with either unreacted cyanate ester groups and/or with cured cyanurate groups.[16-18] This distinction implies that tailoring of the chemical structure of polycyanurate networks may enable mitigation of the undesirable traits while retaining the desirable ones.

In the 1980s, Shimp et al. discovered that a straightforward modification of the chemical structure of bis(aryl) cyanate ester monomers, namely the inclusion of methyl groups positioned *ortho* to the phenyl cyanate oxygen, resulted in decreased water uptake and improved hydrolytic stability of the network.[19,20] In this instance, as is common for thermosetting networks, hydrolytic stability was assessed by monitoring the decrease in glass transition temperature on exposure to water at elevated temperatures. From these results, it was speculated that the placement of methyl groups in position *ortho* to the cyanurate oxygen resulted in steric hindrance of the oxygen, thereby slowing down hydrolytic reactions while inhibiting access to favored sites for water to occupy. A graphical illustration of this concept, along with the structures of the monomers investigated by Shimp, is provided in Figure 1.
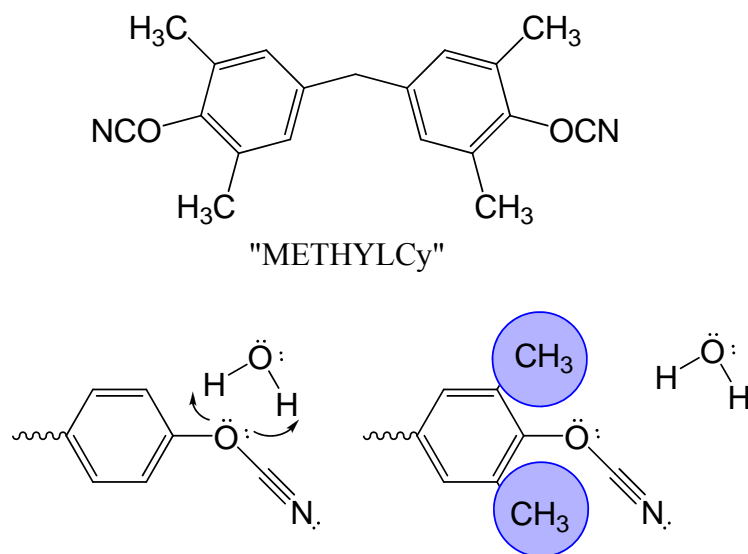
"METHYLCy"

Figure 1. Methylated monomer investigated by Shimp (upper part) and proposed mechanism of improvement in hydrolytic stability (lower part). In the absence of methylation (lower left), water is free to approach the cyanurate oxygen, facilitating interaction, whereas in the presence of methylation (lower right), water is effectively blocked from accessing the oxygen.

Although the hypothesis put forward by Shimp is intuitively appealing, it is important to examine this hypothesis critically in order to advance our understanding of the mechanisms of water uptake in polycyanurate networks. In particular, *ortho-* methylation alters many characteristics of polycyanurate networks, such as: monomer melting point, glass transition temperature at complete conversion to cyanurate, and bulk density of the cured resin. Because the short-term uptake of water in polycyanurates takes place without expansion,[14] it involves the filling of void space within the cured resin. Denser packing of the repeat units in the network would decrease the available space for water uptake and could explain some of the observed behavior without the need for steric hindrance of any particular moiety. Furthermore, as illustrated in Figure 2, a strong correlation (with some exceptions) exists between the number density of cyanurate groups in polycyanurate networks (defined as the gravimetric density divided by the molecular weight per cyanurate equivalent in the cured resin) and moisture uptake, as pointed out recently for co-polymerized polycyanurate networks.[21] *Ortho-* methylation reduces the number density of cyanurate groups, and would therefore be expected to lower the water uptake. Particulary in Figure 2, the water uptake of the networks examined by Shimp (labeled as "METHYLCy") is reasonably close to the general trend, suggesting that *ortho-* methylation is effective in reducing water uptake mainly because it reduces the number density of cyanurate groups.
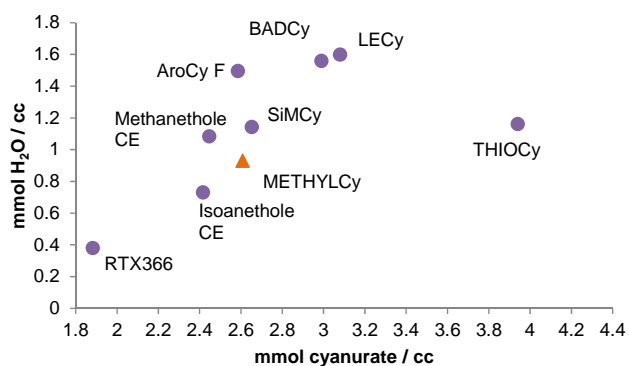
Figure 2. Moisture uptake as a function of cyanurate density for networks derived from di(cyanate ester) monomers. Data for BADCy, LECy, and SiMCy is from Reference 21. Data for Isoanethole CE and Methanethole CE is from Reference 22. Remaining data is from Reference 23.

Correlations such as the one in Figure 2, do not explicitly take into account the effects of conversion. They generally assume complete conversion to cyanurate due to a lack of available data, even when the reported glass transition temperature (T_G) of the networks suggests that such an assumption is invalid. Because conversion strongly affects both water uptake and cyanurate density, a proper examination of the hypothesis put forward by Shimp requires explicit consideration of conversions. During cure, vitrification of the resin may affect the formation of free volume, and subsequently, it may affect moisture uptake, which needs to be considered. In addition, the effect of *ortho-* methylation should be tested in more than one type of monomer, and the effect of *ortho-* methylation should be compared to the effect of adding methyl groups at other locations within the repeat unit. Such a comparison will help distinguish between effects due simply to altering the geometry of the monomer and those effects due specifically to methylation that provides a sterically demanding environment around the cyanurate oxygen. As

a final consideration, it should be noted that the presence of, and choice of, catalysts for cyanate ester cure are known to strongly influence the hydrolytic stability of the networks.[1,16,18,24] The variable of catalyst choice should also be examined.

In what follows, we report the results of a systematic study on the effect of methylation *ortho-* to the cyanurate oxygen on the properties of polycyanurate networks, taking into account important variables such as conversion and catalyst type. We do this by synthesizing *ortho-* methylated analogues of the well-known cyanate ester monomers Primaset® BADCy and Primaset® LECy, which are the cyanated forms of Bisphenol A and Bisphenol E, respectively. The *ortho*-methylated analog of the di(cyanate ester) of Bisphenol E has not been synthesized previously to our knowledge. Using these four monomers allows for a comparative investigation of the effect of introducing methyl groups *ortho-* to the cyanurate oxygen (causing steric hindrance of this oxygen) and the effect of introducing methyl groups at the bridge between aryl groups, a location distant from the cyanurate oxygen.

We found that *ortho-* methylation strongly reduces the water uptake in the networks, in particular at high conversions, whereas methylation of the bridge made no difference. We further found that in systems catalyzed by copper(II) acetylacetonate / nonylphenol, the hydrolytic stability of the networks was improved by *ortho- methylation* but not bridge methylation. However, in networks catalyzed by dibutyl tin dilaurate the hydrolytic stability of the *ortho-* methylated systems was very poor. These results, along with the associated trends in variables such as network packing fraction and the presence or absence of vitrification during cure, tend to confirm the hypothesis that the local vicinity of the cyanurate oxygen (on the molecular scale) represents a preferred site for water uptake in systems with conversions greater than about 80%, and that steric hindrance of the site can mitigate some forms of hydrolytic

6

instability. These concepts are of great importance for the rational design of polycyanurate networks that exhibits superior performance in environments where exposure to moisture is a concern.

Experimental

Monomer Synthesis

4,4'-(ethane-1,1-diyl)bis(2-methylphenol) (5): A cooled (<5 °C) flask containing o-cresol (300 mL, 2.86 mol, 3.8 mol-eq) was equipped with mechanical stirring and then had acetaldehyde (42 mL, 0.75 mol) added. Next, ether (30 mL) was added to dissolve the solids and then to the entire mixture was added 3 mL conc. HCl (3 mL). The temperature rose to 20 °C before falling back to 5 °C. The clear pinkish solution was stirred for an additional 18 hours at room temperature with stirring and then transferred to a 1L single necked round bottom flask. Excess o-cresol was removed under reduced pressure at 100°C to afford 237.25 g of a clear thick oil. This was distilled in a Kugelrohr to yield 178.91 grams of a clear glassy material (97%). This is a mixture of 18 mol-% of the 2,4'-isomer along with about 10 mole% of the trimer. ^{1}H NMR (CDCl$_3$): δ (ppm) 6.98 (s, 2H), 6.96 (d, 2H), 6.70 (d, 2H), 4.66 (br s, 2H), 3.98 (q, 1H), 2.23 (s, 6H), 1.57 (d, 3H).
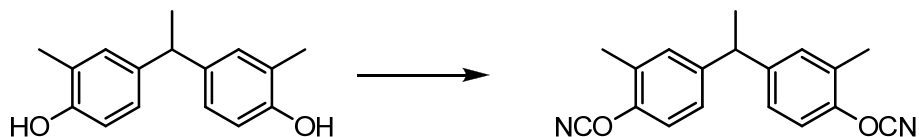
4,4'-(ethane-1,1-diyl)bis((1-cyanato-2-methylbenzene) (3): A solution of 78.48 grams 4,4'-(ethane-1,1-diyl)bis(2-methylphenol) (0.324 mol) and 80 g cyanogen bromide (0.755 moles, 2.3 mol-eq) in 1L ether was cooled to -5 °C (ice salt bath) while a solution of 108 mL triethylamine

(0.776 mol, 2.4 mol-eq) in 100 mL ether was added dropwise over 30 min. The mixture was allowed to warm to room temperature and stirred for three hours then washed with water, dried (MgSO$_4$) and concentrated in vacuum to give 102.07 grams of an off-white solid. This was chromatographed on silica gel using methylene chloride as eluent to afford 45.27 g of a white solid (48%). Mp. 72.1 °C ^{1}H NMR (CDCl$_3$): δ (ppm) 7.34 (d, 2H), 7.09 (d, 2H), 7.04 (s, 2H), 4.10 (q, 1H), 2.28 (s, 6H), 1.60 (d, 3H). ^{13}C NMR (Acetone-d6): 150.17, 144.98, 131.34, 126.81, 126.36, 114.45, 108.94, 43.18, 21.03, 14.39. GC/MS: major peak integrates to 94% 292 (M+), 277 (M+ - Me), minor peak integrates to 2% 292 (M+), minor peak integrates to 4% 267 (M+).
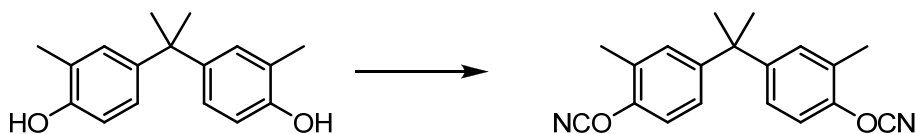
4,4'-(propane-2,2-diyl)bis(1-cyanato-2-methylbenzene) (**4**): A solution of 75 grams 4,4'-(propane-2,2-diyl)bis(2-methylphenol) (0.293 mol) and 65 grams cyanogen bromide (0.614 moles, 2.1 mol-eq) in 1L ether was cooled to -5 °C in an ice salt bath. A solution of 88 mL triethylamine (0.633, 2.15 mol-eq) moles) in 100 mL ether was added dropwise over 30 min keeping the temperature below 0 °C. The solution was allowed to warm to 10°C then washed with water, dried over MgSO$_4$, filtered, and the solution concentrated in under reduced pressure to afford 88.75 g of a white solid (99%). Mp 62-68°C. A recrystallization of material from 400 mL ether gave 70.66 grams of a white solid (79%). Mp 76-77 °C. ^{1}H NMR (CDCl$_3$): δ (ppm) 7.32 (d, 2H), 7.12 (d, 2H), 7.04 (s, 2H), 2.72 (s, 6H), 1.65 (s, 6H).

The nomenclature for all monomers is shown in Figure 3. Note that compounds **1 – 4** represent the monomers compared in this study. Networks **1 – 4** correspond to the thermally

cyclotrimerized versions of monomers **1 – 4**. Note that **1** and **2** are commercially available as Primaset® BADCy and Primaset® LECy. The preparation of compound **4** has been reported previously.[25]
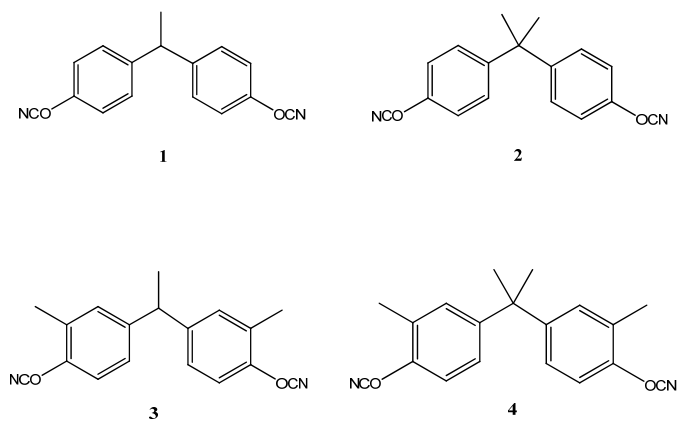
Figure 3. Chemical structures of compounds **1 – 4**.

Preparation of Networks

As-received monomers were further purified by dissolution in dichloromethane, followed by passage through a W-Prep2XY Yamazen flash chromatography column, and rotary evaporation of the purified eluent to remove the solvent. The commercial monomers Primaset® BADCy and Primaset® LECy were obtained from Novoset, Inc. (Peapack, NJ) and used as-received. Catalyst systems utilized included a 30:1 weight mixture of copper(II) acetylacetonate (Roc-Ric, used as-received) dissolved in 4-nonylphenol (97%, mixture of isomers, Aldrich, used as-received), added to monomers at 2 parts per hundred weight, or dibutyl tin dilaurate (DBTDL, Aldrich, 95%), added directly to monomers at 500 parts per million by weight, in line with the procedure described by Marella et al.[18] All monomers except LECy, which is a supercooled liquid at room temperature, were first melted at 90 °C. Catalyst was then added to about 1 g of the liquid monomer in the desired type and amount, and the resultant liquid stirred by hand for a few seconds to achieve homogeneity. (In some cases, no catalyst was added and the preceding

step was therefore omitted.) The formulated monomer was then either placed directly into a hermetically sealed differential scanning calorimetry (DSC) pan and/or poured into one or more silicone rubber molds having a disc-shaped cavity and cured using a pre-determined time-temperature schedule under flowing nitrogen, then cooled and de-molded. The resultant discs measured approximately 12 mm in diameter by 4 mm thick.

Characterization Techniques for Networks

Differential Scanning Calorimetry (DSC)

5-10 mg pieces of cured networks were removed from a molded disc and hermetically sealed in an aluminum DSC pan. Samples were then ramped under 50 mL/min of flowing nitrogen at 10 °C / min, first heating to 350 °C, cooling to 100 °C, then re-heating to 350 °C, using a TA Instruments Q200 differential scanning calorimeter. For selected samples, the maximum temperature was reduced to 300 °C to assess the possibility of chemical degradation during analysis (see Supporting Information).

Thermogravimetric analysis (TGA)

Pieces of cured discs weighing approximately 5 mg were removed and placed in a TA Instruments Q5000 Thermogravimetric Analyzer. These samples were then heated to 600 °C, under nitrogen, and, in separate experiments, in air, at 10 °C / min.

Oscillatory Thermomechanical Analysis (OTMA)

Cured discs were also tested via oscillatory thermomechanical analysis (OTMA) with a TA Instruments Q400 series analyzer under 50 mL/min of nitrogen flow. The discs were initially

held in place with a compressive force of 0.2 N using the standard ~5 mm diameter flat cylindrical probe. The force was then modulated at 0.05 Hz over an amplitude of 0.1 N (with a mean force of 0.1 N) and the temperature was ramped twice (heating and cooling) between -50 °C and 200 °C (to aid in determination of thermal lag) followed by heating to 350 °C, cooling to 100 °C, and re-heating to 350 °C, all at 50 °C/min. For samples previously exposed to hot water, the heating rate was decreased to 20 °C/min and the order of segments were: heating to 350 °C, cooling to 100 °C, two cycles between 100 °C and 200 °C for thermal lag determination, and finally heating to 350 °C. The details of the thermal lag determination procedure are reported in Supporting Information.

Other physical characterization

Sample densities were determined using a Mettler Toledo analytical balance with an attachment for specific gravity determination. De-ionized water was used as the immersion medium. A minimum of four weight measurements were collected and recorded per sample, making use of the cured discs prior to removal of portions for any other testing. For water immersion testing, cured discs were dried to a ± 0.0001 g constant weight in a vacuum dessicator, then weighed and immersed in approximately 250 mL de-ionized water maintained at 85 °C for 96 hours. After removing from the water, samples were patted dry and weighed to determine the moisture uptake (on a dry weight basis).

Results and Discussion

Monomer Characteristics

The overall experimental strategy involved the synthesis of *ortho*- methylated analogs of the well-studied monomers Primaset® LECy and Primaset® BADCy, and then performing structure-property relationship assessments in which important variables such as conversion and

the state of the network during cure (i.e. rubbery or glassy) could be controlled sufficiently to disentangle their effects from those resulting from structural changes. From a structural perspective, LECy, BADCy, and their analogs constitute a set of monomers having 1 (LECy), 2 (BADCy), 3 (monomer **3**), and 4 (monomer **4**) methyl groups per monomer (hence, the numbering system also serves as the methyl group count). Networks made from **1** and **3** have a single methyl group per repeated network segment at the bridge between the two central phenyl rings. Monomers **2** and **4** have two such groups, thus comparisons between **1** and **2**, and between **3** and **4**, show the effects of methyl group addition at the bridging unit. Monomers **3** and **4** differ from **1** and **2** by the addition of two methyl groups located *ortho-* to a cyanurate oxygen, thus comparisons between **1** and **3** and between **2** and **4** show the effect of methyl group addition near the cyanurate oxygen. The ability to independently test the effect of methyl group addition at these two different locations within each repeat unit allows for a convenient way of separating effects that result from steric hindrance of the oxygen from effects that result simply from methylation.

The successful synthesis of monomers that function as analogs of LECy and BADCy can be confirmed by examination of DSC spectra, as shown in Figure 4a and 4b for monomers with no added catalyst, and in Figure 5a and 5b for monomers with 2 phr of nonylphenol / copper(II) acetylacetonate catalyst added (containing 160 ppm Cu on an unmodified monomer weight basis). Despite some minor differences, such as a more rapid onset of cure in the *ortho-* methylated monomers, the shapes of the exotherm and their peak temperatures are similar in both cases.
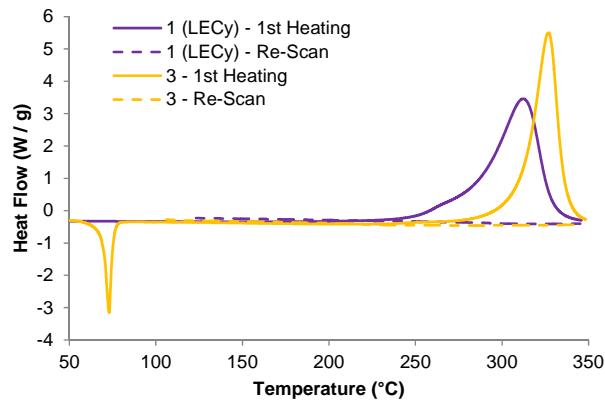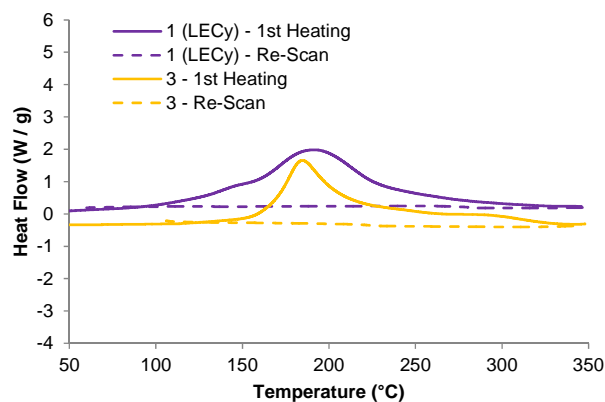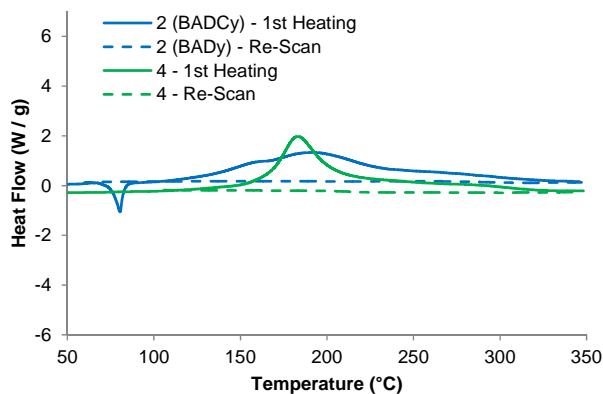
Figure 4a. Comparison of DSC scans for uncured ethylidene-bridged monomers **1** (LECy) and **3** (its *ortho*-methylated analog) with no added catalyst.
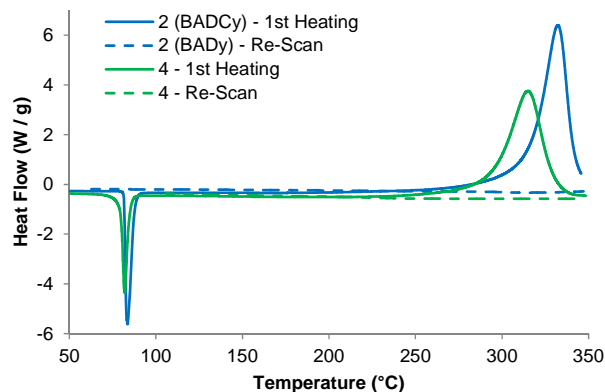
Figure 4b. Comparison of DSC scans for uncured isopropylidene-bridged monomers **2** (BADCy) and **4** (its *ortho*-methylated analog) with no added catalyst.

Figure 5a. Comparison of DSC scans for uncured ethylidene-bridged monomers **1** (LECy) and **3** (its *ortho*-methylated analog) catalyzed with 2 phr nonylphenol / 160 ppm Cu.

Figure 5b. Comparison of DSC scans for uncured ethylidene-bridged monomers **2** (BADCy) and **4** (its *ortho*-methylated analog) catalyzed with 2 phr nonylphenol / 160 ppm Cu.

Interestingly, the melting points of BADCy (**2**) and analog **4** are nearly identical at 82-83 °C, as are the enthalpies of melting. Von't Hoff purity analyses showed these two compounds to be >99% pure. Unlike LECy (**1**), however, which melts at 29 °C,[26] the analog **3** melts at 73 °C, and the Von't Hoff purity is only 96.5% for **3**. The very low melting point of LECy appears to results from the presence of two co-crystallizing forms,[27] thus multiple crystalline forms of **3** may be present and result in an underestimate of purity by the Von't Hoff method. The presence of multiple crystal forms or disordered crystals may also complicate purification of **3**, resulting in a lower overall monomer purity. Overall the DSC data indicate that the purity is high enough and the similarity in processing characteristics great enough that meaningful comparisons in properties with respect to methylation may be undertaken.

Water Uptake in Relation to Free Volume and Vitrification

As stated in the Introduction, the primary purpose of the investigation was to elucidate the mechanism of reduced moisture uptake in polycyanurates cured from *ortho*-methylated di(cyanate ester) monomers. In order to fulfill this purpose, four samples of each of the compounds **1-4** were cured using different cure conditions. These cure conditions were designed to produce two different conversions at a given cure temperature by using a short and a long cure time at each of two temperatures. The temperatures and times were chosen with the goal of accomplishing about 90% conversion in two separate cases: 1) using a long time at a lower temperature, with the network curing in the vitrified state for most of this time, and 2) using a shorter time at a higher temperature, with no vitrification. Under ideal conditions, this experimental design allows the effects of conversion, cure temperature, and vitrification to be checked independently.

Table 1 provides a list of the times and temperatures used for each of the monomers in the study, along with the resultant conversions and glass transition temperature (T_G) values at the end of cure, both of which were obtained by DSC.   For compounds **2** and **4**, the experimental design achieved the goals well, producing samples cured both with and without vitrification at conversions differing by 3% or less at 90% and 85%, respectively, and allowing samples to be compared at points before and after vitrification during isothermal cure at two separate temperatures. For compounds **1** and **3**, the design was less successful but still useful; enabling a comparison of the effect of vitrification in samples with conversions differing by 2% or less at 91% and 92%, respectively. However, in these cases the shorter, rather than the longer time, at the lower temperature serves as the vitrified sample, meaning that pre- and post-vitrification samples can be compared at only one cure temperature. **3** had an unexpectedly low conversion when cured for 24 hours at 170 °C, and showed an unusual residual cure exotherm containing

two peaks, indicating the presence of a side reaction. As a result, inferences based on the behavior of this sample were not attempted. In general, however, the experimental design was sufficient to achieve the goal of providing a means of comparing the different types of methylation while controlling for variables such as conversion and the physical state of the network during cure.

Table 1. Experimental Design and Resultant Sample Parameters

Monomer	Cure Temp (°C)	Cure Time (min)	Conversion[a]	"As-Cured" T_G (°C)[b]	Vitrified During Cure?[c]
1 (LECy)	210	30	0.901 ± 0.009	218	Yes
1 (LECy)	210	1440	0.945 ± 0.007	249	Yes
1 (LECy)	250	5	0.916 ± 0.013	229	No
1 (LECy)	250	210	0.971 ± 0.005	253	Yes
2 (BADCy)	210	30	0.846 ± 0.014	204	No
2 (BADCy)	210	1440	0.912 ± 0.008	248	Yes
2 (BADCy)	250	5	0.892 ± 0.013	226	No
2 (BADCy)	250	210	0.955 ± 0.007	258	Yes
3	170	210	0.913 ± 0.006	175	Yes
3	170	1440	0.862 ± 0.012	170	Yes
3	210	30	0.922 ± 0.009	187	No
3	210	1440	0.992 ± 0.003	229	Yes
4	170	210	0.783 ± 0.014	142	No
4	170	1440	0.869 ± 0.010	174	Yes
4	210	30	0.855 ± 0.012	170	No
4	210	1440	0.984 ± 0.005	235	Yes

a. As measured by DSC with the method specified in Supporting Information Section S2.
b. Measured on 1st DSC scan of cured samples by mid-point of step change in heat capacity or turning point at onset of exotherm if no step change in heat capacity was visible.
c. "Yes" indicates "as cured" T_G of sample was as high as, or higher than, cure temperature.

Figure 6 shows the water uptake as a function of conversion in cured networks of **1** – **4** after immersion at 85 °C for 96 hours. In this and subsequent figures, open symbols represent samples that vitrified during cure, while filled symbols represent samples that did not vitrify. The sample that showed side reactions is also identified. As described by Georjon and Galy for BADCy,[14] and as determined for di(cyanate ester) co-networks in our recent work,[21] there is a clear trend toward increasing water uptake with increasing conversion for all networks. At all

conversions, the uptakes for **1** and **2** are identical, as are those for **3** and **4**. In contrast, the water uptake of **3** and **4** is always lower than that of **1** or **2** at the same conversion in all comparable cases shown. Methylation near the cyanurate oxygen therefore has a significant effect, whereas methylation at the bridge does not. These results provide strong evidence that the cyanurate oxygen is a preferred site for water uptake in polycyanurates, and that creating steric interactions, that is imposing steric hindrance at the site of hydrogen bonding, is an effective means for reducing water uptake, particularly at conversions that approach 100%.
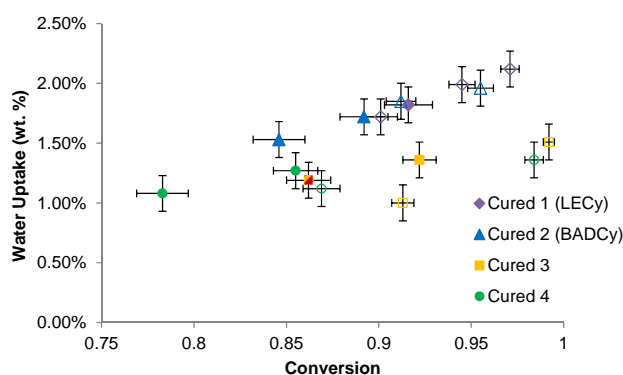
Figure 6. Water uptake as a function of conversion for cured **1-4**. Unfilled symbols represent samples that vitrified during cure, filled symbols represent samples that did not vitrify during cure. Symbols with red striping indicate samples where side reactions were evident. The same labeling scheme is used in subsequent figures.

Figure 6 also shows that the presence or absence of vitrification appears to make no difference in water uptake at a given conversion. This result would not be expected if vitrification led to a more "open" network structure that could accommodate more water, as previously suggested by us[21,28] and others.[14] However, it would be consistent with the idea that a more "open" network is formed at higher conversions due to the necessary intramolecular cyclization,[2] and the possible formation of short macrocyclic loops like those described by Fang and Shimp[2] or Simon *et al.*[29] Although an annealing experiment would be one way to further differentiate between these two

explanations, such an experiment would need to be conducted on fully cured samples in order to avoid altering the conversion during the experiment. Even for the *ortho-* methylated networks, temperatures in excess of 230 °C would be required to conduct such an experiment on catalyzed samples, and such temperatures are just high enough to potentially cause some degradation of the networks.[30] Networks without added catalyst could be more chemically stable, but would require even higher temperatures to reach full conversion. One possibility would be to perform an annealing experiment on a network cured from a monomer such as RTX-366, which has a fully cured T_G near 200 °C.[31]

As mentioned previously, there appears to be a correlation between cyanurate density and water uptake in polycyanurate networks (see Figure 2). This is due to methylation decreasing the number density of cyanurate rings (as confirmed by density data presented below), it could be argued that a lower cyanurate density produced the lower water uptake in **3** and **4**. To further elaborate on this possibility, Figure 7 reprises Figure 6 in a different form; it shows the number density of water molecules absorbed as a function of the number density of cyanurate rings in the network. In a simple model in which each cyanurate ring (or, alternatively, each cyanurate oxygen) acts as a strongly preferred site for water uptake, the curves for all four networks should collapse into a single line. Instead, each network seems to follow a distinct trend. It should be noted that earlier work by us[32] and others[33] has shown that, at lower conversions, from around 70% to around 90%, water uptake decreases as conversion increases. As a result, the trends seen in Figure 7 cannot be reliably extrapolated to lower conversions (at lower conversions, each set of points would pass through a minimum). Furthermore, comparing the trends for **1** and **2**, methylation at the bridge also lowers cyanurate density but has a very different effect on water uptake than methylation *ortho-* to the cyanurate oxygens. There is thus no "universal"

relationship between cyanurate density and moisture uptake that could be used to support the speculation that lower cyanurate density is responsible for the lower water uptake of *ortho-*methylated networks
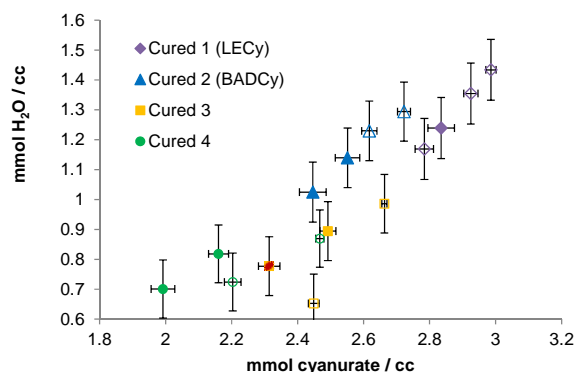
Figure 7. Water uptake as a function of cyanurate density for cured **1-4**. See Figure 6 for a guide to symbols.

To summarize, the water uptake results indicate that *ortho-* methylation is an effective method for reducing water uptake in polycyanurates networks, likely because of steric hindrance provided to the cyanurate oxygen, which appears to be a preferred site for water uptake. The differences are modest at conversions below 85%, but become significant as conversions approach 100%. One potential explanation for such an effect is that conversions above 85% require the formation of more "open" (less tightly packed) network structures. In such "open" structures, thermodynamically favorable interactions between water and the cyanurate oxygens are facilitated, unless these oxygens are sterically hindered by *ortho-* methylation.

If the foregoing statements are true, then a decrease in density and packing fraction with conversion should be observed with increasing conversion in cyanate esters, regardless of cure conditions. Figures 8 and 9, respectively, show the density and packing fraction at room temperature as a function of conversion for networks cured from monomers **1 - 4**. For networks **2** and **4**, there is a clear trend toward lower density and packing fraction with increasing

conversion that is not significantly affected by vitrification or cure temperature. For networks **1** and **3**, there appears to be a downward trend, but the smaller range of conversions studied limits the signal to noise ratio. Note that in previous work,[32] the density of identically catalyzed **1** has been shown to decrease with increasing conversion. The packing fractions for networks **2** and **4** appear identical, while those of **1** and **3** may be slightly higher. Note that the correlation of Bicerano,[34] which has an average deviation of about 1% in this case when compared with other methods, was used to calculate the van der Waals volume (see Supporting Information). In terms of packing fraction then, systematic differences of less than about 0.006 could easily disappear if a different method of calculation of van der Waals volume were chosen. Thus, no significant differences in packing fraction among the four monomers could be detected.
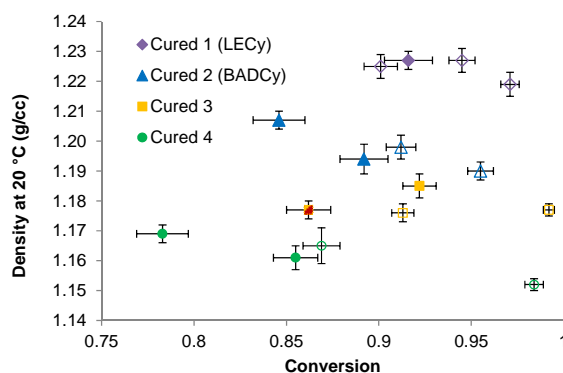
Figure 8. Density as a function of conversion for cured **1-4**. See Figure 6 for a guide to symbols.
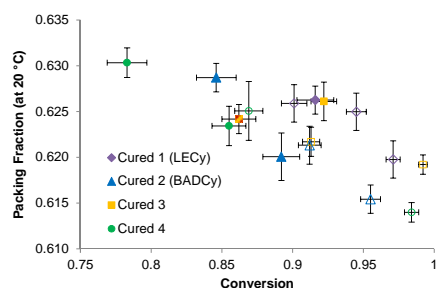
Figure 9. Packing fraction as a function of conversion for cured **1-4**. See Figure 6 for a guide to symbols.

An important question related to packing fraction and density is whether a significant difference exists between vitrified and non-vitrified samples. Of the four networks studied, only network **3** shows a lower density for vitrified samples. Given that network **3** showed anomalous behavior due to side reactions, and given that the difference is not reproduced in the other, very similar networks, the difference is likely due to an uncontrolled variation rather than to a systematic effect of vitrification that is unique to **3**. Thus, vitrification during cure, if it affects packing densities at all, is likely to affect packing much less than systematic effects due to an increase in conversion. Furthermore, if van der Waals volume was simply being converted to free volume during cure without an overall change in sample volume, then the actual density (deriving from an unchanging mass divided by an unchanging volume) should not change with conversion, whereas there is ample evidence that it systematically declines. The decrease in the coefficient of thermal expansion with increasing conversion noted for polycyanurate networks would produce some overall decrease in density as conversion increased, however, the magnitude of the decrease in density with increasing conversion is much too large to be explained by this effect.

For the present study, it can be concluded that *ortho-* methylation of cyanurate groups does not lead to lower uptake because a lower T_G at full cure allows free volume to relax more readily in

the sample under similar conditions. The best explanation appears to be that *ortho-* methylation lowers moisture uptake by steric hindrance of the cyanurate oxygen, a preferred site for water uptake. Note that because *ortho-* methylation does not appear to increase the packing fraction of the network, this effect is not simply due to methyl groups "filling holes" that water prefers to occupy, rather the local arrangements of atoms in the network are altered such that there are fewer favorable locations (and/or reduced thermodynamic favorability) for water to occupy near the polar cyanurate oxygen (and potential hydrogen-bonding site).

Thus, the density and packing data demonstrate that at higher conversions, there is more free volume available within the networks, and, as seen in Figure 6, water uptake becomes more sensitive to the local molecular structure of repeat unit segments near the cyanurate oxygen. At lower conversions, there is less free volume, and water is hindered from accessing favored sites regardless of the local repeat unit structure. Therefore, *ortho-* methylation makes less of a difference in water uptake. This particular aspect of water uptake in polycyanurate networks has not been widely recognized previously.

Hydrolytic Stability via Glass Transition Temperature Decreases

Although the reduced water uptake associated with *ortho-* methylated polycyanurate networks offers some direct technological advantages, such as lower out-gassing for space structures, a modest reduction in take-off weight for unprotected aerospace structures in humid environments, and reduced risk of blistering on rapid heating, much of the technological interest in attaining lower water uptake in polycyanurate networks stems from the presumed correlation between higher water uptake and greater "knock down" in thermo-mechanical performance when the networks are utilized in wet environments. The most common measure of the "knock down" is

the decrease in the glass transition temperature of the networks produced by exposure to hot/wet conditions. The resultant measure of performance is the associated "wet" T_G of the network, which is typically utilized to establish a maximum service temperature in combination with an engineering safety factor.

Having established that *ortho-* methylation in polycyanurate networks leads to lower water uptake, an important follow-on consideration is the effect of *ortho-* methylation on the "wet" T_G of the networks. Figure 10 presents the dry T_G of networks **1-4** as a function of conversion. The dry T_G values follow the diBenedetto equation[35] as expected; with methylation at the bridge resulting in a roughly 15 °C increase in T_G at a given conversion. The addition of two *ortho-* methyl groups per monomer, however, decreases the dry T_G by 50-60 °C at a given conversion. To reconcile these very different effects of adding methyl groups, it is helpful to separate out the different structural effects with the aid of Figure 11, in which the dry T_G is plotted as a function of cross-link density. At identical conversions (indicated by the circled points), bridge group methylation decreases cross-link density by 10%, while the addition of two *ortho-* methyl groups decreases cross-link density by 13%. At the same cross-link density, however, the addition of a bridge methyl group increases T_G by about 50 °C, while the addition of two *ortho-* methyl groups raises T_G by at most about 20 °C (to visualize this effect, compare the trends among identically colored points in Figure 11 and estimate the vertical offset). Methyl groups may therefore be thought of as "segment stiffeners" in networks with identical cross-link densities. The bridge methyl group, however, is more effective, as it constrains the degree of bending in the more flexible aliphatic backbone portion of the segment, whereas the aromatic methyl groups simply add side group bulk to the already rigid phenyl groups. The stiffening effect of methylation of the bridge is great enough to compensate for the decreased cross-link density, whereas the less

potent stiffening effects of *ortho-* methyl groups only partly compensate for decreased cross-link density.
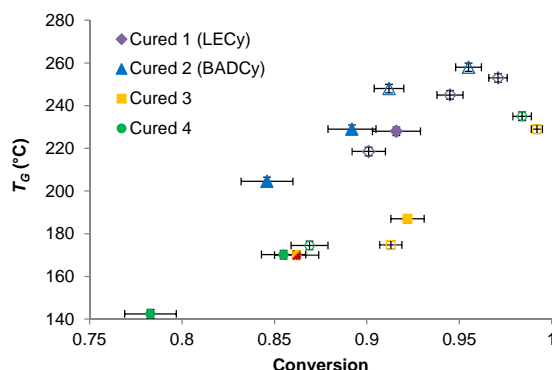
Figure 10. Dry T_G as a function of conversion for cured **1**-**4**. See Figure 6 for a guide to symbols.
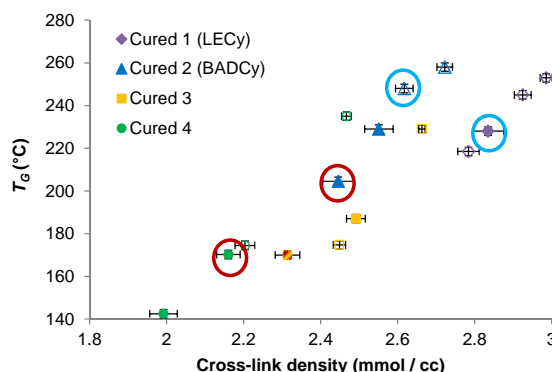
Figure 11. Dry T_G as a function of cross-link (i.e. cyanurate) density for cured **1**-**4**. See Figure 6 for a guide to symbols. The pairs of matched colored circles indicate samples with identical conversions (blue, ~90%, showing effect of bridge group methylation; red, ~85%, showing effect of *ortho-* methylation).

Figure 12 shows the "wet" T_G as a function of conversion for networks **1**-**4**. Although the effect of conversion is much smaller, and even near zero in network **3**, the general trends are

qualitatively similar to those seen in Figure 10. Methylation at the bridge increases the "wet" T_G

by about 0 - 10 °C while *ortho-* methylation results in a 30-40 °C decrease in "wet" T_G at the

same conversion. In terms of "knock down", there is thus an approximately 20 °C lower "knock

down" in the *ortho-* methylated networks, however, this improvement is insufficient to

compensate for the lower dry T_G of the *ortho-* methylated networks. The measured "knock

down" depends on plasticization of the networks by any moisture remaining after heating to the

T_G (previous experiments[21,36] have shown that some, but not all, moisture remains under these

conditions), along with permanent degradation of the network due to hydrolysis. Because these

effects represent a mixture of intrinsic material properties and extrinsic sample properties, the

interpretation should be limited to qualitative analysis of trends and differences. Thus, in terms

of hot/wet performance, for the specific networks studied, there is actually a penalty for *ortho-*

methylation in terms of the maximum use temperature. Whether or not *ortho-* methylation

represents a useful strategy for applications therefore depends on the relative importance of

reduced water uptake compared to maximum use temperatures.
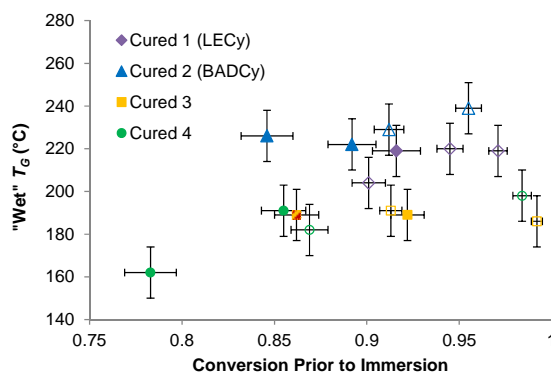
Figure 12. T_G as a function of conversion for cured **1-4** after immersion in 85 °C water for 96

hours. See Figure 6 for a guide to symbols.

The aforementioned results for copper-catalyzed polycyanurates are in contrast to the earlier work in zinc-catalyzed *ortho*-methylated polycyanurate networks reported by Shimp et al.[20] in which both reduced water uptake as well as improvements in "wet" T_G were observed. To gain some additional insight into what role, if any, the choice of catalyst played in the above results, some comparative studies using different catalyst types were undertaken. Specifically, polycyanurate networks with no added catalyst, the 2 parts per hundred nonylphenol / 160 ppm Cu catalyzed networks for which detailed results are reported above (referred to herein as "Cu-Acac catalyzed", and networks catalyzed by addition of 500 ppm of dibutyl tin dilaurate (DBTDL) were compared. The DBTDL-catalyzed networks were of interest because recent work by Marella et al.[18] showed improved hot/wet performance in DBTDL-catalyzed networks of the cyanated phenol-formaldehyde resin PT-30 compared to systems catalyzed with other metals. DBTDL has also been studied previously as a catalyst for **1** (LECy)[37] and **2** (BADCy).[38-43]

Table 2 compares the key characteristics of networks of **3** and **4** cured at 210 °C for 24 hours using the three catalyst types mentioned previously. The addition of catalyst results in a higher degree of conversion, but generally decreases the dry T_G at full conversion due to plasticization of the network by incorporated nonylphenol. The effects of adding the Cu-Acac catalyst package are small, but effects arising from addition of the DBTDL catalyst are more significant. In terms of the difference between dry (as-cured) T_G and "wet" T_G, the networks with no added catalyst fare best, with the T_G decreasing by only about 5 °C. This very small change is in line with previously studied polycyanurate networks.[26] The incorporation of the Cu-Acac catalyst causes a more significant reduction in T_G on exposure to hot water of 20 - 30 °C, in line with the

observations of Marella *et al.*[18] as well as the slightly higher water uptake.   The introduction of DBTDL, however, results in severe damage to the samples on exposure to hot water, with networks **3** and **4** undergoing disintegration during the 96 hour test. In the case of **4**, the sample became so damaged that not even the remaining fragments could be tested after recovery. It is unclear why the effect of DBTDL addition on hydrolytic stability of networks **3** and **4** was markedly different from the reports of Marella *et al*, in which addition of DBTDL improved the hydrolytic stability of the cyanated phenolic resin PT-30.[18]

   In addition to greatly decreasing hydrolytic stability, the incorporation of DBTDL as a catalyst also results in some loss of thermo-chemical stability, as seen by the decomposition temperature data in Table 2, whereas the incorporation of Cu-Acac results in no significant loss of thermo-chemical stability. The density of the DBTDL catalyzed networks is also consistently higher than the others, and while the "as cured" T_G values are reasonable for the conversions measured, the fully cured T_G values are quite a bit lower than expected given the conversions and "as cured" T_G values.   These features all suggest that side reactions, especially at elevated temperatures, are much more pronounced when DBTDL is used as a catalyst for networks **3** and **4**. The presence of side reactions will lead to errors in the measurement of conversion by DSC, as well as to a potential decrease in T_G of the "fully cured" network on exposure to heating to 350 °C. Indeed, the T_G of the "fully cured" network is often a few °C lower than the "as cured" T_G, potentially due to side reactions in monomers **3** and **4** at elevated temperatures. In fact, some level of side reactions may be present in all versions of networks **1 - 4**, however, when all of the data is considered, the side reactions have more pronounced effects for the DBTDL-catalyzed networks. More significant side reactions would be one possible reason for the greatly decreased hydrolytic stability of the DBTDL-catalyzed networks. The occurrence of these side reactions

may be a direct consequence of the added steric hindrance around the reacting cyanuarte during

cyclotrimerization of the *ortho-* methylated monomers. A complete set of comparative data for

the variously catalyzed networks may be found in Supporting Information.

Table 2. Effect of Cure Catalyst on Key Properties of Networks **3** and **4**

Mon-omer	Catalyst	Con-version	"As Cured" T_G (°C)[a]	"Fully Cured" T_G (°C)[b]	"Wet" TG (°C)[c]	TGA 5% Weight Loss in N_2 / Air (°C)	Water Uptake (%)	Density (g/cc)
3	Not Added	0.994± 0.002	246	244	240	401/403	1.21%	1.142
3	Cu-Acac	0.995± 0.006	226	216	195	402/404	1.46%	1.165
3	DBTDL	0.996 ± 0.012	196	199	<100*	395/396	13.82%	1.180
4	Not Added	0.957 ± 0.017	226	233	222	401/401	1.05%	1.159
4	Cu-Acac	0.990 ± 0.007	236	228	214	399/400	1.18%	1.154
4	DBTDL	0.959 ± 0.047	185	192	68*	378/389	-3.68%*	1.162

a. Measured on 1st DSC scan of cured samples by mid-point of step change in heat capacity or turning point at onset of exotherm if no step change in heat capacity was visible.

b. Measured on 2nd DSC scan of cured sample (after heating to 350 °C at 10 °C / min) by mid-point of step change in heat capacity.

c. Measured by OTMA by temperature at peak loss component of stiffness.

Conclusions

A comparison of the physical properties of polycyanurate networks based on 2,2-bis(4-cyanatophenyl)propane (BADCy) and 1,1-bis(4-cyanatophenyl)ethane (LECy) with and without a single methyl group *ortho*- to each aryl- cyanurate linkage showed that *ortho*- methylation was effective at reducing moisture uptake, particularly at conversions above 80%, whereas the effect of methylation at the bridges between phenyl rings in the network segments was negligible. These differences were observed even though *ortho*- methylation appeared to have no significant impact on either the packing fraction or its dependence on conversion in these networks. Vitrification during cure had little effect on either free volume development or moisture uptake. These results tend to confirm that steric hindrance from an *ortho*- methyl group inhibits absorption of water. Such an effect is likely best explained by decreasing the thermodynamic favorability of hydrogen bonding and/or dipole-dipole interaction with the cyanurate oxygen by creating an unfavorable steric environment. The hydrolytic stability of the *ortho*- methylated networks, as inferred from the relative decrease in glass transition temperature on immersion in water for 96 hours at 85 °C, was moderately improved. However, because the dry glass transition temperature of the *ortho*- methylated networks was significantly lower, the "wet" glass transition temperature of the *ortho*- methylated networks was still 30 – 40 °C lower than the analogous commercial networks. An examination of the effect of two different catalysts, 2 parts per hundred of a 30 : 1 by weight mixture of nonylphenol and copper(II) acetylacetonate and 500 parts per million of dibutyl tin dilaurate (DBTDL), compared to analogous uncatalyzed networks, showed very significant differences in stability, with networks catalyzed by dibutyl tin

dilaurate showing significant side reactions at elevated temperature and severe hydrolytic degradation. These results show that *ortho-* methylation mitigates some, but not all, forms of hydrolytic instability in polycyanurate networks.

ASSOCIATED CONTENT

Supporting Information. Section S1: Tabulated list of all monomers, catalyst systems, and experiment types. Section S2: Details of DSC conversion measurements. Section S3: Raw DSC data. Section S4: Details of OTMA thermal lag determination. Section S5: Raw OTMA data. Section S6: Raw TGA data. Section S7: Determination of van der Waals volume. This material is available free of charge via the Internet at http://pubs.acs.org.

AUTHOR INFORMATION

Corresponding Author

*andrew.guenthner@us.af.mil

Present Addresses

†Michael E. Wright, Cobalt Technologies, Mountain View, CA 94043 USA

research internship at the Air Force Research Laboratory, under which a portion of this work was

completed.

REFERENCES

1. *Chemistry and Technology of Cyanate Ester Resins*, Hamerton, I., Ed.; Chapman & Hall: London, 1994.
2. Fang, T.; Shimp, D. A. *Prog. Polym. Sci.* **1995**, *20*, 61-118.
3. Nair, C. P. R.; Mathew, D.; Ninan, K. N. In *New Polymerization Techniques and Synthetic Methodologies*, Abe, A.; Albertsson, A.-C.; Cantow, H. J., Eds.; Springer-Verlag: Berlin, 2001; Vol. 155, pp 1-99.
4. Hamerton, I.; Hay, J. N. *High Perform. Polym.* **1998,** *10*, 163-174.
5. Deutsch, A.; Surovic, C. W.; Lanzetta, A. P.; Ainspan, H. A.; Abbiate, J. C.; Veihbeck, A.; Hedrick, J. C.; Shaw, J. M.; Tisdale, S. L.; Foster, E. F.; Coteus, P. W. *IEEE Trans. Compon. Packag. Manuf. Technol. Part B-Adv. Packag.* **1996,** *19*, 331-337
6. Esslinger, J. R.; Fruchtnicht, O. C. *SAMPE J.* **2004,** *40*, 9-15
7. Wienhold, P. D.; Persons, D. F. *SAMPE J.* **2003,** *39* (6), 6-17.
8. Fabian, P.; Haynes, M.; Babcock, H.; Hooker, M. *IEEE Trans. Appl. Supercond.* **2013,** *23*, No. 7700204.
9. Munshi, N. A.; Walsh, J. K.; Hooker, M. W.; Babcock, H. K.; Haight, A. H.; Durso, S. R.; Kawaguchi, A.; Hough, P. *IEEE Trans. Appl. Supercond.* **2013,** *23*, No. 7700104.
10. Shivakumar, K. N.; Chen, H.; Holloway, G. *J. Reinf. Plast. Compos.* **2009**, *28*, 675-689.
11. Morgan, B.; Madhukar, M.; Walsh, J.; Hooker, M.; Grandlienard, S. *J. Compos. Mater.* **2010,** *44*, 821-837.
12. Chen, P. C.; Saha, T. T.; Smith, A. M.; Romeo, R. *Optical Engineering* **1998,** *37*, 666-676.
13. Nishimura, A.; Izumi, Y.; Imaizumi, M.; Nishijima, S.; Hemmi, T.; Shikama, T. *Fusion Eng. Des.* **2011,** *86*, 1558-1561.
14. Georjon, O.; Galy, J. *Polymer* **1998,** *39*, 339-345.
15. Reams, J. T.; Guenthner, A. J.; Lamison, K. R.; Yandek, G. R.; Swanson, D. D.; Mabry, J. M. *J. Polym. Sci., Part B: Polym. Phys.* **2014**, *52*, 1061-1070.
16. Shimp, D. A.; Ising, S. J. *Polym. Mat. Sci. Eng.* **1992**, *66*, 504.
17. Kasehagen, L. J.; Haury, I.; Macosko, C. W.; Shimp, D. A.,. *J. Appl. Polym. Sci.* **1997,** *64*, 107-113.
18. Marella, V. V.; Throckmorton, J. A.; Palmese, G. R. *Polym. Degrad. Stabil.* **2014**, *104*, 104-111.
19. Shimp, D. A. *Polym. Mat. Sci. Eng.* **1986**, *54*, 107-113.
20. Shimp, D. A. U. S. Patent 4,604,452 (1986).
21. Guenthner, A. J.; Lamison, K. R.; Vij, V.; Reams, J. T.; Yandek, G. R.; Mabry, J. M. *Macromolecules* **2012**, *45*, 211-220.
22. Davis, M. C.; Guenthner, A. J.; Groshens, T. J.; Reams, J. T.; Mabry, J. M. *J. Polym. Sci,. Part A: Polym. Chem.* **2012**, *50*, 4127-4136.
23. *Chemistry and Technology of Cyanate Ester Resins*, Hamerton, I., Ed.; Chapman & Hall: London, 1994, Appendix A, Table A-3, pp. 332-333.
24. Yeh, R. H.; Lin, P. W.; Lin, K. F. *J. Polym. Res.-Taiwan* **2002,** *9*, 31-36.
25. Pankratov, V. A.; Vinogrodova, S. V.; Korshak, V. V. *Russ. Chem. Rev.* **1977**, *46*, 278.

26. Snow, A. W. "The synthesis, manufacture and characterization of cyanate ester monomers" in Hamerton, I. (Ed.), *Chemistry and Technology of Cyanate Ester Resins*. Chapman & Hall: London, 1994, p. 35.

27. Guenthner, A. J.; Reams, J. T.; Lamison, K. R.; Ramirez, S. M.; Swanson, D. D.; Yandek, G. R.; Sahagun, C. M.; Davis, M. C.; Mabry, J. M. *ACS Appl. Mater. Interfaces* **2013**, *5*, 8772-8783.

28. Corley, C. A..; Guenthner, A. J.; Sahagun, C. M.; Lamison, K. R.; Reams, J. T.; Hassan, M. K.; Morgan, S. E.; Iacono, S. T.; Mabry, J. M. *ACS Macro Lett.* **2014**, *3*, 105-109.

29. Simon, S. L.; Gillham, J. K. *J. Appl. Polym. Sci.* **1993**, *47*, 461-485.

30. Goertzen, W. K.; Kessler, M. R., *Composites Part A* **2008,** *39*, 761-768.

31. Li, Q. X.; Simon, S. L. *Macromolecules* **2007**, *40*, 2246-2256.

32. Reams, J. T.; Guenthner, A. J.; Lamison, K. R.; Vij, V.; Lubin, L. M.; Mabry, J. M. *ACS Appl. Matl. Interfaces* **2012**, *4*, 527-535.

33. Ising, S. J.; Shimp, D. A.; Christenson, J. R. in *3rd International SAMPE Electronics Conference*, SAMPE International Business Office, 1989; pp 360-370.

34. Bicerano, J., *Prediction of Polymer Properties*. 3rd ed.; Marcel Dekker, Inc.: New York, 2002; pp. 66-78.

35. Pascault, J. P.; Williams, R. J. J. *J. Polym. Sci,. Part B: Polym. Phys.* **1990**, *28*, 85-95.

36. Davis, M. C.; Guenthner, A. J.; Sahagun, C. M.; Lamison, K. R.; Reams, J. T.; Mabry, J. M. *Polymer* **2013**, *54*, 6902-6909.

37. Li, W. F.; Liang, G. Z.; Xin, W. L. *Polym. Int.* **2004**, *53*, 869-876.

38. Dai, S. K.; Zhou, D. X.; Gu, A. J.; Liang, G. Z.; Yuan, L. *Polym. Eng. Sci.* **2011**, *51*, 2236-2244.

39. Nagendiran, S.; Chozhan, C. K.; Alagar, M.; Hamerton, I. *High Perform. Polym.* **2008**, *20*, 323-347.

40. Nagendiran, S.; Premkumar, S.; Alagar, M. *J. Appl. Polym. Sci.* **2007**, *106*, 1263-1273.

41. Matthew, D.; Nair, C. P. R.; Ninan, K. N. *J. Appl. Polym. Sci.* **2000**, *77*, 75-88.

42. Nair, C. P. R.; Francis, T. *J. Appl. Polym. Sci.* **1999**, *74*, 3365-3375.

43. Matthew, D.; Nair, C. P. R.; Krishnan, K.; Ninan, K. N. *J. Polym. Sci. Part A: Polym. Chem.* **1999**, *37*, 1103-1114.

For Table of Contents Use Only

"Mechanisms of Decreased Moisture Uptake in *ortho*- Methylated Di(Cyanate Esters)"

Andrew J. Guenthner,[1]* Michael E. Wright,[2,†] Andrew P. Chafin,[2] Josiah T. Reams,[3] Kevin R. Lamison,[3] Michael D. Ford,[3] Shawn P. J. Kirby,[4] Jacob J. Zavala,[3] Joseph M. Mabry[1]

[1] Aerospace Systems Directorate, Air Force Research Laboratory, Edwards AFB, 93524 USA
[2] Naval Air Warfare Center, Weapons Division, China Lake, CA 93555 USA
[3] ERC Incorporated, Air Force Research Laboratory, Edwards AFB, CA 93524 USA
[4] California State University, Long Beach, Long Beach, CA 90840 USA

* andrew.guenthner@us.af.mil

†Present address: Cobalt Technologies, Mountain View, CA 94043 USA

S1. Guide to Nomenclature and Experimental Descriptions
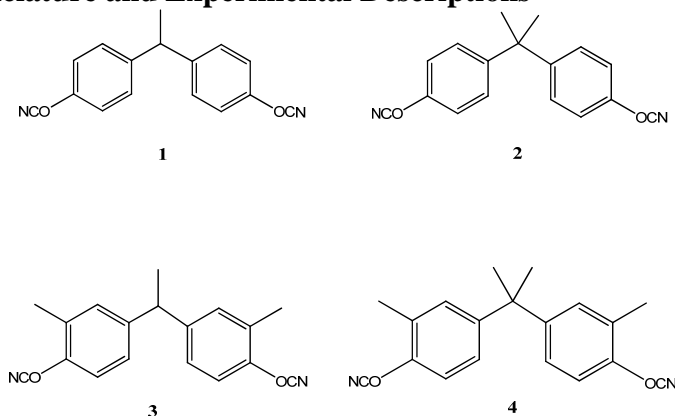
Figure S1. Chemical structures and numbering system for monomers. Note that the assigned number corresponds to the number of methyl groups present in the monomer. **1** is the commercial product Primaset® LECy and **2** is the commercial product Primaset® BADCy.

Table S1: Description of Catalyst Systems Employed

Label	Description
Not Added	No catalyst added to monomer (some residual phenols likely present)
Cu-Acac	2 parts per hundred monomer by weight of pre-mixed 30:1 by weight nonylphenol and copper(II) acetylacetonate added to molten monomer
DBTDL	500 parts per million monomer by weight dibutyl tin dilaurate added directly to molten monomer

Table S2: Description of Experiment Types

Type	Description
Cure Condition	Monomers **1-4** cured at two temperatures for two times, designed to produce a range of conversions and vitrification behavior; cure times are always denoted in minutes and describe only the second step. All cures consisted of an initial step of 150 °C for 60 minutes, followed by the time and temperature denoted. All ramp rates were 5 °C / min. Measurements taken include conversion by DSC, T_G after cure and after heating to 350 °C at 10 °C / min (assumed to result in complete conversion of cyanate esters to cyanurates, i.e. "full cure" as denoted by the suffix "-fc" in subscripts, measured by DSC and TMA, density, water uptake, and "wet" T_G values (including after heating to 350 °C at 10 °C / min) by TMA.
Catalyst Choice	Monomers **3** and **4** only, cured for 1 hour at 150 °C followed by 24 hours at 210 °C, using no catalyst added, Cu-Acac catalyst, and DBTDL catalyst (see Table S1). Cure times for these experiments are always denoted in hours. Measurements taken include conversion by DSC, T_G after cure and after heating to 350 °C at 10 °C / min (assumed to result in complete conversion of cyanate esters to cyanurates, i.e. "full cure" as denoted by the suffix "-fc" in subscripts, measured by DSC and TMA, density, water uptake, and "wet" T_G values (including after heating to 350 °C at 10 °C / min) by TMA, and TGA ramped heating under nitrogen and in air. Note that the experiments using Cu-Acac replicate one of the conditions used in the "cure condition" experiments in order to provide a point of comparison.
DSC Scan Temperature Range	Replication of 12 DSC experiments (cure condition experiments on monomers **3** and **4**), and catalyst choice experiments that do not replicate the cure condition experiments on monomers **3** and **4**. In .each case, the DSC conversion and T_G measurements are repeated using a maximum heating temperature of 300 °C rather than 350 °C, in order to investigate the assumption of full cure and the possibility of degradation, when heating to these temperatures.
Auxiliary DSC Experiments	The melting characteristics of all four monomers are determined by a separate single DSC heating scan. The enthalpy of cure for each monomer / catalyst combination examined in the "Catalyst Choice" experiments is also determined by DSC.

S2. Conversion Measurements by DSC

For well-studied polycyanurates networks at high monomer conversions, an ideal way to determine conversion would be to utilize DSC experiments to measure the "as cured" T_G and then utilize the diBenedetto equation[S1] to compute the conversion. The uncertainty in a measurement of T_G using the mid-point method by DSC is only about 2 °C, which corresponds to an uncertainty of less than 0.005 in conversion assuming no error in diBenedetto parameters. Such a level of precision is considerably better than what is currently offered by any other method. In reality, however, diBenedetto equation parameters must ultimately be determined experimentally, and the experiments utilized for their determination suffer from many forms of both uncertainty and systematic error, such that the actual uncertainty in determining conversions based on T_G measurements is considerably larger. Moreover, for newly synthesized monomers, no diBenedetto equation parameters are typically available.

Conversions for polycyanurates networks are typically determined utilizing residual enthalpies of cyclotrimerization, with the diBenedetto equation providing a number of useful ways to check the data. For instance, for any physically realistic values of the diBenedetto equation parameters, the T_G must always increase with increasing conversion, as must the derivative of T_G with respect to conversion. Therefore, if the T_G of a polycyanurate network is 100 °C at a conversion of 0.7, and 150 °C at 0.8, the diBenedetto equation requires that it must exceed 200 °C at a conversion of 0.9. Moreover, the values of the diBenedetto equation parameters tend to follow consistent patterns with respect to structure for polycyanurate networks, allowing T_G and conversion pairings to be checked for reasonableness. Finally, well-known relationships exist in polycyanurates between cure temperatures, order of magnitude cure times, and T_G, values for polycyanurate networks, so in cases where the pairing between a T_G

value and a conversion seems unreasonable, it is typically easy to discriminate between an unreasonable measured value of conversion and an unreasonable measured value of T_G as the cause.

The foregoing considerations are often enough to preclude measurement errors of more than about 0.05 (absolute) in the determination of conversion in polycyanurate networks with values of $T_{G\infty}$ (that is, the value of T_G at complete conversion) below about 325 °C. An absolute uncertainty of about 5% in conversion also happens to be about the level at which considerations related to the selection of baselines become important in DSC measurements. The prevailing practice in most cases has been simply to live with an uncertainty of 0.05 in conversion values obtained by DSC, and to manually select a baseline for integration of heat flows that follows any reasonable method.

An examination of the reproducibility of DSC traces, along with considerations such as probable weighing errors, suggest that much more precise measurements of conversion, with precisions near 0.01, are possible, if only an appropriate method of baseline selection is utilized. To see the impact of such improvements, one need only visualize data such as Figure 6 in the main manuscript with horizontal error bars of 0.05 in each direction (with the corresponding variation in data point location). Under such circumstances, variations in key parameters such as water uptake with respect to conversion, and their implications for structure-property relationship development, would be impossible to obtain reliably. Thus, it has long been recognized in kinetic studies,[S2] a good method for determining a DSC baseline is a highly valuable tool in understanding many key phenomena in polycyanurate networks.

The main difficulty in determining baselines for DSC exotherms is that the heat capacity, which also determines the DSC heat flow signal, can change during the course of an exothermic

event. The most significant cause for the change in heat capacity is the glass transition, which typically increases heat capacity by about 0.3 J/g °C in polycyanurate networks at high conversion. Other changes, such as the changing thermal environment during instrument heating, can lead to slight shifts in baselines. In addition to these, polycyanurate networks undergo some thermal degradation at elevated temperatures. At temperatures above 350 °C, the degradation signal is strong enough to mask even the glass transition. At lower temperatures, degradation can certainly affect the baseline. The fact that in many cases, the glass transition temperature of polycyanurate networks actually decreases slightly after heating to 350 °C indicates that degradation is possibly significant enough to affect the baseline. In principle, modulated DSC can be used to eliminate the effects of changing heat capacity. In practice, however, we have observed the advantages of modulated DSC to be limited. The algorithms that separate the reversible from the irreversible signals in modulated DSC tend to be imprecise (due to difficulty in maintaining a programmed temperature change) when exotherms are comparatively large, as they often are in polycyanurate networks. Moreover, modulated DSC requires very slow heating rates; in practice, the T_G increases significantly during measurement when such slow heating rates are utilized, eliminating the benefit of simultaneous conversion and T_G measurement. We have found that the use of inferred information based on the near-universal behavior of polycyanurate networks, along with re-scanning procedures to estimate baseline shifts, constitute a more reliable basis for baseline estimation than reliance on modulated DSC.

There are several desirable characteristics that must be balanced when developing a method for generating baselines. A key characteristic is objectivity, an algorithm should avoid having to rely on the judgments of operators, yet it must be able to work under a wide variety of circumstances, from samples with excess enthalpy near the T_G, to samples that show a clearly

shifted step transition with a large exotherm, to samples that show no apparent T_G during residual cure. Another important characteristic is a measure of uncertainty; any method should include a means for estimating the uncertainty inherent in the procedure. Finally, any method should take into account as much as possible that is known about the sample, while maintaining simplicity.

A key starting point for any method is the use of re-scanning to establish a preliminary baseline, as exemplified by Sheng et al.[S3] Figure S2 shows a typical DSC scan (thick solid line) with the re-scanned baseline (no offset, thick dashed line), for monomer **4** cured at 210 °C for 30 minutes (Cu-Acac catalyzed). The thin lines depict three possible baselines that might be selected based on a simple visual examination of the first heating curve. The thin solid line connects the inflection point with the final minimum, while the dotted line connects the two local minima, and the dashed line makes use of the slopes at the two minima. In contrast, the re-scan method uses the 2nd heating as a baseline, truncated at around point B where the two thick lines intersect. Note how the re-scanned baseline yields the largest area under the curve.
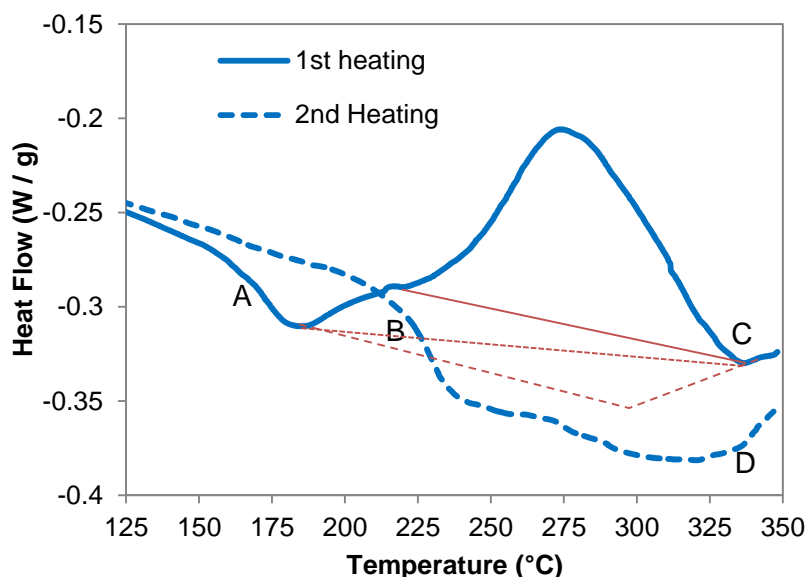
Figure S2. DSC scan of monomer **4** cured at 210 °C for 30 minutes (Cu-Acac catalyzed) thick (blue) line – 1st heating, thick (blue) dashed line – re-scan baseline with no offset, thin (red) lines show potential baselines assigned by operator judgment.

Although experience with DSC baselines might suggest that the re-scanned baseline is the worst candidate, a more careful examination of the behavior of polycyanurate networks leads to the opposite conclusion. The region near "B" on the second heating corresponds to the T_G of the fully cured network, with a heat capacity increase of about 0.05 W/g (0.3 J / g °C), as expected. The "dip" in the curve starting near "A" actually has two parts, a step increase in heat capacity followed by the initiation of cure. That the T_G really is near "A" at about 175 °C, and not at some temperature below 125 °C or near 225 °C can be confirmed using the approximate area of the curve (roughly 40-80 J / g for the given baselines), which implies a conversion of roughly 0.88 – 0.94. (Conversions are determined from residual heats of cure using the formula $\alpha = 1 - (\Delta H_r/\Delta H_0)$, where α represents the conversion, ΔH_r represents the residual heat of cyclotrimerization, that is, the quantity determined by integrating the DSC scan relative to the baseline, and ΔH_0 represents the separately measured heat of cyclotrimerization of the uncured monomer). A T_G below 125 °C would imply an increase of 100 °C or more for a conversion change of 0.12 at most, or at least 8 - 16 °C for every 1% change. Such a steep dependence is usually not seen at T_G values below about 250 °C. On the other hand, a T_G near 225 °C would imply no change of T_G with conversion, which is also not physically realistic. A T_G near 175 °C would imply a 4 – 8 °C increase in T_G for every 0.01 increase in conversion, which is just as expected for T_G values of 150 – 250 °C. The magnitude of the increase in heat capacity at a conversion of 0.88 – 0.94 will be quite similar to that at full conversion. Yet the magnitude of the step change in heat flow visible near "A" is significantly smaller than 0.05, which indicates that the initiation of residual cure actually masks the full step change. A step change of 0.05 near "A" should bring the baseline to a point congruous with the portion of the second scan above the T_G at full cure.

Thus, the thin "visual" baselines all underestimate the true area under the curve. Only if a completely unmasked T_G is present at a low enough temperature that residual cure is not immediately initiated afterword will a visual baseline be correct, and for polycyanurate networks, where cure is often initiated even below T_G, such an occurrence is rare. To quantify by how much a visual baseline will underestimate the extent of residual cure, in the case of a "half buried" T_G, the missed portion of the residual cure exotherm would amount to 0.025 W / g multiplied by the time needed to complete residual cure, at 10 °C / min. in the example above, which is typical, this time is about 900 s. Thus, the missed area represents about 22.5 J / g, or slightly more than 0.03 in terms of residual conversion missed. The use of an unadjusted re-scanned baseline, however, also underestimates the residual cure because the baseline is correct only above the T_G at full cure. The magnitude of this error, as can be seen from Figure S2, is roughly half of the step height (0.05 W / g) times the difference in time between scanning at the "as cured" and "fully cured" T_G values, that is, about 50 °C, corresponding to 300 s, altogether about 7.5 J / g, or slightly more than 0.01 in terms of conversion.   The re-scanned baseline will therefore be most accurate when the conversion is near one, and least accurate when there is a substantial shift in T_G.

As mentioned previously, the re-scanned baseline is typically used as a starting point and further adjusted. In a method we described previously,[S4] the re-scanned baseline is offset by an amount given by the minimum difference (most negative, not absolute) for the re-scanned minus the original scanned heat flow value. This type of offset is illustrated by the thick dotted line in Figure S3, which displays the same experimental data shown in Figure S2. The method for generating this type of baseline has the advantages of simplicity and objectivity, but when the original data contains a shifted T_G value that is not totally masked, it generates an offset that is

too large. A more appropriate offset is shown by the thin dotted line in Figure S3, based on alignment of the signals at 50 °C below the end-point of the T_G in the first heating. This offset, however, involves a somewhat arbitrary choice of the matching temperature. As described later, the need for this arbitrary choice can be used to estimate uncertainties associated with the procedure. It should be pointed out that the original curve is not expected to cross over the offset baseline even at the end of cure (that is, there is no endothermic event at the conclusion of cure). This fact may also be used to constrain the offset value in cases where a low-temperature value is unavailable.
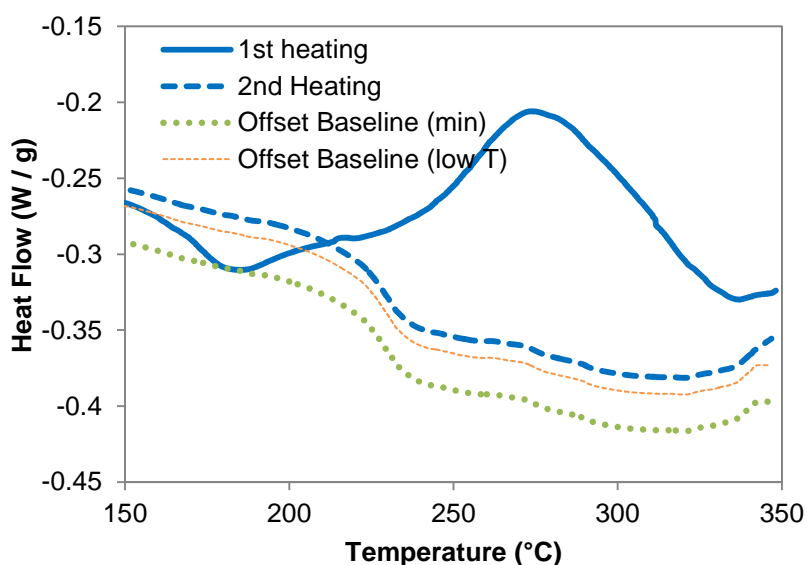
Figure S3. Baselines generated by offsetting the re-scanned signal (same experimental data as in Figure S2). The thick dotted line represents the use of the signal minimum with respect to the re-scan (objective but inaccurate), whereas the thin dotted line represents matching of the signal to the re-scan at an arbitrarily chosen temperature below T_G (more accurate but less objective).

The "visual" baselines shown in Figure S2 also differ from the re-scanned baselines shown in Figure S3 in that the "visual" baselines incorporate the implicit closure of the residual cure exotherm at point "C". For polycyanurate networks with T_G values above 350 °C, an

"open," or incomplete, exotherm often results from vitrification of samples during cure,[S4] however, the T_G values for all the polycyanurates in this study is generally below 300 °C, and often not more than about 225 °C. As a result, vitrification is not responsible for the "open" ends of the residual cure exotherms observed. The most likely explanation appears to be side reactions, herein termed "degradation," that generate heat but do not constitute cyclotrimerization of cyanate esters to cyanurates. If one compares the effects of different catalysts on the DSC behavior seen above 300 °C (see Figures S31-S36 below), one finds that systems with no added catalyst show very little upward curvature and nearly parallel lines for the first and second scans. In these cases a simple offset is sufficient to create a closed exotherm. For systems catalyzed with Cu-Acac, however, there tends to be an upturn in the signal after about 325 °C, especially for samples cured at higher temperatures or for longer times. For samples catalyzed with DBTDL, there is a very significant upturn. The T_G values after heating to 350 °C are lower for systems that experience longer cure times in seven out of the eight cases reported herein, suggesting that side reactions do take place; T_G values are also significantly lower after heating to 350 °C for the DBTDL-catalyzed systems, which are less thermally stable according to TGA data (see Section S6).

Because "degradation" is associated with an unexpected upturn in the signals, a simple way to account for it is to truncate the baseline using a line connecting the minimum in the re-scanned baseline and the point with minimum heat evolution (using a preliminary assumption that the re-scanned baseline is correct). An alternative, and more conservative approach, is to use a line connecting the turning point (that is, the point where the second derivative is maximum) on the re-scanned baseline with the end-point of the first scan. This alternative

procedure effectively closes the exotherm at 350 °C, whereas the former closes the exotherm at its uncorrected minimum. Figure S4 illustrates the use of these two alternative procedures.
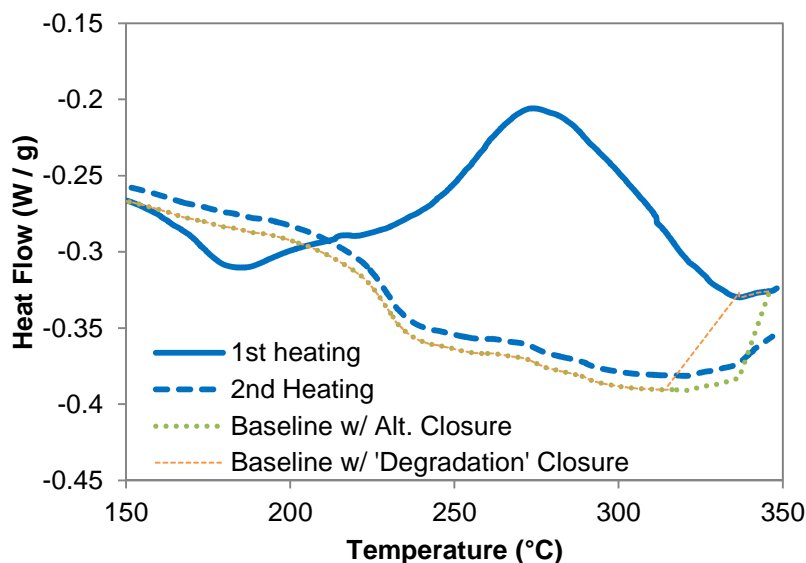
Figure S4. Baselines from Figure S3 with forced curve closure at high temperatures. The most likely reason for the incomplete closure is believed to be other chemical reactions, herein grouped under the term "degradation" that does not produce cyanurates.

The final feature that can improve the accuracy of baselines is a means of accounting for the shift in T_G during cure. To incorporate this function, a linear fit of the offset re-scanned baseline was measured above the T_G. The line described by this fit was then utilized in place of the signal from the 2nd scan for all temperatures below the region where the fit was performed and above the original scan T_G end-point, which is assumed to correspond to the local turning point (maximum second derivative) in the original scan.   Figure S5 shows the offset baselines with and without a T_G shift as computed by the methods described above.   Such a baseline implies that a significant portion of the exotherm is "hidden" by the interplay of unseen changes in heat capacity and side reactions. Superficially, such a conclusion seems difficult to accept.

However, in order for this implication to be false, many known facts about the physical properties of cyanate ester resins (such as the dependence of heat capacity on conversion and the presence of detectable side reactions) would also need to be false.
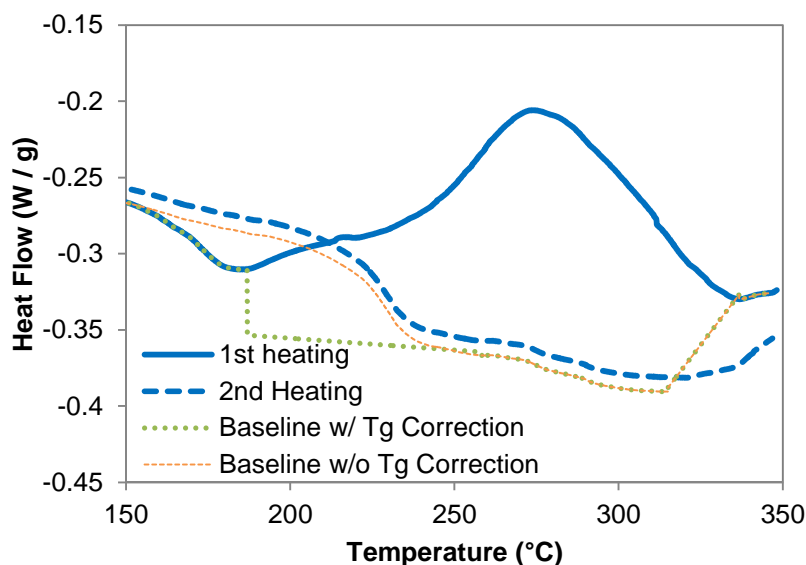
Figure S5. Comparison of baselines with (dotted line) and without (dashed line) a T_G shift, for the same data shown in Figures S2-S4.

Having established a method for estimation of the baseline, an important follow-on consideration is the uncertainty in the estimate. Although a formal estimate of uncertainty is very difficult given the complex nature of the likely distributions of the variables, a reasonable estimate may be derived from a sensitivity analysis. As mentioned previously, there are typically multiple ways to estimate the parameters needed to establish the baseline. By comparison of the effect of alternate choices on the area of the residual exotherm, one can obtain an estimate of sensitivity, and these sensitivities may be combined assuming that the various factors are uncorrelated to arrive at a final uncertainty estimate.

Figure S6 illustrates the three factors examined in the sensitivity analysis and their effects on the area of the residual cure exotherm. Recall that in estimating the offset needed for the re-

scanned baseline, an arbitrary choice of "low temperature" was used to make the estimate (50 °C below the original scan T_G end-point). To estimate the sensitivity to this choice, the baseline is recomputed using an offset based on matching the curves at 25 °C below the T_G end-point, which is close to the minimum difference that can be considered "below T_G." The area of the exotherm is then re-computed and the difference in areas is used as the uncertainty due to this factor. As Figure S5 illustrates, the difference in area will be equal to the offset difference (in W/g) multiplied by the time difference corresponding to the temperature difference between the original T_G end-point and the start of degradation. In most cases, the offset difference is about 0.005 W/g, resulting in a sensitivity of around 5 J/g.
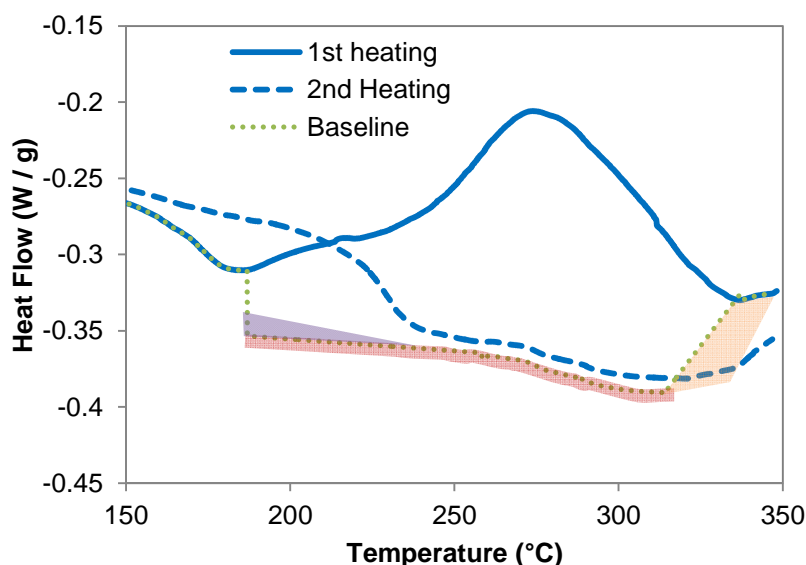
Figure S6. Graphical illustration of sources in uncertainty for the baseline, including slope of the extrapolated baseline (purple), offset value (red), and exotherm closure (orange), for the same data shown in Figures S2-S5. The area of the shaded regions corresponds to the uncertainty (in J/g) in the estimated area of the exotherm due to each factor.

A second factor leading to uncertainty is the slope of the baseline extrapolated from the T_G end-point in the re-scan to the T_G end-point in the original scan. To estimate this error, a measure of the likely difference in the baseline heat flow value at the T_G end-point in the original

scan is needed. Although one could attempt to use error estimates relating to the regression used to generate the line, this approach will ignore systematic sources of error, which are likely to be significant contributors. A more elegant approach is to consider that the change in heat capacity at T_G is typically 0.3 J / g °C (0.05 W/g at 10 °C / min), therefore the difference between the size of the "step" at T_G and 0.05 W / g indicates the uncertainty. Because a partial step change in heat capacity may be visible at T_G, one cannot simply use the size of the discontinuity in the baseline as the step size. However, having measured heat flow values at 50 °C and 25 °C below the T_G end-point in order to compute the offsets, one may extrapolate these values to the T_G end-point to determine a value for the "top" of the step, then decrease the value by 0.05 W / g to serve as the comparative point for the sensitivity analysis. The effect of this difference on the area of the exotherm is illustrated in Figure S6. Because it scales only with the change in T_G end-points between scans, it tends to be smaller than the other factors, typically accounting for just 1-2 J / g.

The last factor considered in the sensitivity analysis is the impact of "degradation". As mentioned in the discussion of Figure S4, there are two alternate ways, one more conservative than the other, to estimate the baseline in the region affected by "degradation". A comparison between these two cases provides a natural basis for the determination of sensitivity, using the difference in the computed residual cure exotherm areas. As shown in Figure S6, the area tends to scale as the heat flow difference needed to "close" the curve, typically 0.05 W / g at 350 °C, and the temperature range affected, typically only about 25 °C, which implies an error of about 7.5 J / g at 10 °C / min. Thus, in most cases, uncertainty about the "degradation" contributes the most to the uncertainty in the area of the curve.

One limitation of the above method for determination of baselines is for systems such as uncured resin that are never in the glassy state prior to cure. In such cases, either the turning

point corresponding to the onset of cure or a low-temperature cut-off point may be used to determine the start of cure. The baseline above T_G can then be extrapolated back to this point. In such cases, an offset value cannot be determined with precision, therefore it is assumed to be zero. In such cases, a correction for thermal degradation may then be applied as normal. In order to estimate the error, the maximum possible offset may be used as an alternate case for sensitivity analysis, with the maximum (most upward) possible value determined by the lesser of the heat flows at the end point or the cure onset / low-temperature cutoff. This procedure allows the maximum offset while adhering to the "no endothermic events" assumption. The sensitivity to uncertainty in the slope cannot be performed and so is assumed to be zero, while the sensitivity analysis for "degradation" may be carried out as described above. This alternate procedure was utilized for the uncured resin systems studied, with a low-temperature cutoff of 100 °C utilized for uncured **1** (LECy) and **2** (BADCy) because no turning point was observed in these samples.

In order to validate the newly developed method described above, we computed two sets of diBenedetto equation parameters for cured **1-4** using the 16 samples from the cure condition experiment that were heated to 350 °C. For one set, conversions were estimated by DSC using residual heats of cure, with manually selected baselines drawn between the most prominent turning points at the beginning and end of each exotherm (like the "middle" baseline shown in Figure S2) for each of the four partly cured samples as well as the uncured monomer. For the second set, the conversions derived using the newly developed method were substituted. The diBenedetto equation[S1] was then fitted to the four conversion / T_G points for each monomer, using the Solver algorithm in Microsoft Excel, with the uncured T_G set to -50 °C for **1** (LECy),[S5] -38 °C for **2** (BADCy),[S5] and -45 °C (the average of BADCy and LECy to the nearest 5 °C) for

3 and **4** and the other two parameters adjusted to minimize the sum of squared residuals between predicted and experimentally observed T_G values.

Tables S3 and S4 summarize the results of the validation experiments. From Table S3, it is clear that the manual baseline method results in consistently higher conversion estimates. This result is due to the partially or completely "buried" T_G signal in the DSC measurement, which in effect "hides" a portion of the exotherm underneath the apparent manually-selected baseline. Note that, when an error of 0.05 is assumed for conversion measurements, the effect would be insignificant for most cases, and, even in the worst case the difference is about 0.07. Thus, as long as an error of 0.05 is taken into account, along with the potential for much of such an error to be systematic, then the use of manually-selected baselines would be sufficient. For higher precision measurements, though, the manually-selected baselines provide significantly different results. These differences have cascading effects, for instance, when determining the parameters of the diBenedetto equation. Systematic differences in conversion result in systematic differences in estimated equation parameters, with the value of the parameter λ altered quite significantly by the method of baseline selection.

In order to assess which method is more likely to be accurate, various aspects of the predicted diBenedetto parameters may be examined. For both methods, the average rms deviation in predicted T_G values is about 4 °C, with manual baselines providing smaller errors in two cases and the new method giving smaller errors in the other two. When the predicted value of the T_G at full cure is examined, however, it is clear that the new method is more accurate. For BADCy and LECy, the new method matches the average post-cured T_G seen in DSC experiments quite well. The post-cured T_G, however, can vary widely (from 265 °C to 285 °C for LECy, for instance), and in cases such as network **3** where one sample experienced significant side

reactions, it can be quite a bit lower than the maximum T_G observed by DSC for the network. In fact, for networks **3** and **4**, the post-cured T_G values are lower than some of the "as-cured" T_G values when "as cured" conversions are near 100%. This result indicates that some degradation of the network does occur on heating, introducing errors into the post-cured values. It should also be noted that the maximum observed network T_G values match post-cured values reported for BADCy and LECy from earlier studies[S5,S6] to within 10 °C, whereas the average values are lower. Thus, comparison with the maximum observed T_G seems most appropriate for the estimate of $T_{G\infty}$, and in that respect, the new method showed an average under-prediction of just 4 °C, whereas the manual method resulted in an average under-prediction of 12 °C. There are two possibilities, either the manual method is more accurate and the new method underestimates conversion, or the manual method overestimates conversion and the new method is more accurate. In the former case, one would expect the new method to result in an over-prediction of $T_{G\infty}$ when using the diBenedetto equation, whereas in the latter case, one would expect the manual method to result in under-prediction of $T_{G\infty}$ when using the diBenedetto equation. The latter case is a significantly better description of the observed data; therefore the new method appears to provide a more accurate estimate of conversion.

A final point worth noting, the new method has been developed for di(cyanate ester) systems with glass transition temperatures in the range of 150 – 250 °C. Although the method may be valid for other thermosetting resin systems with similar T_G values, it has not been tested in such systems. For thermosetting resins with a significantly higher T_G, in which complete cure may not be possible without introducing significant degradation, or for thermosetting resins without a well-defined network structure that gives rise to a well-defined T_G value, the method

may not be superior to manual estimation of baselines. For other types of reactions studied by DSC that do not conceal a well-defined T_G, this method is likely not applicable.

Table S3: Validation of DSC Baseline Generation Method: Comparison of Conversions

Monomer	Cure Temp (°C)	Cure Time (min)	Conversion (manual baseline)	Conversion (new method)	"As-Cured" T_G (°C)*
1 (LECy)	210	30	0.943	0.901 ± 0.009	218
1 (LECy)	210	1440	0.977	0.945 ± 0.007	249
1 (LECy)	250	5	0.959	0.916 ± 0.013	229
1 (LECy)	250	210	0.989	0.971 ± 0.005	253
2 (BADCy)	210	30	0.901	0.846 ± 0.014	204
2 (BADCy)	210	1440	0.961	0.912 ± 0.008	248
2 (BADCy)	250	5	0.950	0.892 ± 0.013	229
2 (BADCy)	250	210	0.984	0.955 ± 0.007	258
3	170	210	0.951	0.913 ± 0.006	175
3	170	1440	0.919	0.862 ± 0.012	170
3	210	30	0.963	0.922 ± 0.009	187
3	210	1440	0.995	0.992 ± 0.003	226
4	170	210	0.856	0.783 ± 0.014	142
4	170	1440	0.918	0.869 ± 0.010	174
4	210	30	0.920	0.855 ± 0.012	170
4	210	1440	0.997	0.984 ± 0.005	235

*average of DSC transition mid-point measurements for all samples

Table S4: Validation of DSC Baseline Generation Method: diBenedetto Parameters

Monomer	Baseline Method	T_{G0} (°C) (fixed)	$T_{G\infty}$ (°C) (fitted)	$T_{G,full-cure}$* (°C) by DSC	λ (fitted)	rms Prediction Error (°C)
1 (LECy)	Manual	-50	263	274 / 285	0.36	1.0
2 (BADCy)	Manual	-38	271	288 / 296	0.40	4.0
3	Manual	-45	228	208 / 229	0.27	8.2
4	Manual	-45	236	229 / 235	0.32	3.4
1 (LECy)	New	-50	271	274 / 285	0.59	2.1
2 (BADCy)	New	-38	287	288 / 296	0.56	4.9
3	New	-45	230	208 / 229	0.49	6.8
4	New	-45	243	229 / 235	0.50	1.5

* average of all four samples, after heating to 350 °C at 10 °C / min. / Maximum of any "as-cured" or "post-cured" T_G observed among the four samples

S3. Raw DSC Data

S3.1 Cure Condition Experiments and Associated DSC Scan Temperature Range Experiments
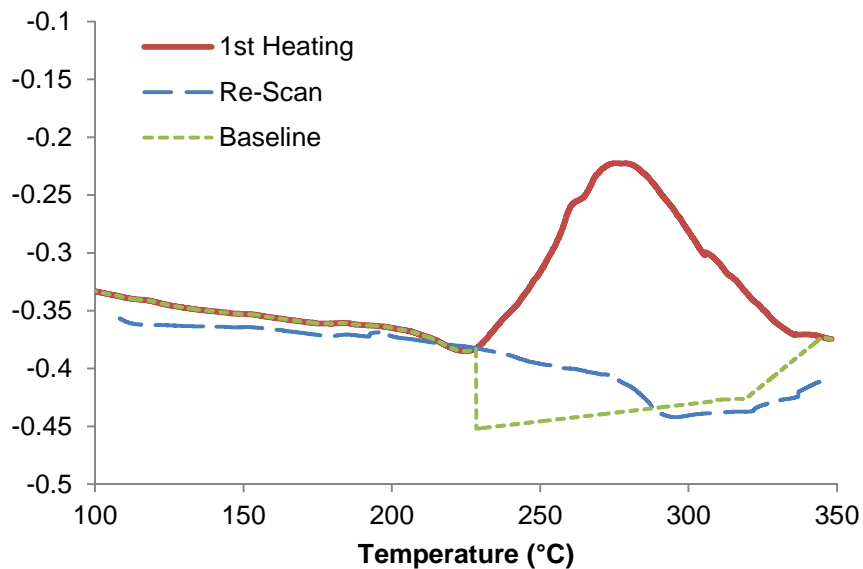
Figure S7. DSC scan of **1** (LECy) after curing at 210 °C for 30 minutes.
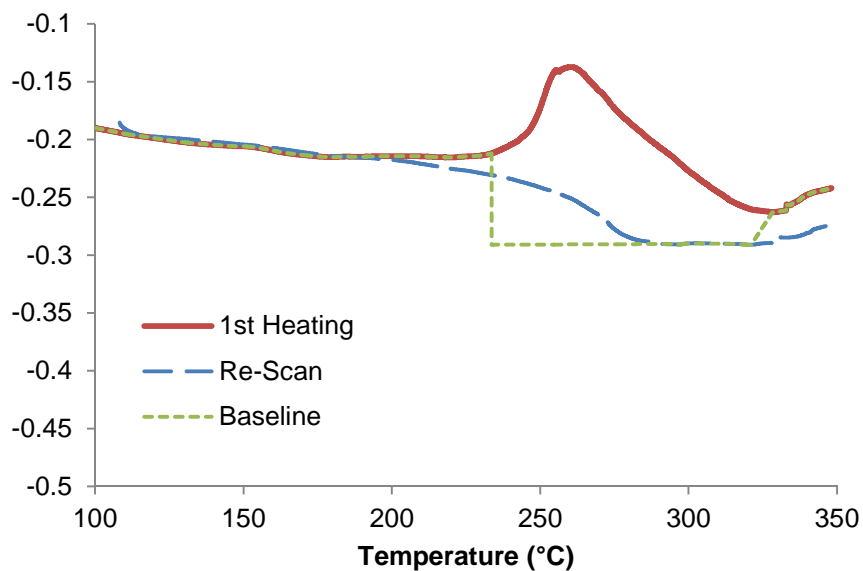
Figure S8. DSC scan of **1** (LECy) after curing at 210 °C for 1440 minutes.
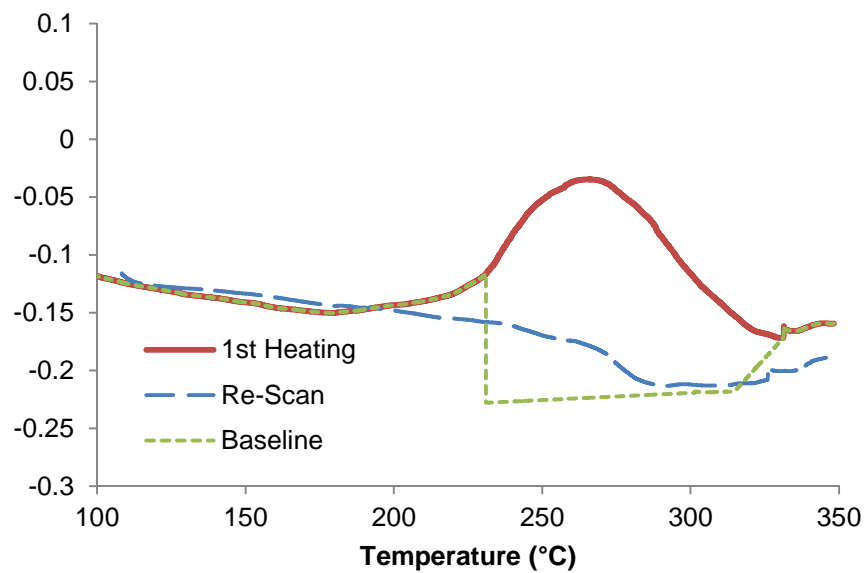
Figure S9. DSC scan of **1** (LECy) after curing at 250 °C for 5 minutes.
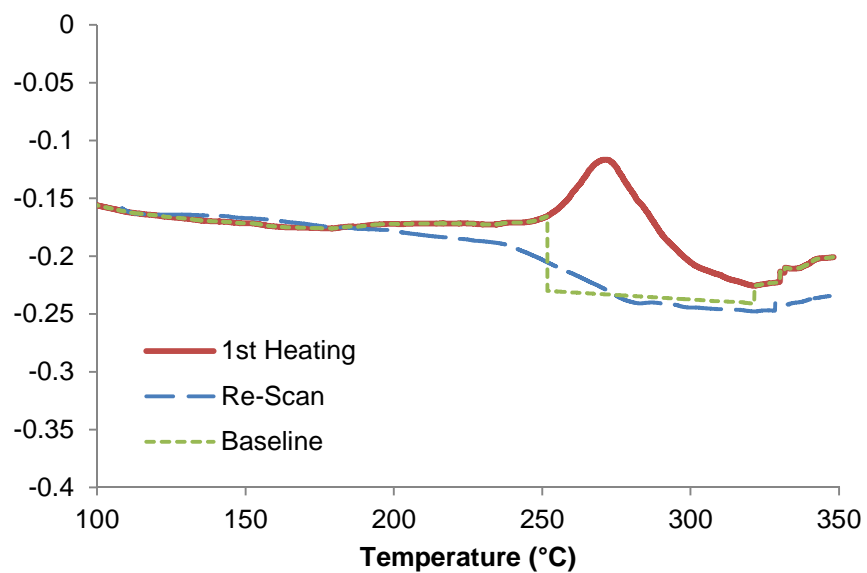
Figure S10. DSC scan of **1** (LECy) after curing at 250 °C for 210 minutes.
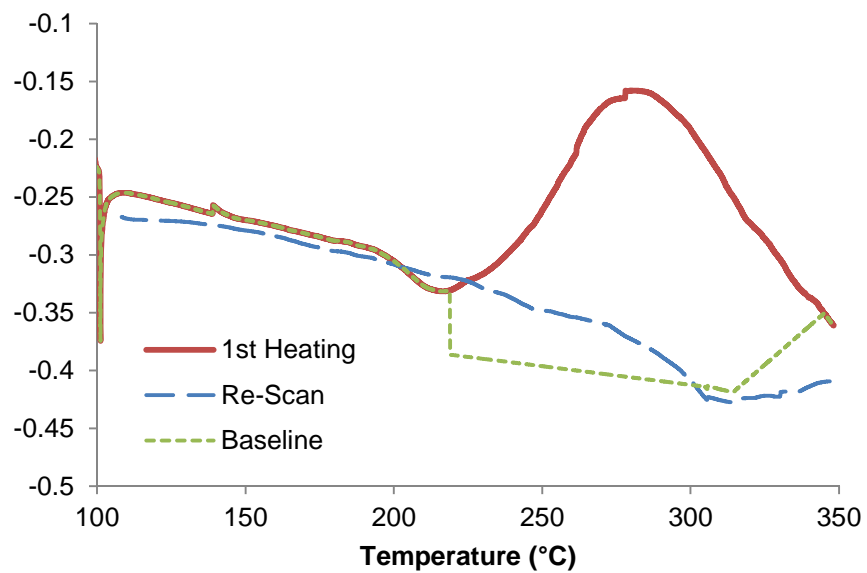
Figure S11. DSC scan of **2** (BADCy) after curing at 210 °C for 30 minutes.
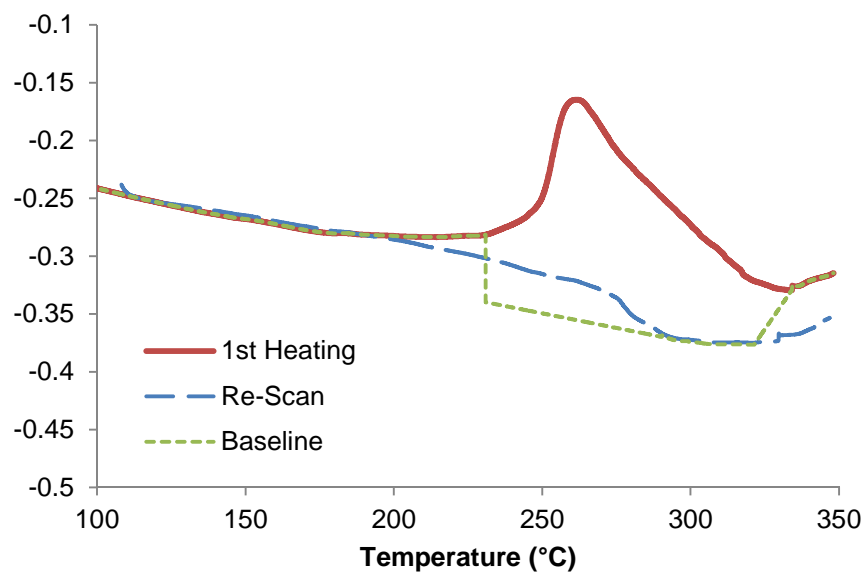
Figure S12. DSC scan of **2** (BADCy) after curing at 210 °C for 1440 minutes.
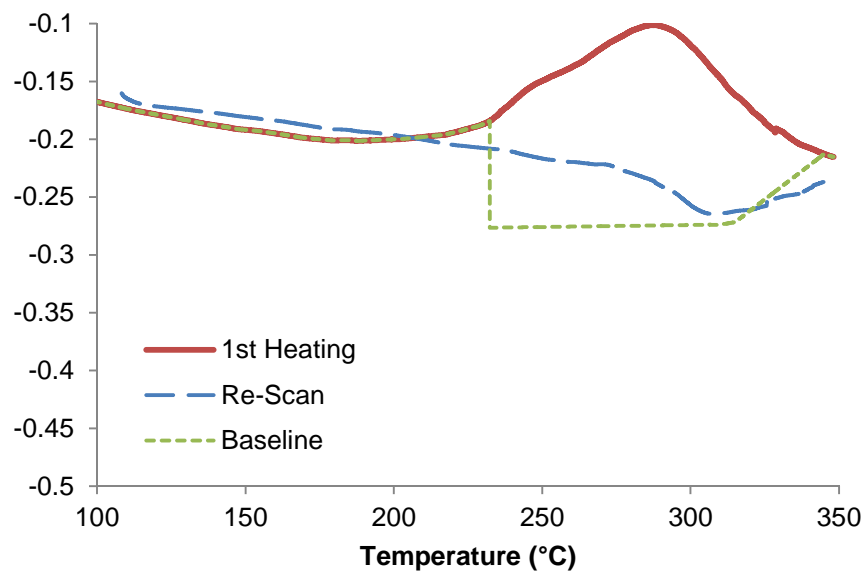
Figure S13. DSC scan of **2** (BADCy) after curing at 250 °C for 5 minutes.
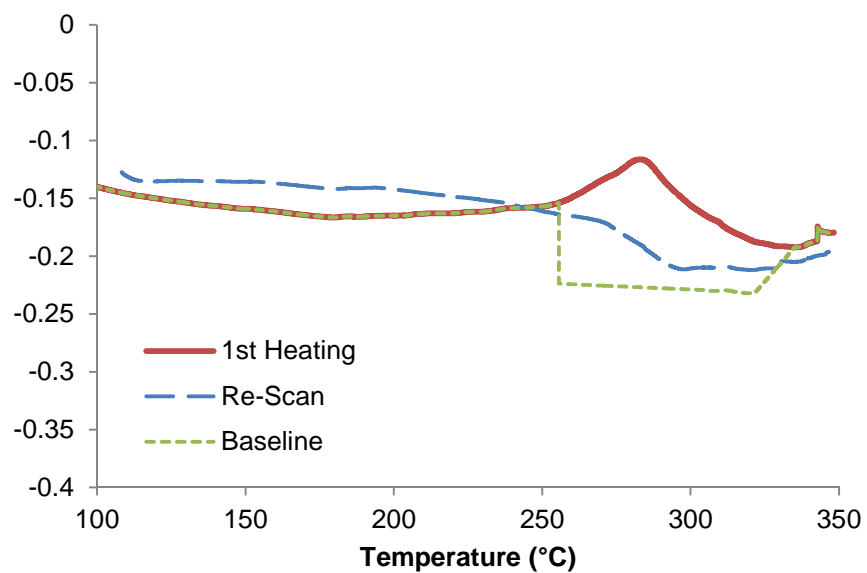
Figure S14. DSC scan of **2** (BADCy) after curing at 250 °C for 210 minutes.

22
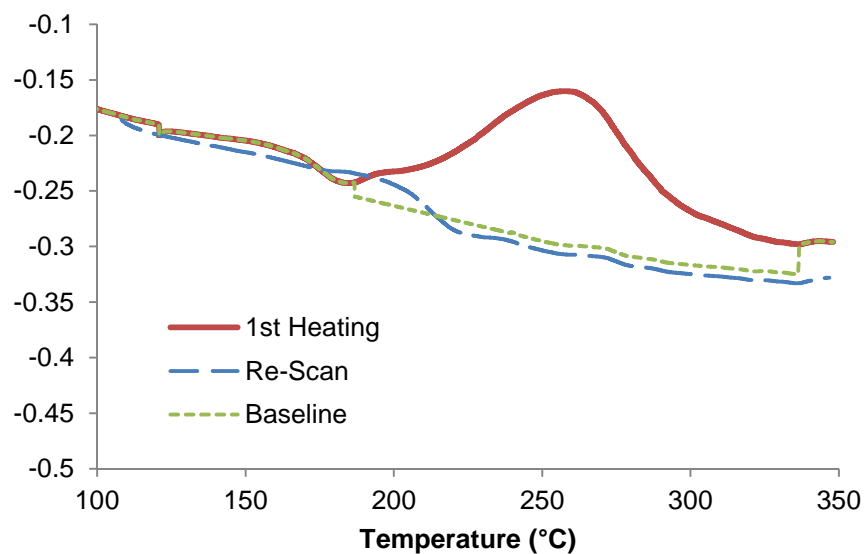
Figure S15. DSC scan of **3** after curing at 170 °C for 210 minutes.
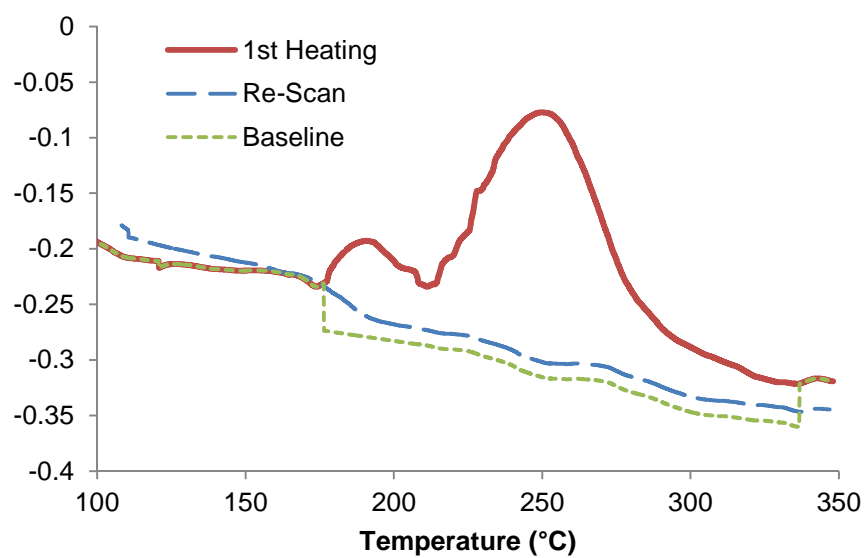
Figure S16. DSC scan of **3** after curing at 170 °C for 1440 minutes.
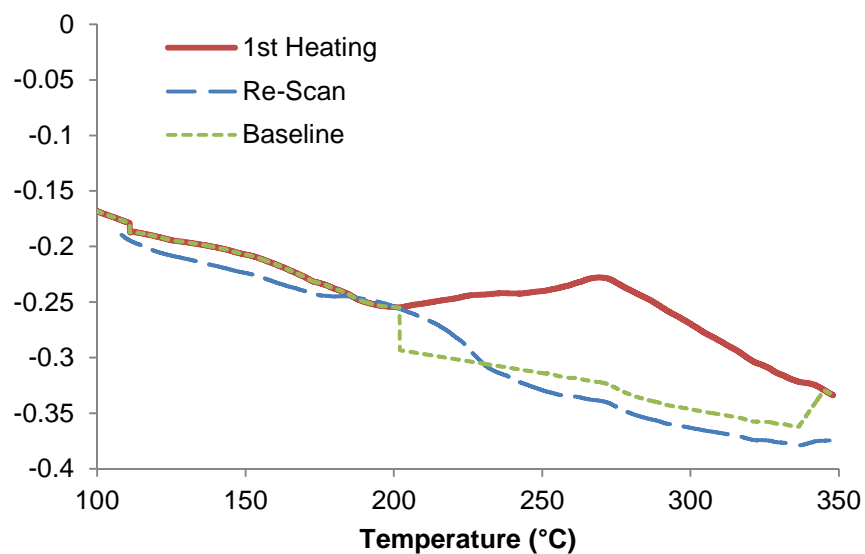
Figure S17. DSC scan of **3** after curing at 210 °C for 30 minutes.
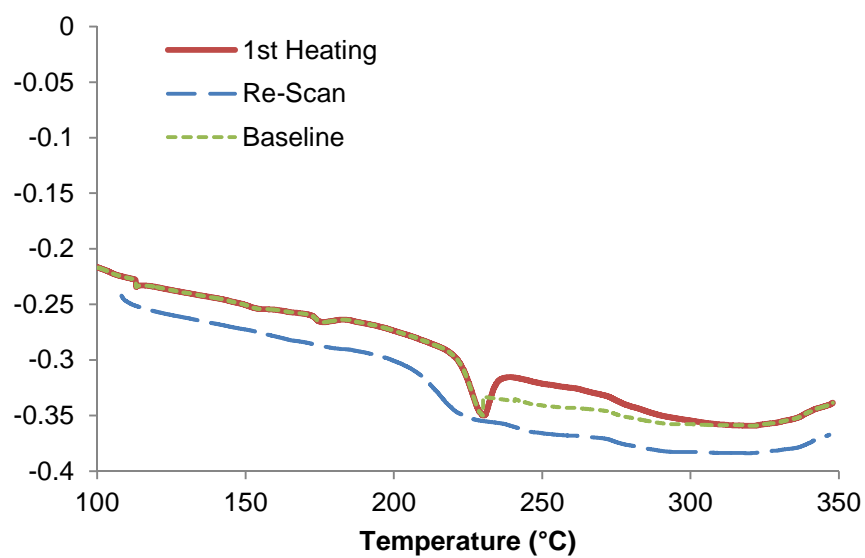
Figure S18. DSC scan of **3** after curing at 210 °C for 1440 minutes.
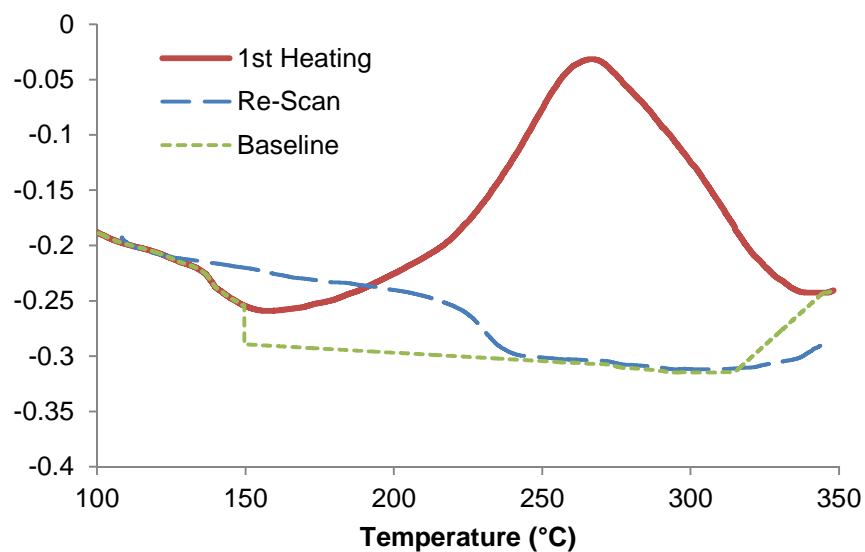
Figure S19. DSC scan of **4** after curing at 170 °C for 210 minutes.
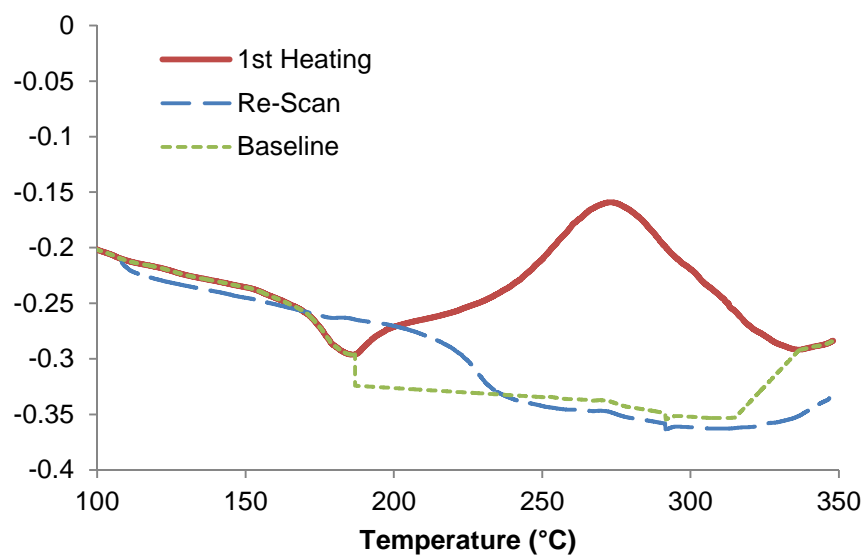
Figure S20. DSC scan of **4** after curing at 170 °C for 1440 minutes.
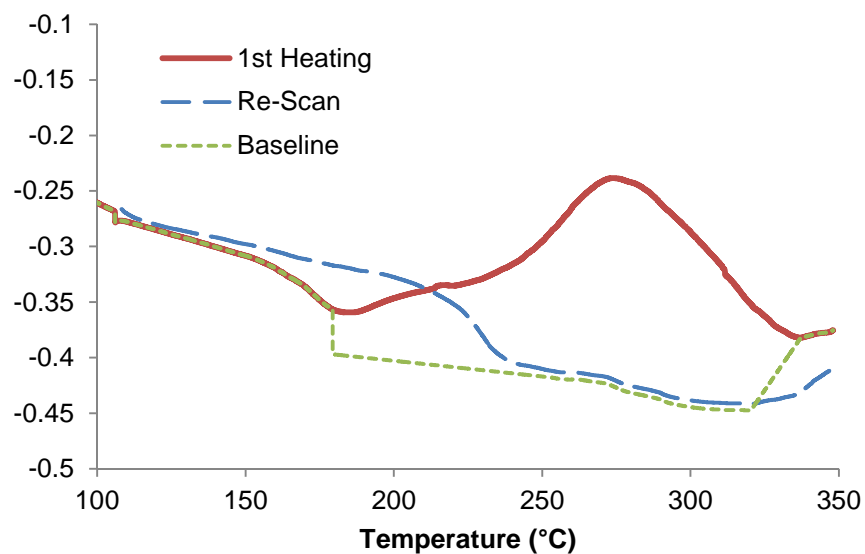
Figure S21. DSC scan of **4** after curing at 210 °C for 30 minutes.
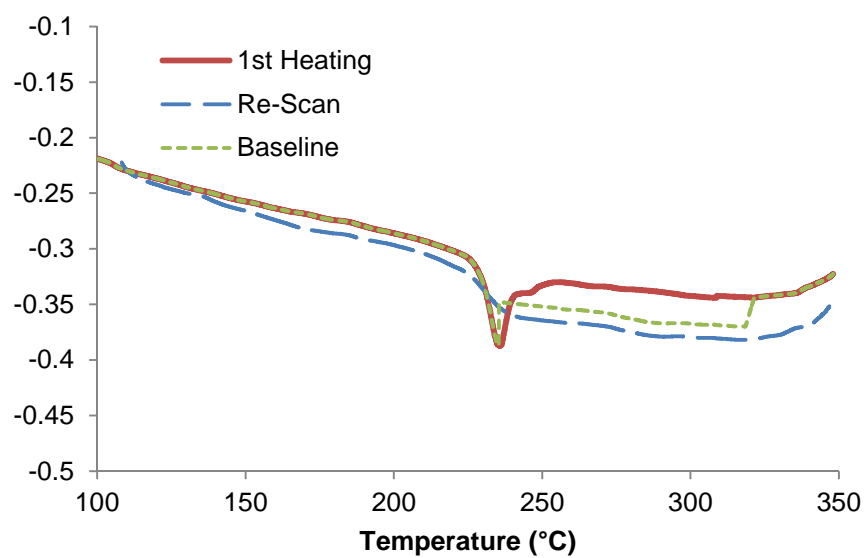
Figure S22. DSC scan of **4** after curing at 210 °C for 1440 minutes.
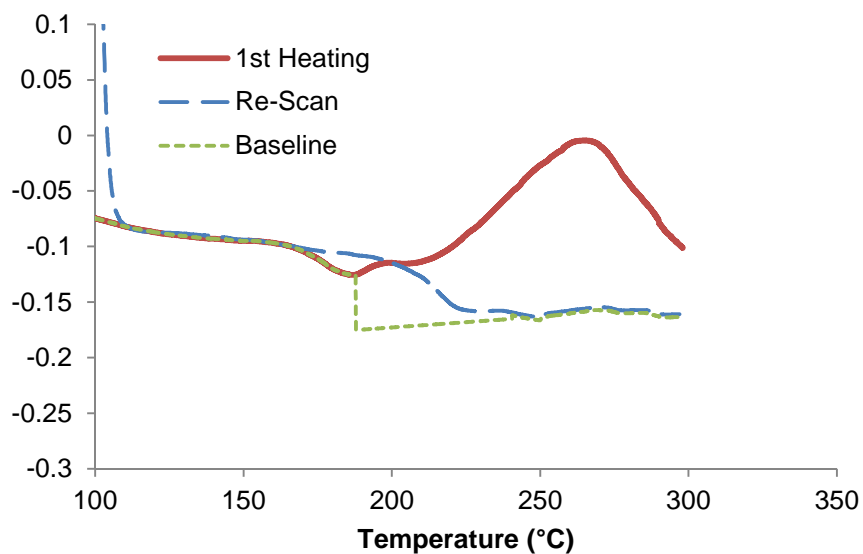
Figure S23. DSC scan of **3** after curing at 170 °C for 210 minutes (maximum scan temperature 300 °C).
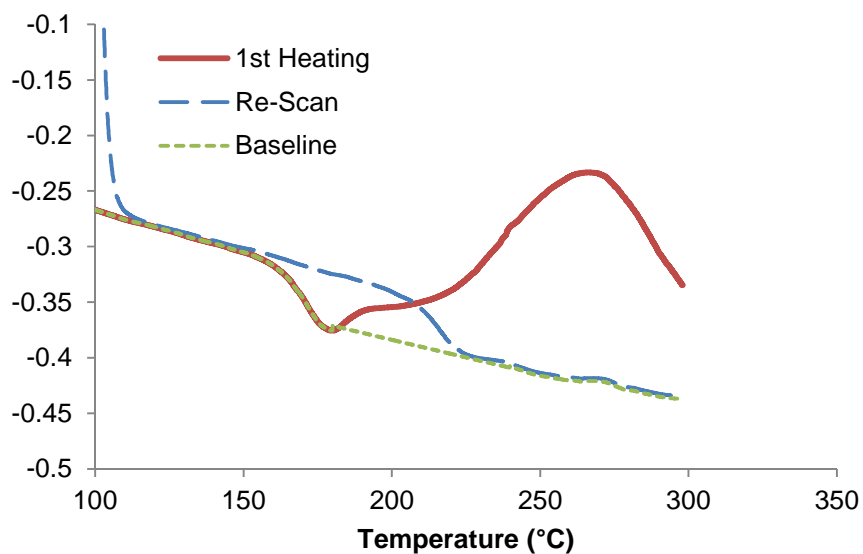
Figure S24. DSC scan of **3** after curing at 170 °C for 1440 minutes (maximum scan temperature 300 °C).
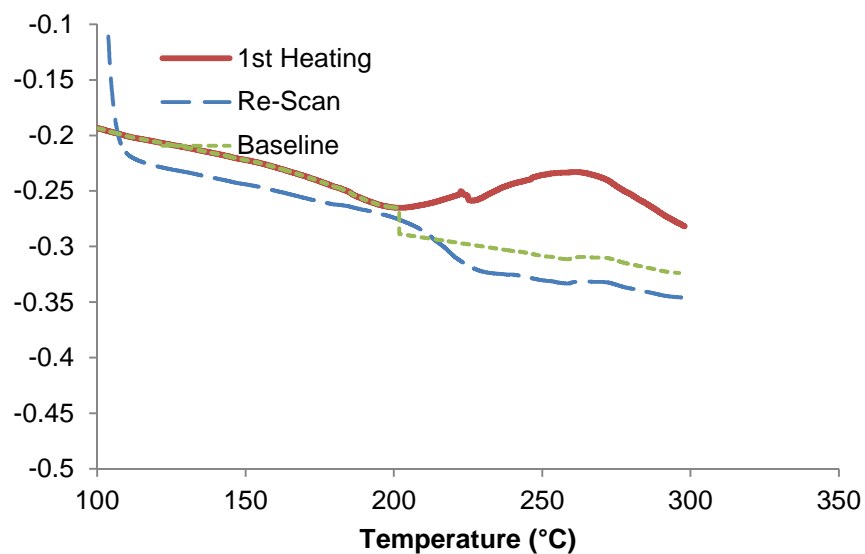
Figure S25. DSC scan of **3** after curing at 210 °C for 30 minutes (maximum scan temperature 300 °C).
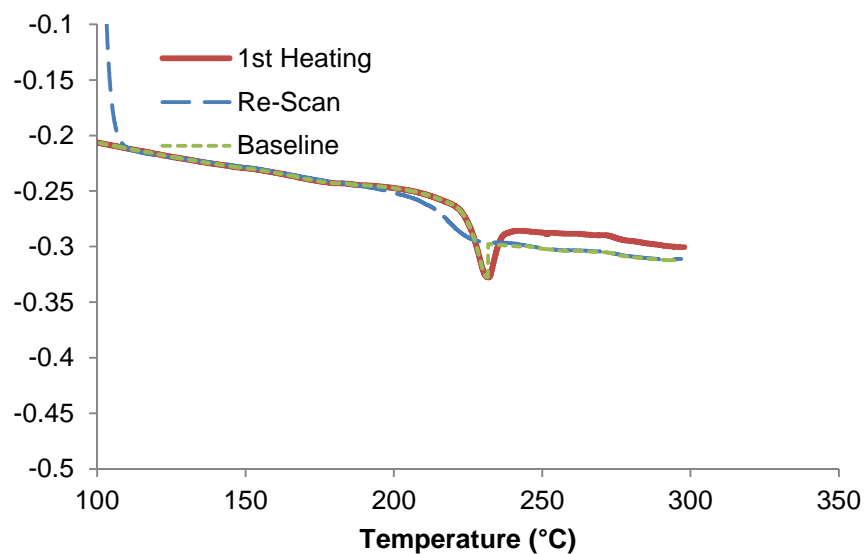
Figure S26. DSC scan of **3** after curing at 210 °C for 1440 minutes (maximum scan temperature 300 °C).
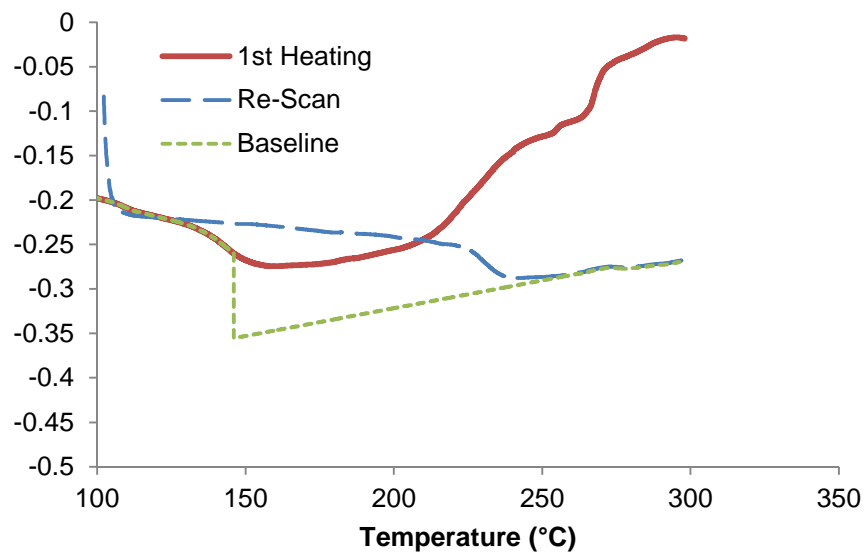
Figure S27. DSC scan of **4** after curing at 170 °C for 210 minutes (maximum scan temperature 300 °C).
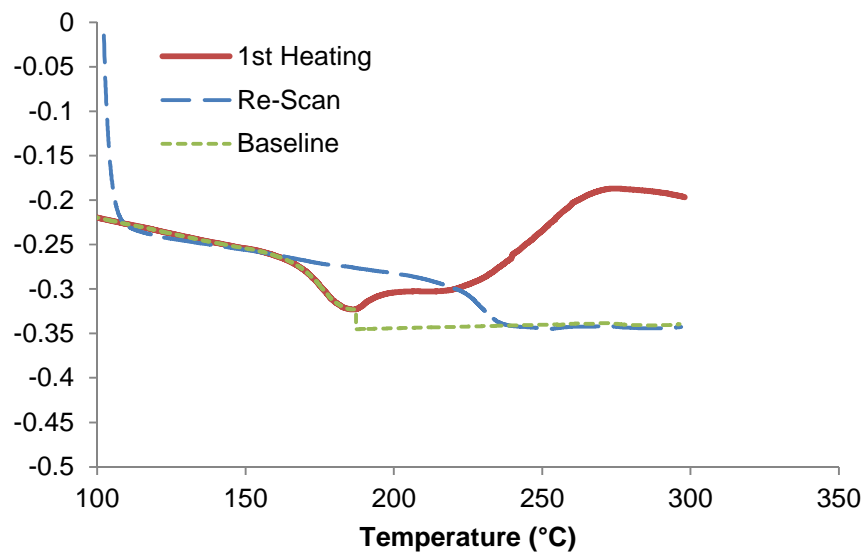
Figure S28. DSC scan of **4** after curing at 170 °C for 1440 minutes (maximum scan temperature 300 °C).
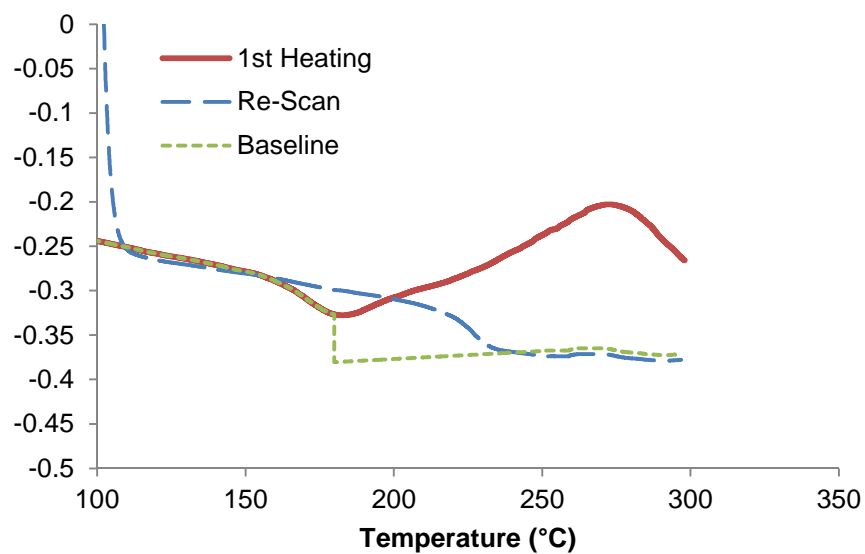
Figure S29. DSC scan of **4** after curing at 210 °C for 30 minutes (maximum scan temperature 300 °C).
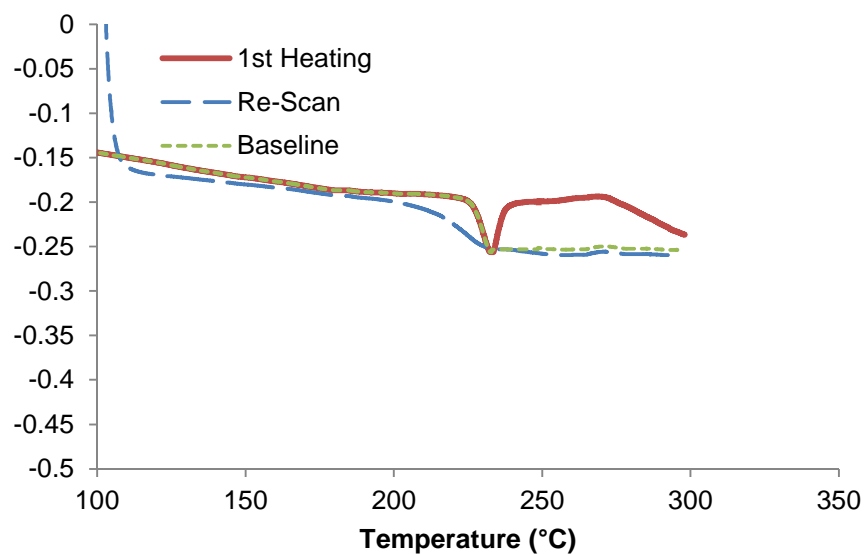
Figure S30. DSC scan of **4** after curing at 210 °C for 1440 minutes (maximum scan temperature 300 °C).

Table S5. DSC Conversion Analysis of Cured Networks (Cu-Acac Catalyzed, Cure Condition Experiments)

Monomer / Max Scan Temp (°C)	Max Cure Temp (°C) / time (min)	T_G (°C)	ΔH_r (J/g)[a]	ΔH_r (kJ/eq.)[a]	Conversion (α)	$T_{G\text{-}fc}$ (°C)[b]
1 / 350	210 / 30	216-221	88 ± 6	11.7±0.8	0.901 ± 0.009	281 – 289
1 / 350	210 / 1440	245	50 ± 5	6.6 ± 0.7	0.945 ± 0.007	266 – 273
1 / 350	250 / 5	228	75 ± 10	10 ± 1	0.916 ± 0.013	272 - 282
1 / 350	250 / 210	253	26 ± 4	3.4 ± 0.5	0.971 ± 0.005	250 - 280
2 / 350	210 / 30	199-210	113 ± 8	16 ± 1	0.846 ± 0.014	288 - 305
2 / 350	210 / 1440	248	64 ± 5	9.0 ± 0.6	0.912 ± 0.008	273 - 285
2 / 350	250 / 5	229	79 ± 8	11 ± 1	0.892 ± 0.013	285 - 304
2 / 350	250 / 210	258	33 ± 5	4.6 ± 0.7	0.955 ± 0.007	276 - 292
3 / 350	170 / 210	168-182	63 ± 3	9.2 ± 0.4	0.913 ± 0.006	203 - 220
3 / 350	170 / 1440	169-173	100 ± 7	15 ± 1	0.862 ± 0.012	177 - 190
3 / 350	210 / 30	182-189	57 ± 6	8.2 ± 0.9	0.922 ± 0.009	219 - 230
3 / 350	210 / 1440	229	5 ± 2	0.8 ± 0.3	0.992 ± 0.003	207 - 222
4 / 350	170 / 210	136 – 146	151 ± 7	23 ± 1	0.783 ± 0.014	223 – 237
4 / 350	170 / 1440	170 – 180	92 ± 6	14 ± 1	0.869 ± 0.010	221 – 234
4 / 350	210 / 30	163 – 179	101 ± 7	15 ± 1	0.855 ± 0.012	217 – 236
4 / 350	210 / 1440	235	11 ± 3	1.7 ± 0.6	0.984 ± 0.005	226 – 238
3 / 300*	170 / 210	168-181	65 ± 3	9.5 ± 0.4	0.910 ± 0.006	205 – 221
3 / 300*	170 / 1440	163-175	73 ± 3	10.7±0.4	0.899 ± 0.006	211 – 221
3 / 300*	210 / 30	181-192	32 ± 3	4.7 ± 0.4	0.956 ± 0.005	209 - 226
3 / 300*	210 / 1440	232	5 ± 3	0.8 ± 0.4	0.993 ± 0.004	210 - 227
4 / 300*	170 / 210	136-152	120±18	18 ± 3	0.828 ± 0.027	225 – 237
4 / 300*	170 / 1440	168-180	61 ± 4	9.4 ± 0.6	0.912 ± 0.007	224 – 237
4 / 300*	210 / 30	161-178	78 ± 6	11.9±0.9	0.888 ± 0.010	220 - 232
4 / 300*	210 / 1440	233	18 ± 3	2.7 ± 0.5	0.975 ± 0.005	214 - 230

* Incomplete cure was observed when using a maximum scan temperature of 300 °C, therefore conversions obtained are not reliable.
a. Residual heat of cure.
b. Glass transition temperature after heating to the maximum scan temperature at 10 °C/min.

S3.2 Catalyst Choice Experiments with Associated DSC Scan Temperature Range Experiments
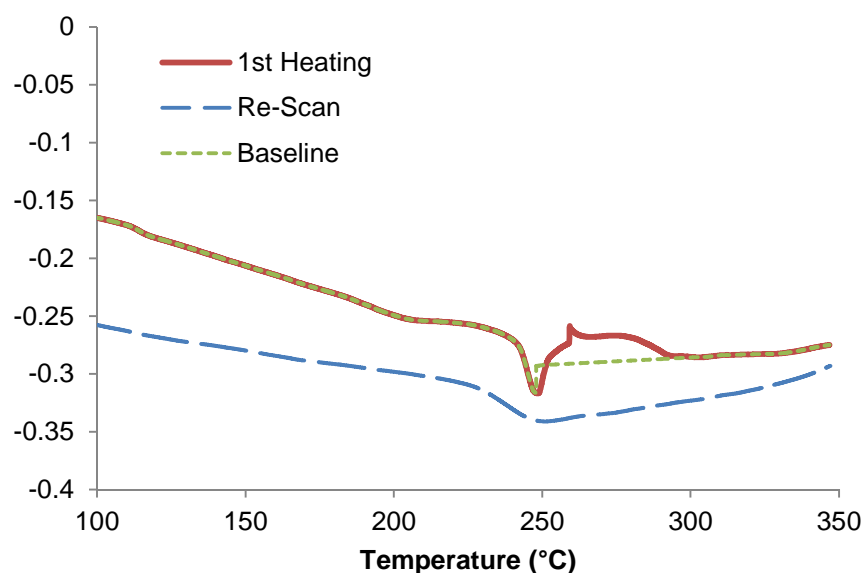
Figure S31. DSC scan of **3** (no catalyst added) after curing for 24 hours at 210 °C.
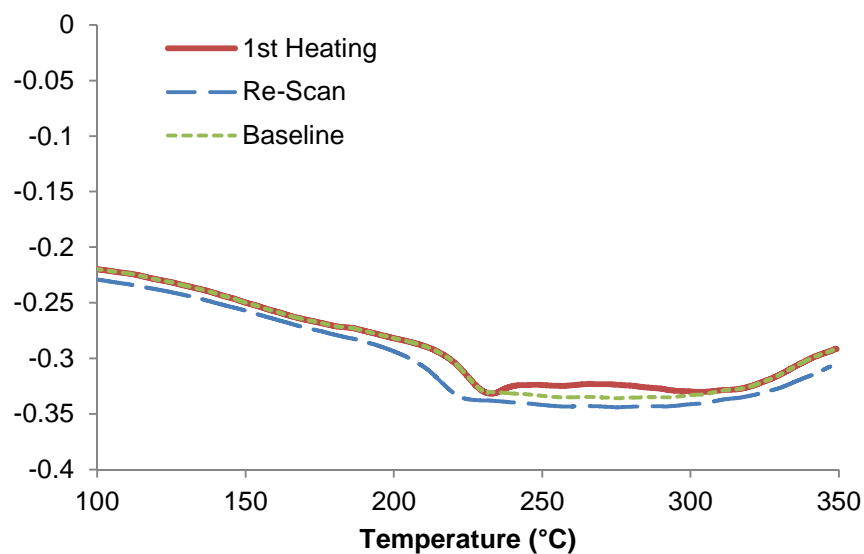
Figure S32. DSC scan of **3** catalyzed with Cu-Acac/nonylphenol after curing for 24 hours at 210 °C.
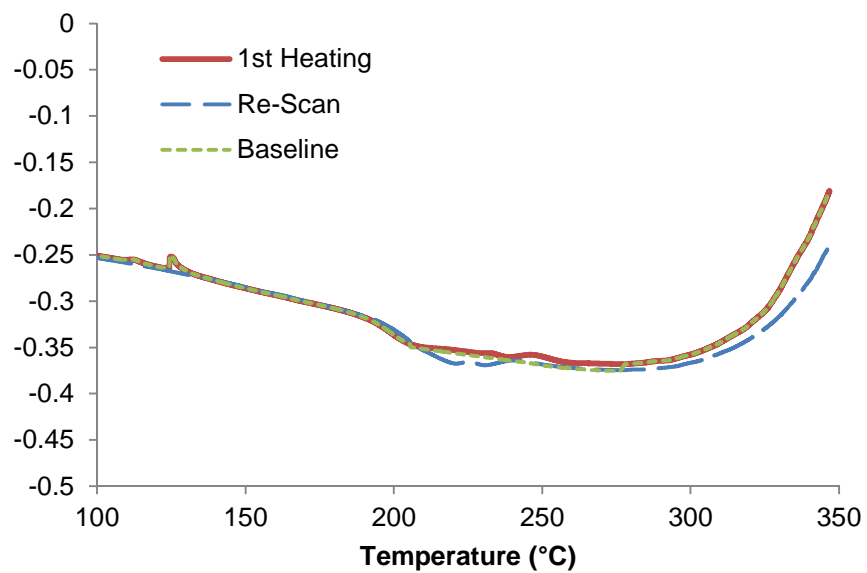
Figure S33. DSC scan of **3** catalyzed with DBTDL after curing for 24 hours at 210 °C.
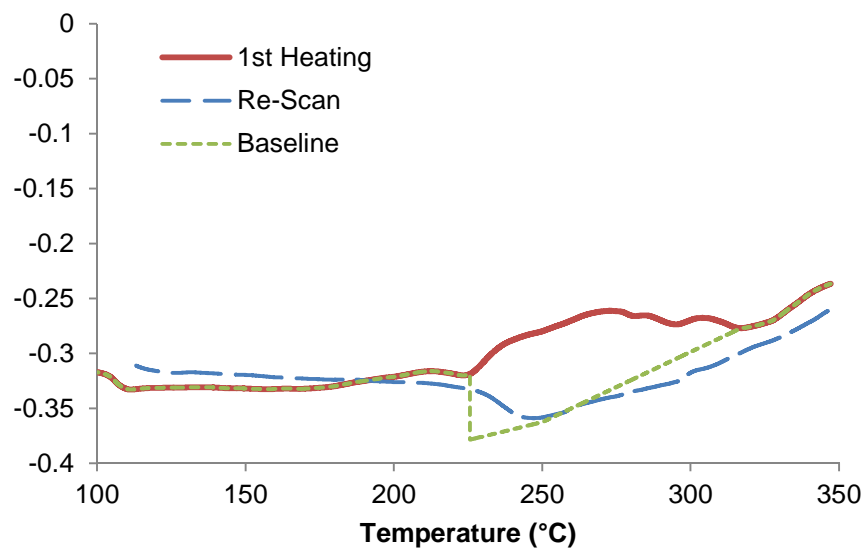
Figure S34. DSC scan of **4** (no catalyst added) after curing for 24 hours at 210 °C.
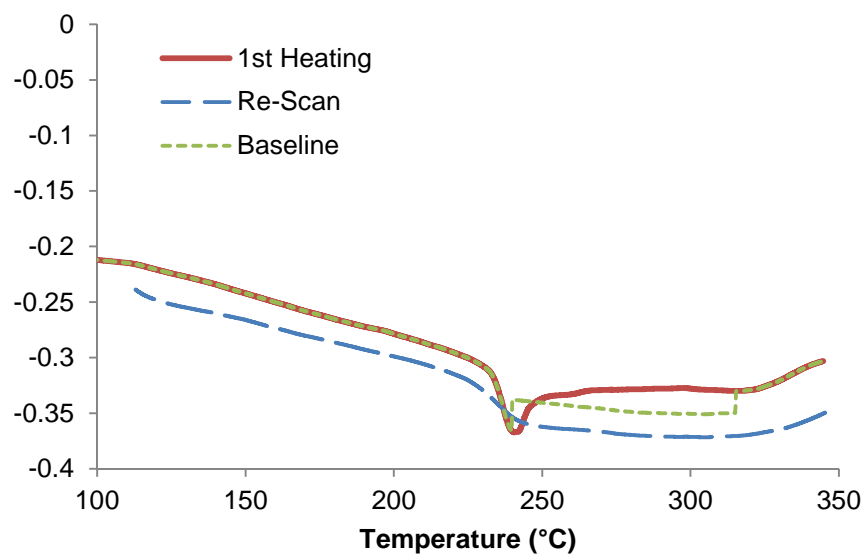
Figure S35. DSC scan of **4** catalyzed with Cu-acac/nonylphenol after curing for 24 hours at 210 °C.
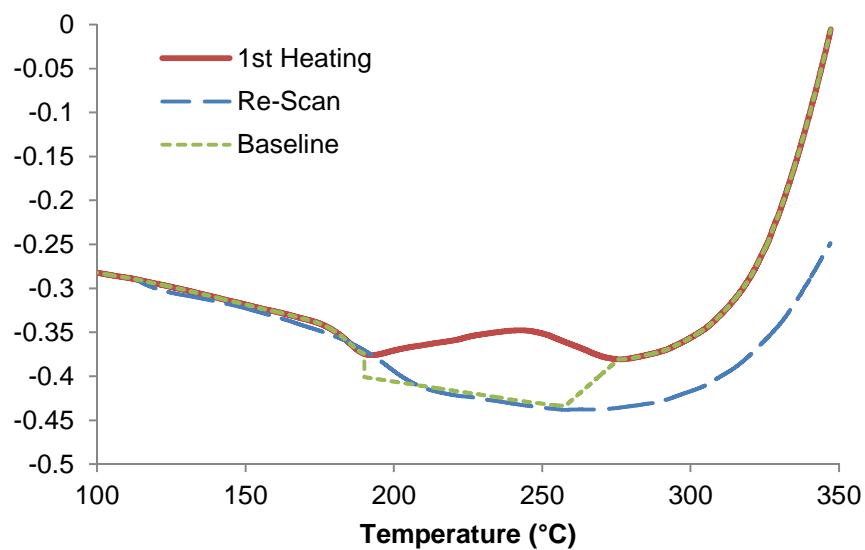
Figure S36. DSC scan of **4** catalyzed with DBTDL after curing for 24 hours at 210 °C.
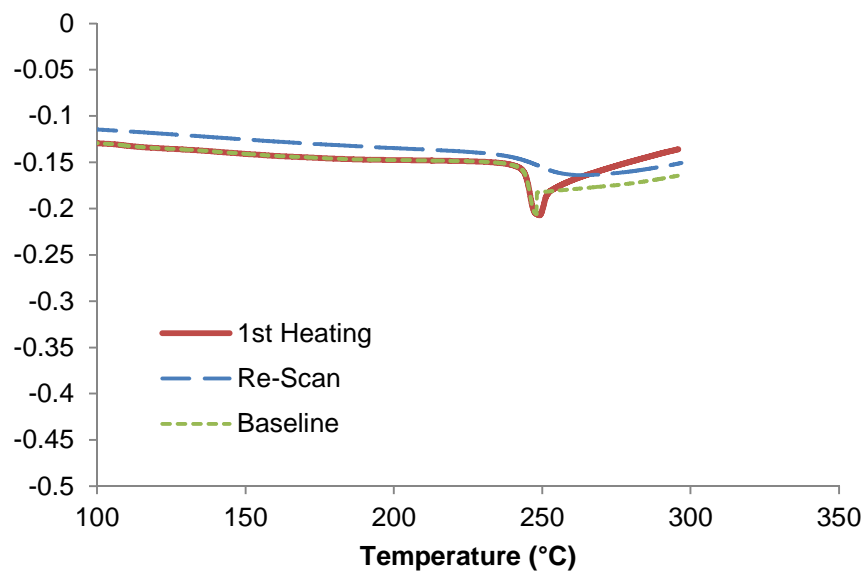
Figure S37. DSC scan of **3** (no catalyst added) after curing for 24 hours at 210 °C (max scan temperature 300 °C).
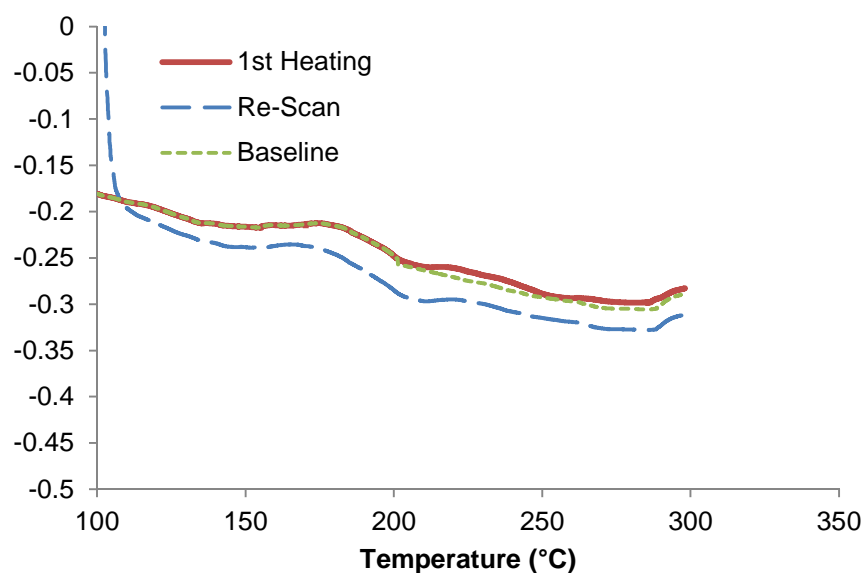
Figure S38. DSC scan of **3** (catalyzed with DBTDL) after curing for 24 hours at 210 °C (max scan temperature 300 °C).
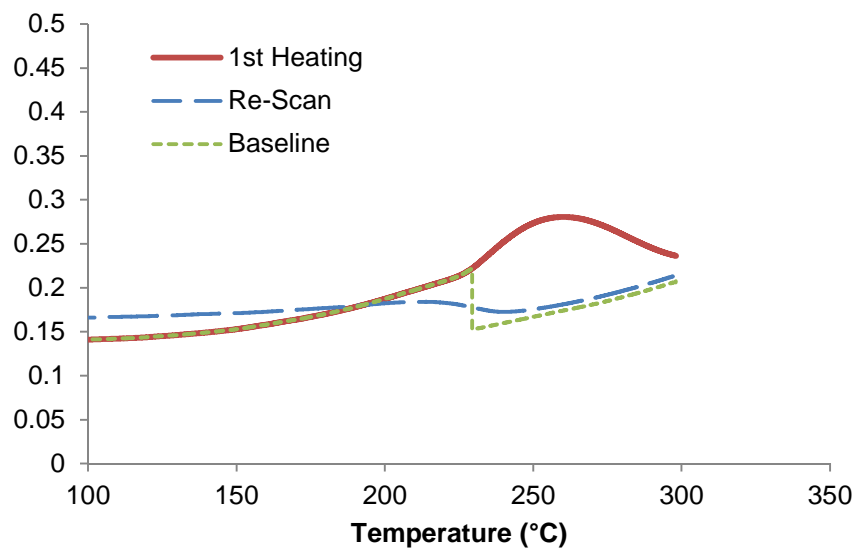
Figure S39. DSC scan of **4** (no catalyst added) after curing for 24 hours at 210 °C (max scan temperature 300 °C).
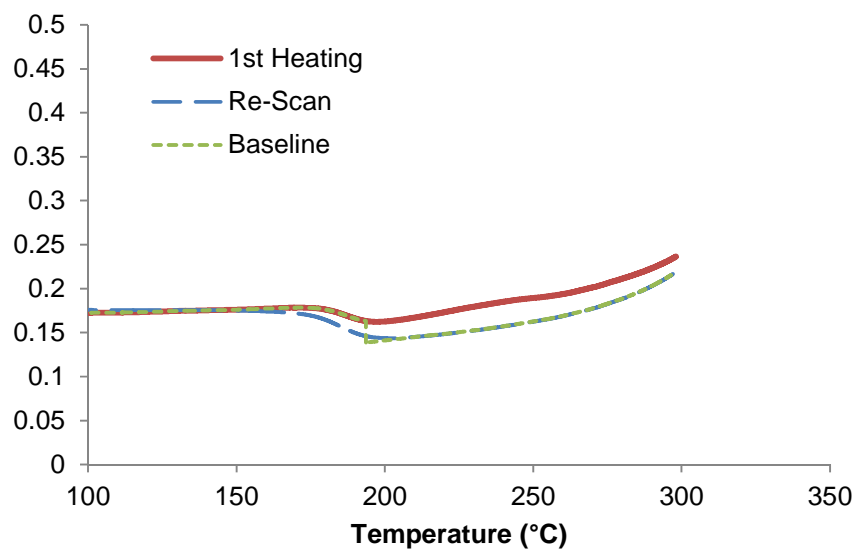
Figure S40. DSC scan of **4** (catalyzed with DBTDL) after curing for 24 hours at 210 °C (max scan temperature 300 °C).

Table S6. DSC Conversion Analysis for Catalyst Choice Experiments

Monomer / Max Scan Temp (°C)	Catalyst	T_G (°C)	ΔH_r (J/g)[a]	ΔH_r (kJ/eq.)[a]	Conversion (α)	$T_{G\text{-}fc}$ (°C)[b]
3 / 350	Not Added	242-247	4 ± 2	0.6 ± 0.2	0.994 ± 0.002	228-248
3 / 350	Cu-AcAc	217-228	3 ± 4	0.5 ± 0.6	0.995 ± 0.006	206-222
3 / 350	DBTDL	192-205	2 ± 8	0.3 ± 1.2	0.996 ± 0.012	197-212
4 / 350	Not Added	226 ± 3	32 ± 13	5 ± 2	0.957 ± 0.017	228-243
4 / 350	Cu-AcAc	234-242	7 ± 5	1.1 ± 0.7	0.990 ± 0.007	226-242
4 / 350	DBTDL	178-190	28 ± 32	4 ± 5	0.959 ± 0.047	188-208
3 / 300*	Not Added	242-253	5.4±0.8	0.8 ± 0.1	0.992 ± 0.001	242-257
3 / 300*	DBTDL	185-204	4 ± 4	0.6 ± 0.6	0.994 ± 0.006	182-203
4 / 300*	Not Added	227 ± 1	34 ± 6	5 ± 1	0.953 ± 0.009	220-239
4 / 300*	DBTDL	180-195	15 ± 4	2.3 ± 0.6	0.978 ± 0.006	177-195

* Incomplete cure was observed when using a maximum scan temperature of 300 °C, therefore conversions obtained are not reliable.

a. Residual heat of cure.

b. Glass transition temperature after heating to the maximum scan temperature at 10 °C/min.

S3.3 Uncured Monomers
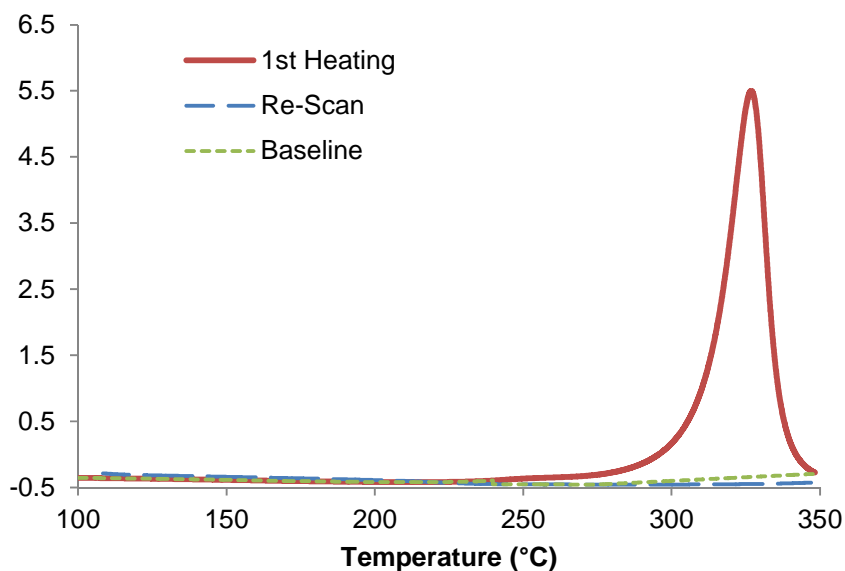
Figure S41. DSC scan of uncured **3** with no catalyst added.
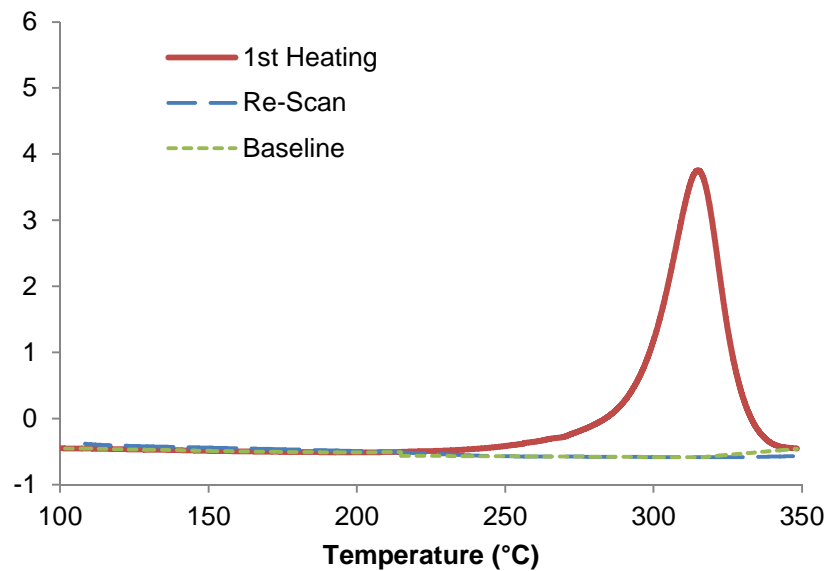
Figure S42. DSC scan of uncured **4** with no catalyst added.
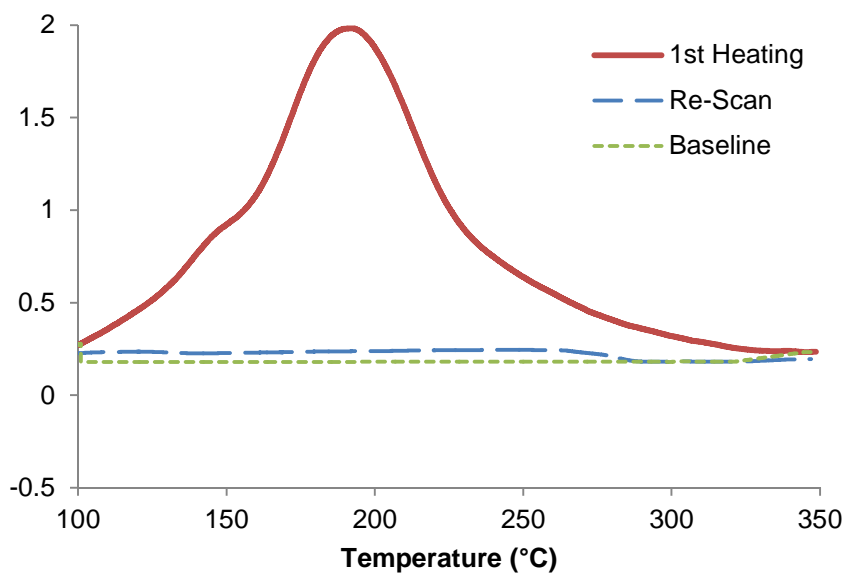
Figure S43. DSC scan of uncured **1** (LECy) with 2 phr nonylphenol / Cu-Acac.
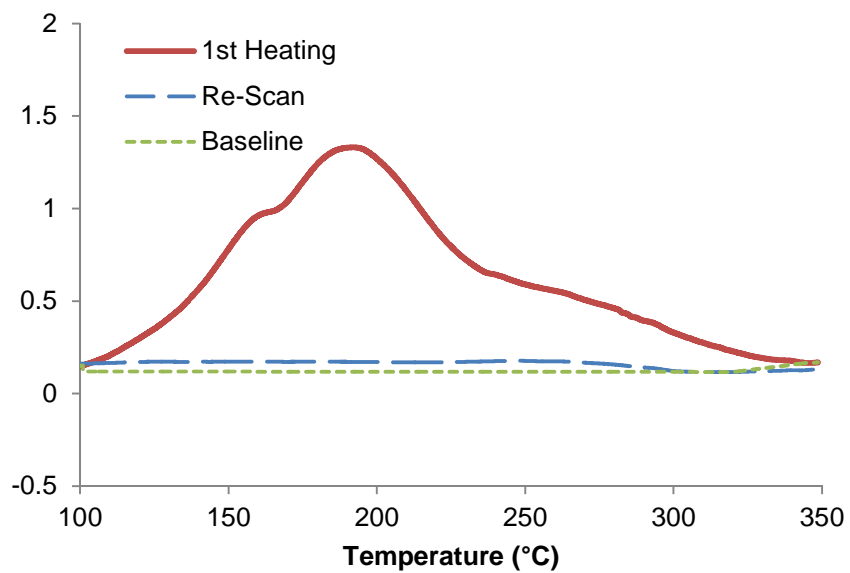
Figure S44. DSC scan of uncured **2** (BADCy) with 2 phr nonylphenol / Cu-Acac.
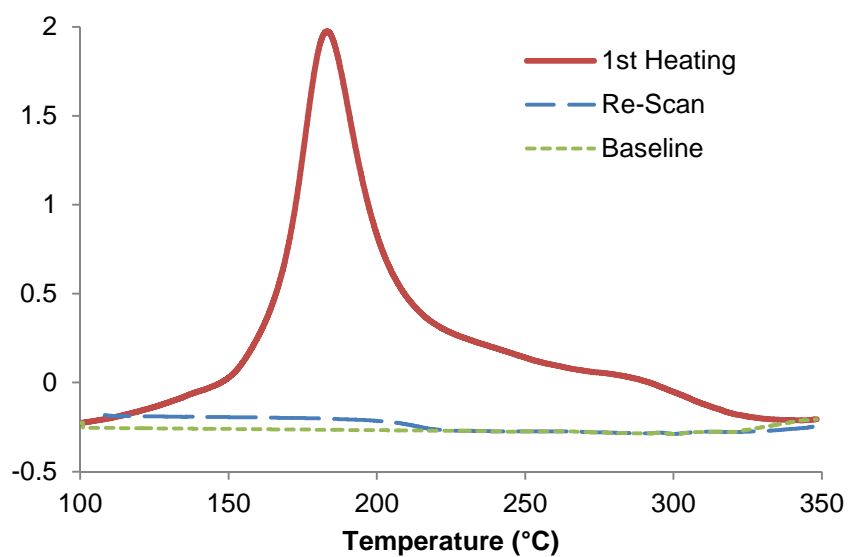
Figure S45. DSC scan of uncured **3** catalyzed with 2 phr nonylphenol / Cu-Acac.
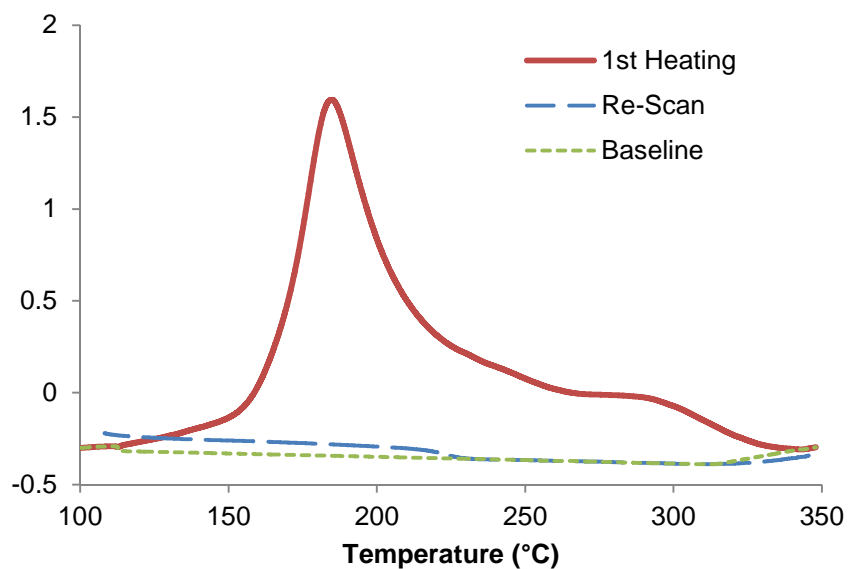
Figure S46. DSC scan of uncured **4** catalyzed with 2 phr nonylphenol / Cu-Acac.
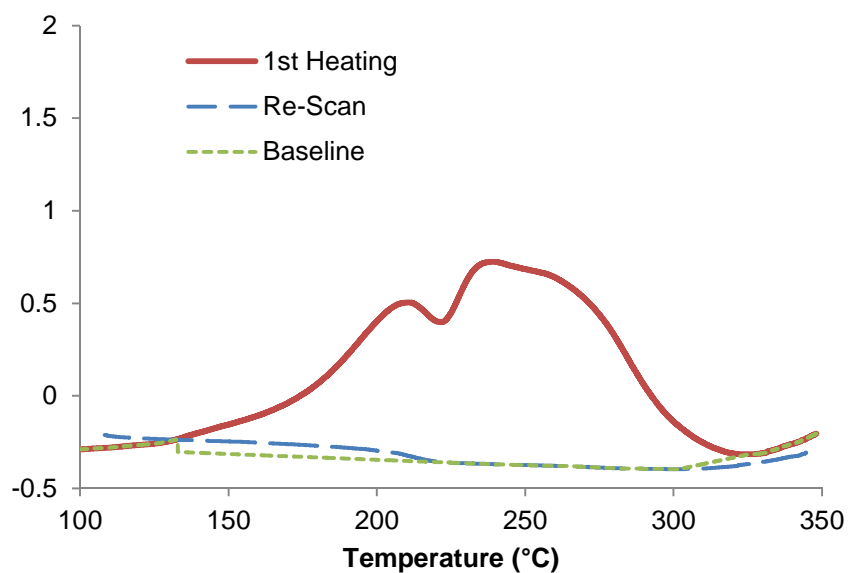
Figure S47. DSC scan of uncured **3** catalyzed with DBTDL (run 1).
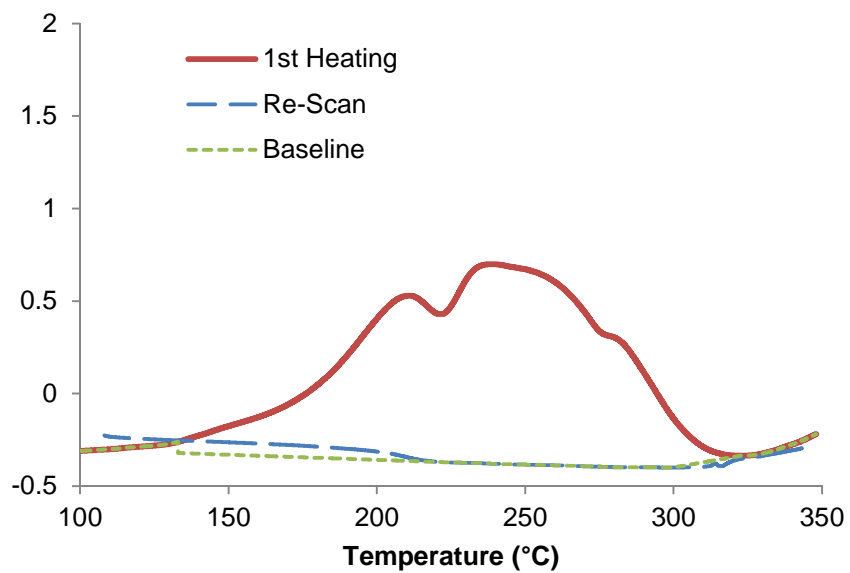
Figure S48. DSC scan of uncured **3** catalyzed with DBTDL (run 2).
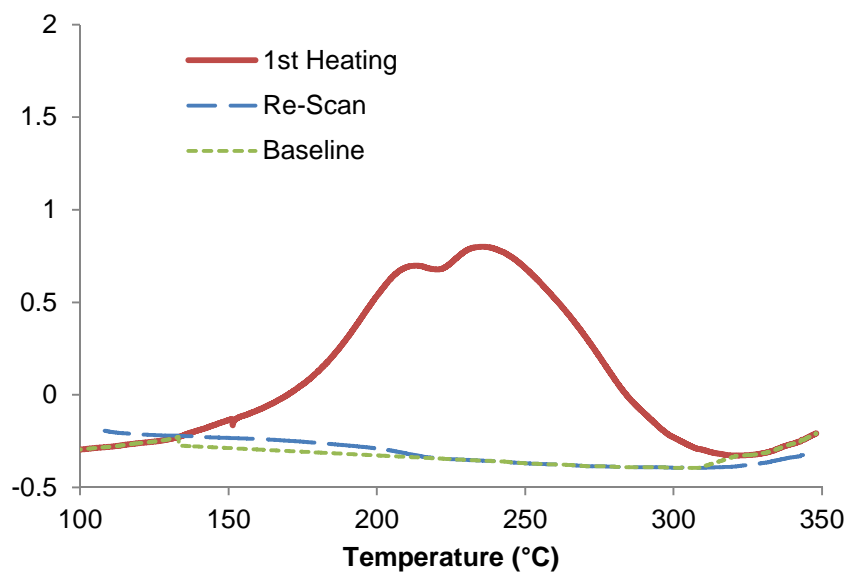
Figure S49. DSC scan of uncured **3** catalyzed with DBTDL (run 3).
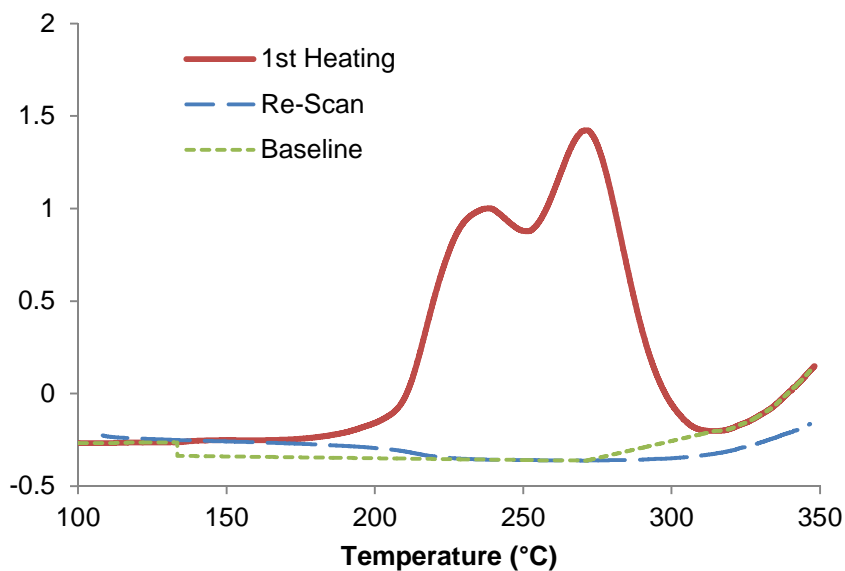
Figure S50. DSC scan of uncured **4** catalyzed with DBTDL.

Table S7. DSC Analysis of Uncured Samples

Monomer	Catalyst	T_{onset} (°C)[a]	T_{peak} (°C)[a]	ΔH_0 (J/g)[a]	ΔH_0 (kJ/eq.)[a]	T_{G-fc} (°C)[b]
3	Not Added	219	327	695 ± 32	101 ± 5	208-239
4	Not Added	211	315	732 ± 37	112 ± 6	213-242
1 (LECy)	Cu-Acac	107	192	903 ± 57	119 ± 8	272-288
2 (BADCy)	Cu-Acac	108	192	737 ± 44	102 ± 6	281-302
3	Cu-Acac	114	183	722 ± 38	105 ± 6	205-219
4	Cu-Acac	123	185	697 ± 28	107 ± 4	218-229
3 run 1	DBTDL	125	239	643 ± 71	94 ± 10	205-219
3 run 2[a]	DBTDL	138	239	640 ± 60	93 ± 9	202-217
3 run 3 [a]	DBTDL	130	236	641 ± 50	94 ± 7	202-217
4	DBTDL	205	271	679 ± 77	104 ± 12	204-222

Samples heated at 10 °C / min. to 350 °C, cooled to 100 °C, then heated again at 10 °C / min. to 350 °C.

a. "Onset" and "Peak" refer to primary exothermic event, with the integrated peak area being used to determine ΔH_0.

b. Glass transition temperature after heating to the maximum scan temperature at 10 °C/min.

c. Replicated runs for checking reproducibility.

Table S8. DSC Melting Endotherm Parameters

Monomer	Catalyst	T_m (°C)	Van't Hoff purity	ΔH_m (J/g)	ΔH_m (kJ/mol)
1	Not Added	n/a (29)[d]	n/a	n/a	n/a
2[c]	Not Added	82.8 ± 0.2	99.2 ± 0.2%	105 ± 9	29.2 ± 2.5
3	Not Added	73.0	96.5%[b]	83.1 ± 0.4[a,b]	24.2 ± 0.1[a,b]
4	Not Added	82.0	99.0%	92.4 ± 1.2[a]	28.3 ± 0.4[a]

a. Uncertainty associated with analysis of a single sample, does not reflect sample-to-sample variation.
b. Sample crystallizaes with difficulty, purity reflects both amorphous sample and actual chemical impurities.
c. Data originally reported in Ref. S8; uncertainties based on sample-to-sample variation.
d. Exists as a supercooled liquid at room temperature; melting point reported by Ref. S9.

S4. Determination of Thermal Lag in TMA Data

Previously, we have published a procedure for the determination of thermal lag in di(cyanate ester) samples heated at 10 °C/min.[S7] Although this procedure can be utilized with a variety of heating rates, herein we present an updated method for handling samples heated at very rapid rates, namely 50 °C/min, which builds upon the previous method.

To summarize briefly, when TMA samples, which typically take the form of cylinders measuring around 12 mm in diameter by 3-5 mm tall, are heated or cooled at an appreciable rate, a temperature gradient develops between the sample surface (where the instrument thermocouple is placed) and the interior of the sample. The sample response, however, depends in general on the temperature throughout the sample, rather than strictly at the surface. The exact dependence depends on which response is being measured, how the probe makes contact with the sample, how strain gradients are distributed within the sample, and so forth, and is very difficult to determine. Therefore for the purposes of this discussion we will describe the sample response as depending on the average temperature of the sample, even though such an assumption is just a

reasonable approximation. In general, the average temperature of the sample will lag behind the surface temperature during heating or cooling. The lag time will depend on the sample geometry and heat transport characteristics, and is well approximated by a single time constant, typically 30 to 60 seconds for 3-5 mm thick samples. When this time constant is multiplied by a given heating (or cooling) rate, a temperature difference between the surface and average temperatures of the sample may be inferred. This difference is referred to as the "thermal lag" of the sample.

Figure S51 illustrates the experimental procedure for determination of thermal lag, and is taken from a sample used in Ref. S7, with a ramp rate of 10 °C / min. After an initial heating, the sample is cycled twice over the range 100 °C to 200 °C. This dry sample has been previously cured to 210 °C, with a T_G somewhere near 250 °C, so cycling at these temperatures should be entirely in the glassy state with no chemical reactions taking place. Under these conditions, the only contribution to changes in the length of the sample (as measured by displacement in the probe) should be from thermal expansion of the sample or mechanical instabilities caused by the absence of a perfectly flat and level surface on which the probe rests. Moreover, over the temperature range encountered, the thermal expansion should be close to linear.
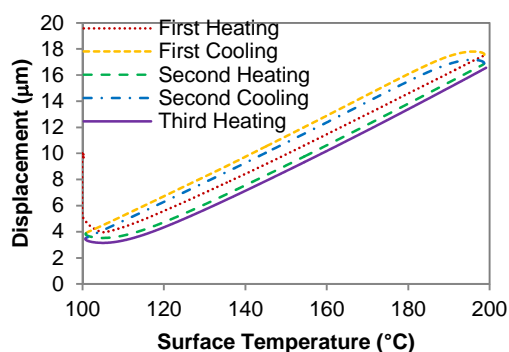
Figure S51. Raw signals used to determine thermal lag in a TMA experiment. The sample is a co-network of 50 wt% BADCy and 50 wt% LECy, cured at 210 °C for 24 hours under dry N$_2$, catalyzed with the same Cu-Acac / nonylphenol mixture reported in this work.

Except for the first two minutes or so of scanning, corresponding to 20 °C, the displacement does appear to be linear with temperature on all scans. For a given heating scan, there is a negative displacement between the first and second scan, and a much smaller negative displacement between the second and third scan, very similar to that seen between the first and second cooling scan. These negative displacements are likely the result of the aforementioned mechanical instabilities in probe contact, with the probe essentially "settling" into a more stable position as the scanning progresses. After two heating and cooling cycles, the probe has "settled" enough that mechanical instabilities become insignificant. The lines also appear to be parallel, with the initial non-linear portion of the scans appearing to cause a net horizontal displacement of the lines.

The apparent horizontal displacement of the lines is in fact due to thermal lag. On the final heating and cooling scans, as seen in Figure S52, mechanical instabilities have become small enough that we may safely assume that linear thermal expansion is the only cause of displacement. In that case, the displacement is proportional to the average temperature of the sample. The nonlinear, relatively flat portions of the curves near the start of each scan therefore represent instances in which the surface temperature changes while the average temperature does not. This phenomenon is simply explained as the result of thermal lag, that is, only the outer portions of the sample begin heating or cooling, causing the average temperature to change little until the change in heat flow propagates through the bulk of the sample. Because of the symmetry of the heat transport equation, the lag patterns for heating and cooling are "mirror images" of one another. This means that the horizontal displacement between the lines at a given displacement in Figure S52 equals twice the thermal lag, that is, the line is displaced rightward by thermal lag during heating, and leftward by an equal amount during cooling at the

45

same rate. To compute the thermal lag, one then needs only to choose an appropriate displacement, find the corresponding temperatures for heating and cooling runs, then subtract and divide by two. The resultant thermal lag may then be assumed proportional to the heating rate. The TMA scan as a whole may then be corrected by measuring the heating rate at each point and applying the proportionate thermal lag (the proportionality constant has units of time, as expected).
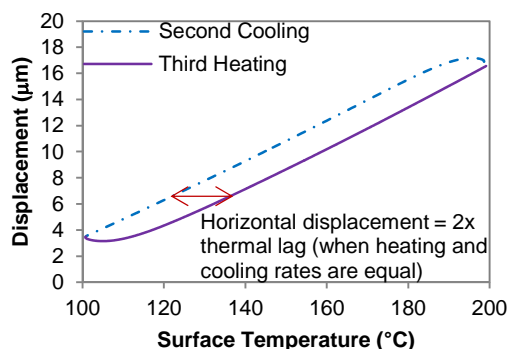
Figure S52. Method for determination of thermal lag from single cycle data.

Figure S53 shows the results of applying the thermal lag correction to the data in Figure S52. As expected, the curves collapse into a single line over nearly the entire range. To demonstrate that the correction also has value when applied to the determination of the glass transition temperature, Figures S54 and S55 compare the loss component of stiffness scan on cooling and re-heating the same sample through the glass transition temperature, without (Figure S54) and with (Figure S55) the thermal lag applied. Note that the data used to calculate the lag is displacement data, which is based on the mean of the modulated signal, while the data used to calculate the loss component of stiffness depends on the amplitude and phase of the modulated signal. Therefore, the two signals are independent, and thus the coincidence seen in Figure S55 is not simply caused by shifting the curves in Figure S54 arbitrarily until they merge.
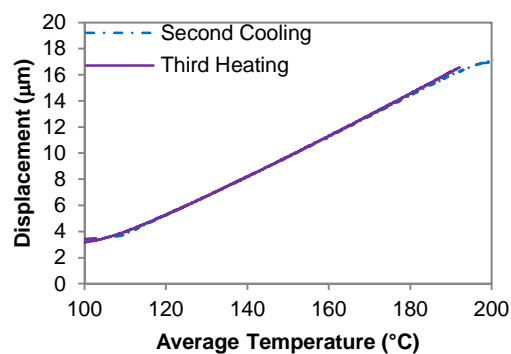
Figure S53. Results of applying thermal lag correction to displacement data during thermal lag determination cycle.
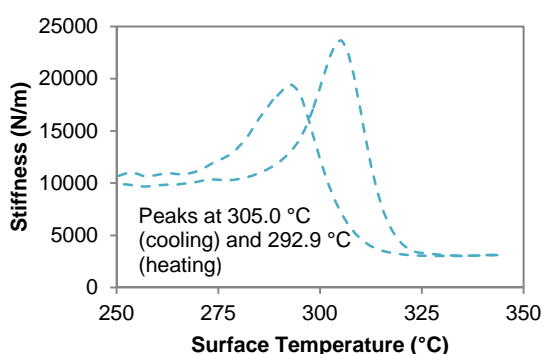
Figure S54. Loss component of stiffness as a function of temperature during cooling and re-heating of the sample used for Figures S51-S53, after heating to 350 °C at the completion of the thermal lag determination cycle, without applied thermal lag correction.
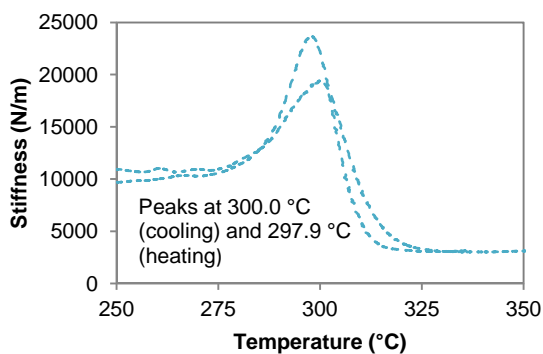
Figure S55. Data for Figure S54, with thermal lag correction applied.

A key consideration for this method is the locations of the corresponding displacement points used to compute the thermal lag. For samples heated at 10 °C or 20 °C, as in Ref. S7, a

point in the displacement loop corresponding to 25% of the distance covered from the bottom to the top was used, and has proven to be a good choice in many subsequent experiments. The 25% value represents a compromise between the need to be far enough from the edges of the loop to avoid nonlinearities, while being toward the lower end of the temperature scale where the sample is stiffer and probe settling (or sample creep) is less likely. The only adjustment required for this method is to use a wider temperature range in the loop at faster heating rates, to ensure enough time elapses to minimize the nonlinearities during the thermal lag determination cycle.

Figure S56 shows the displacement as a function of corrected temperature for the entire TMA run, which consists of the thermal lag determination loop, plus a heating, cooling, and re-heating to 350 °C in order to measure "as cured" and "fully cured" T_G values. Anywhere the displacement curves coincide represents a reasonable choice of reference point for thermal lag determination. In particular, below, and just above the T_G (indicated by the kink in the displacement curve), the coincidence is good for the final cooling and re-heating, providing another option for thermal lag determination that produces the same results as utilizing a separate set of heating and cooling cycles. At the first encounter with T_G there is displacement due to stress relaxation, and above T_G there is displacement due to creep, causing lack of coincidence.
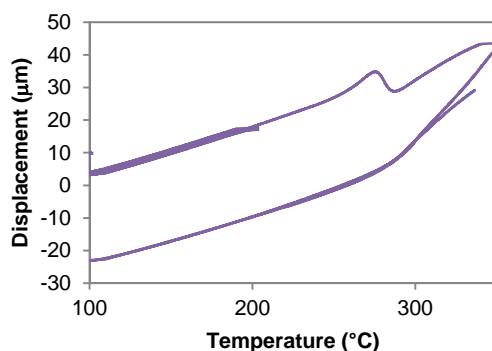
Figure S56. Displacement as a function of temperature (with thermal lag correction applied) for the entire TMA scan described in Figures S51-S55.

For samples heated at 20 °C / min., the method outlined in Ref. S7 and again above was used in this work with an appropriately wide temperature range during lag determination. However, for samples heated at 50 °C / min., we could not design a loop that was wide enough to accommodate the needed lag time while remaining well below T_G, which for monomers **3** and **4** is lower than for LECy and BADCy (limitations on the cooling capability of the TMA furnace prevent us from simply shifting the loop to arbitrarily lower temperatures). Figure S57 shows an example (for **4**, cured at 210 °C for 24 hours, with no catalyst added), of the widest available lag loop. Although there may appear to be displacements that bridge linear segments of the heating and cooling loops at about 20 µm, the cooling rate is not entirely constant, so that application of a thermal lag proportional to heating rate results in the curve shown in Figure S58. In Figure S58, it is clear that there are no parallel lines that cross the same displacement in the heating and cooling curves.
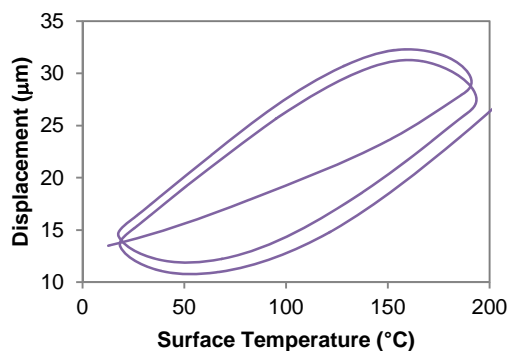
Figure S57. Displacement as a function of surface temperature during the thermal lag determination loop for **4** after curing without catalyst at 210 °C for 24 hours.
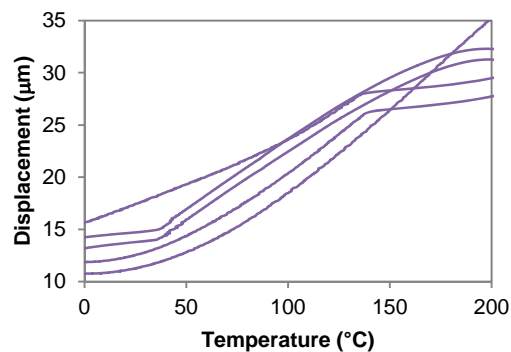
Figure S58. Displacement as a function of temperature (with thermal lag correction applied) for **4** after curing without catalyst at 210 °C for 24 hours.

As a result of these limitations, the displacements just above T_G were used to determine the thermal lag, instead of the displacements within the intended low-temperature cycling portion of the experiment. An examination of the coincidence of the dynamic mechanical functions in the "cooling and 2nd heating" experiments seen in Section S5 testifies to the validity of this technique. In Tables S9 – S11, the difference in the loss component peak temperature is tabulated as the uncertainty in the T_G at full cure (which can be viewed as really a measure of the uncertainty in the thermal lag determination). The uncertainties in the coefficient of thermal expansion (CTE) measurements were determined by assuming thermal lag was overestimated by the uncertainty listed in the T_G measurement, measuring the CTE again, and recording the difference as the characteristic measurement uncertainty (i.e. the sensitivity of CTE measurements to the uncertainty in thermal lag determination was utilized).

S5. Raw TMA Data

S5.1. Dry TMA (Catalyst Choice Experiments)
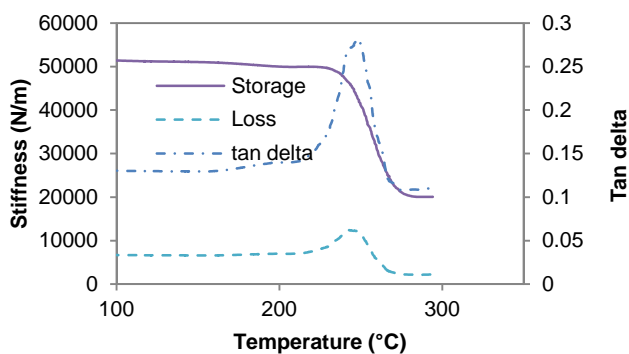
Figure S59. TMA (1st heating) of cured **3** (no catalyst).
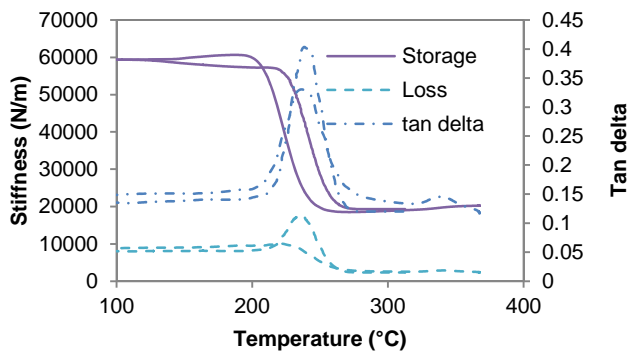
Figure S60. TMA (cooling and 2nd heating) of cured **3** (no catalyst).
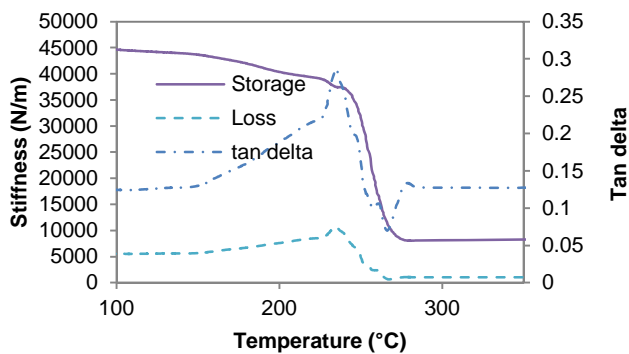
Figure S61. TMA (1st heating) of cured **3** (catalyzed with Cu-Acac).
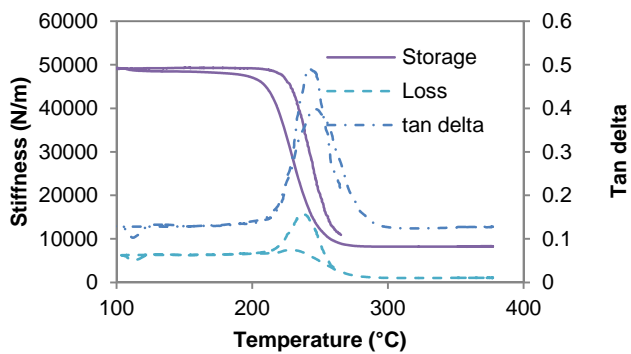
Figure S62. TMA (cooling and 2nd heating) of cured **3** (catalyzed with Cu-Acac).
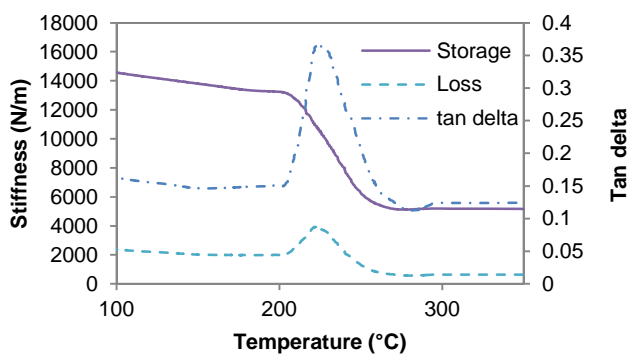
Figure S63. TMA (1st heating) of cured **3** (catalyzed with DBTDL).
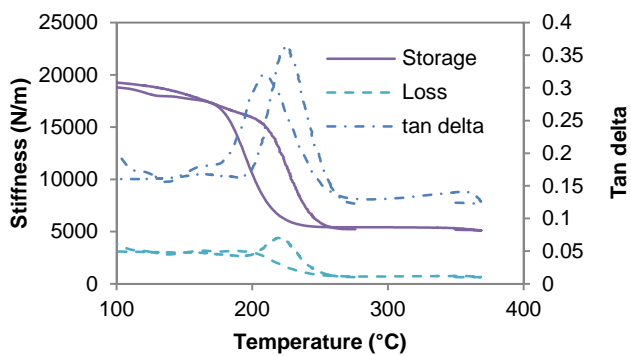
Figure S64. TMA (cooling and 2nd heating) of cured **3** (catalyzed with DBTDL).
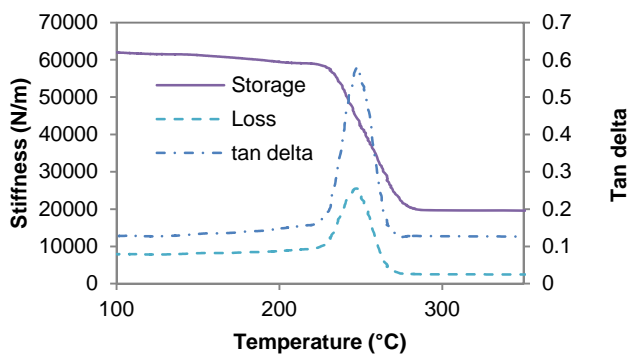
Figure S65. TMA (1st heating) of cured **4** (no catalyst).
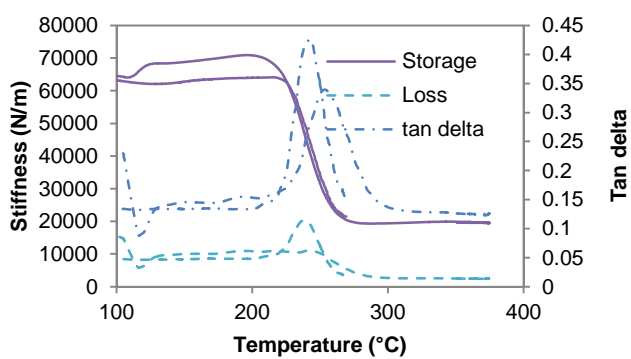
Figure S66. TMA (cooling and 2nd heating) of cured **4** (no catalyst).
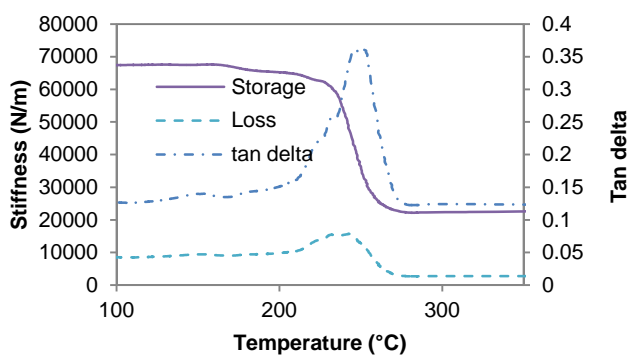
Figure S67. TMA (1st heating) of cured **4** (catalyzed with Cu-Acac).
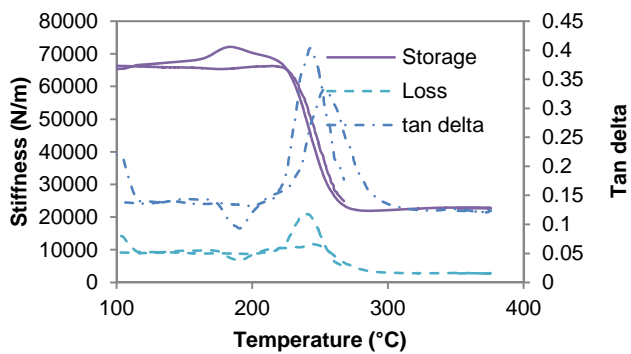
Figure S68. TMA (cooling and 2nd heating) of cured **4** (catalyzed with Cu-Acac).
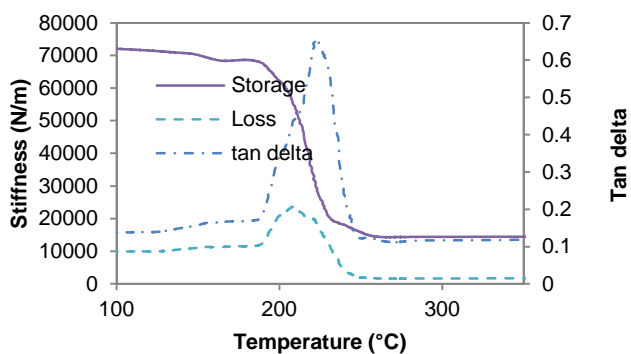
Figure S69. TMA (1st heating) of cured **4** (catalyzed with DBTDL).
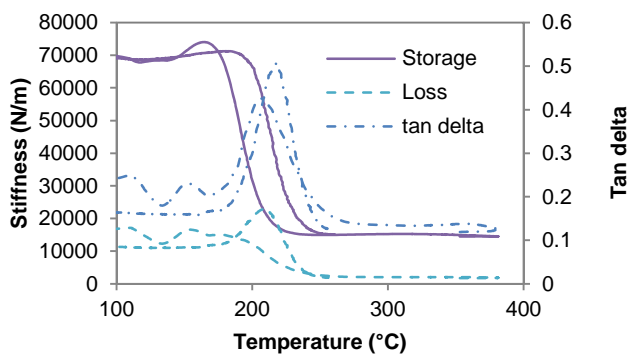
Figure S70. TMA (cooling and 2nd heating) of cured **4** (catalyzed with DBTDL).

Table S9. Thermo-mechanical Data for Dry Samples

Mono-mer	Catalyst	T_G[a] (°C)	$T_{G\text{-}fc}$[b] (°C)	CTE (µm / m °C)[c]	CTE_{fc} (µm / m °C)[b,c]	S'_r (N/m)[d]	$S'_{r\text{-}fc}$(N/m)[d,b]
3	Not Added	246	236 ± 7	72 ± 1	51 ± 5	21000	20000
3	Cu-AcAc	235	238 ± 6	77 ± 4	63 ± 4	13000	11000
3	DBTDL	223	220 ± 9	125 ± 8	107 ± 2	6000	6000
4	Not Added	247	237 ± 2	78 ± 4	61 ± 1	21000	22000
4	Cu-AcAc	243	241 ± 1	75 ± 1	57 ± 4	22000	25000
4	DBTDL	208	208 ± 6	69 ± 4	54 ± 4	15000	18000

a. Peak temperature of loss component of stiffness.
b. The suffix "-fc" indicates measurement done at "full cure", that is, after heating to 350 °C.
c. Measured at 150 °C using a ± 5 °C window.
d. Storage component of stiffness at T_G + 30 °C (T_G as defined in note a).

## S5.2. "Wet" TMA (Cure Condition Experiments)
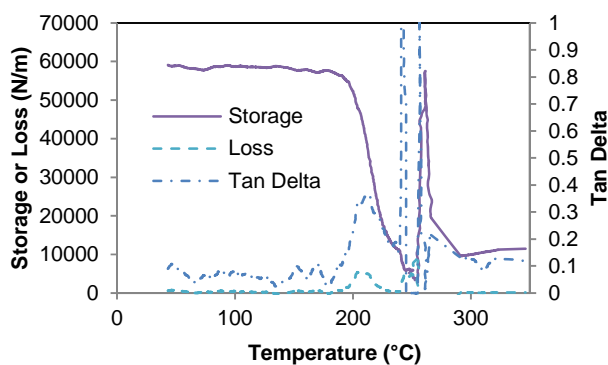
Figure S71. TMA (1st heating) of Cu-Acac catalyzed **1** (LECy) cured at 210 °C for 30 minutes, after 96 hours immersion in 85 °C water.
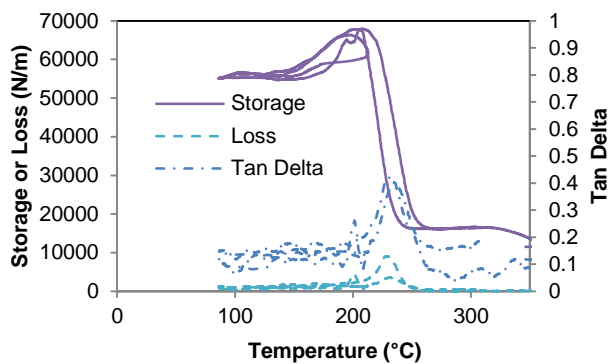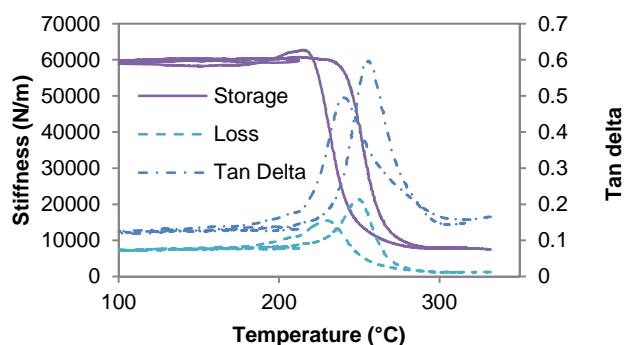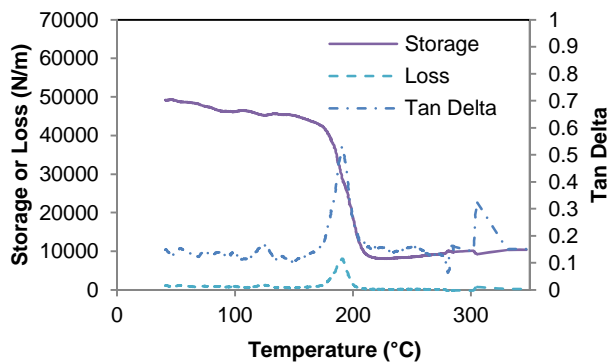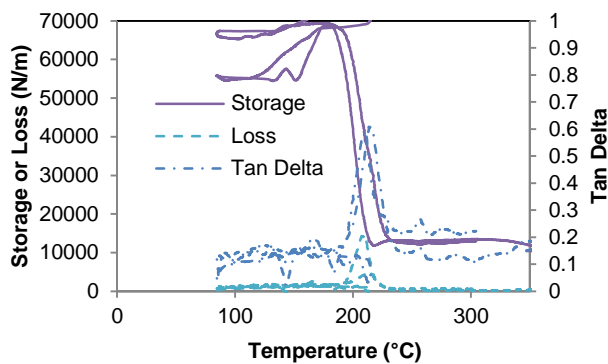
Figure S72. TMA (1st cooling and 2nd heating) of Cu-Acac catalyzed **1** (LECy) cured at 210 °C for 30 minutes, after 96 hours immersion in 85 °C water.
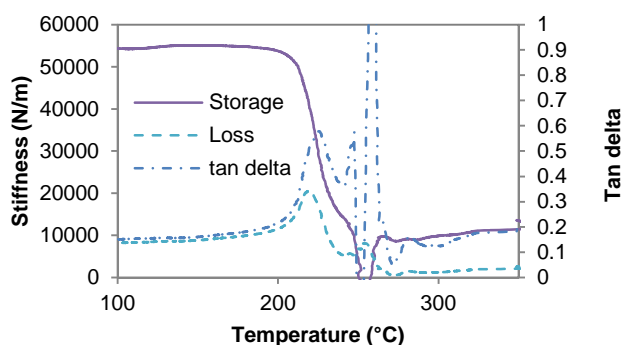
Figure S73. TMA (1st heating) of Cu-Acac catalyzed **1** (LECy) cured at 210 °C for 24 hours, after 96 hours immersion in 85 °C water.
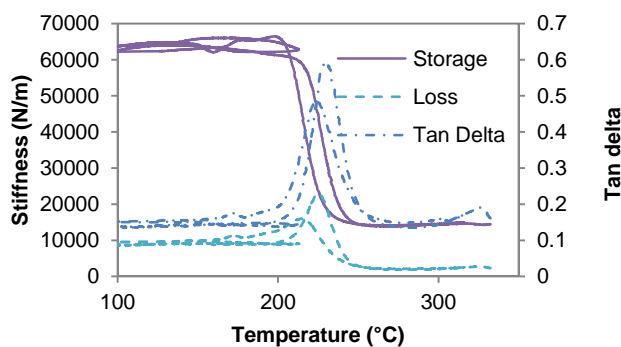
Figure S74. TMA (1st cooling and 2nd heating of Cu-Acac catalyzed **1** (LECy) cured at 210 °C for 24 hours, after 96 hours immersion in 85 °C water.
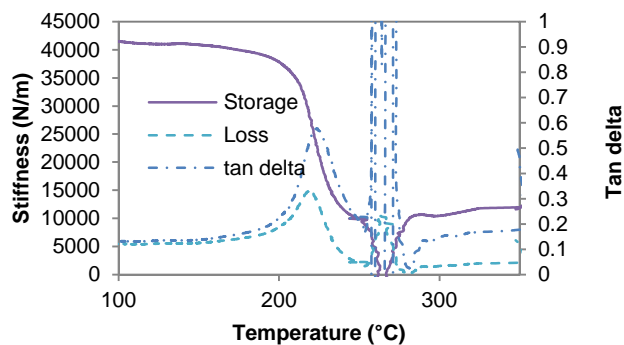
Figure S75. TMA (1st heating) of Cu-Acac catalyzed **1** (LECy) cured at 250 °C for 5 minutes, after 96 hours immersion in 85 °C water.
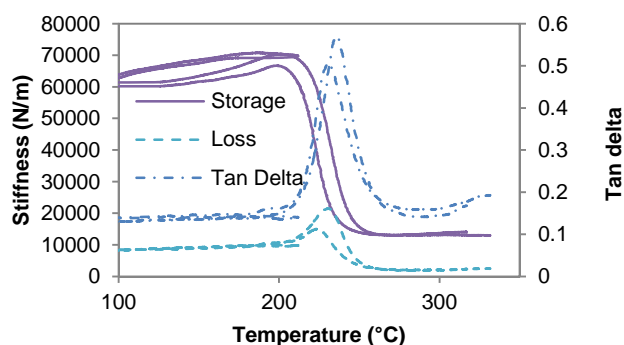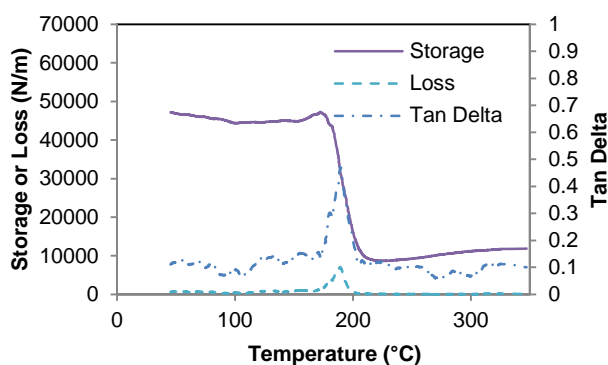

Figure S76. TMA (1st cooling and 2nd heating) of Cu-Acac catalyzed **1** (LECy) cured at 250 °C for 5 minutes, after 96 hours immersion in 85 °C water.
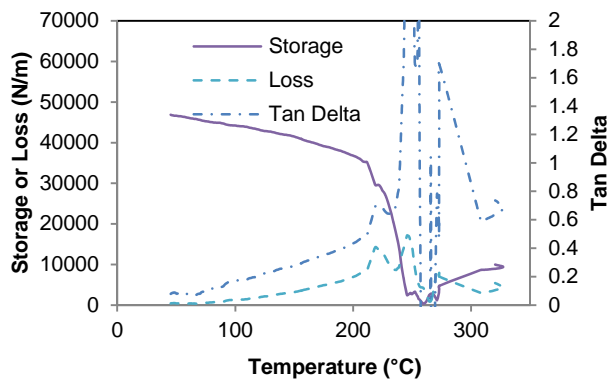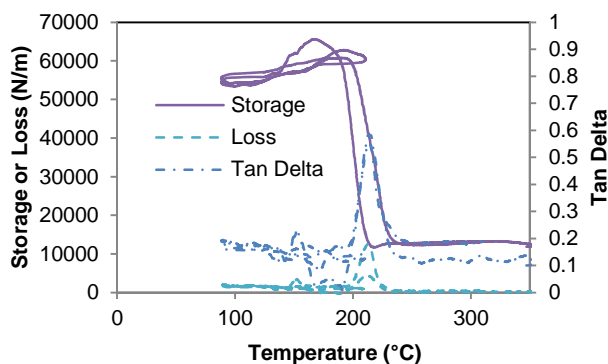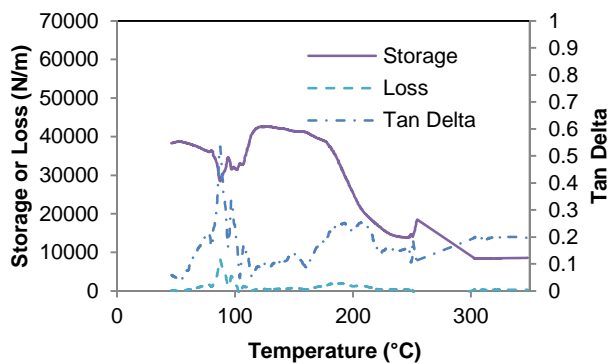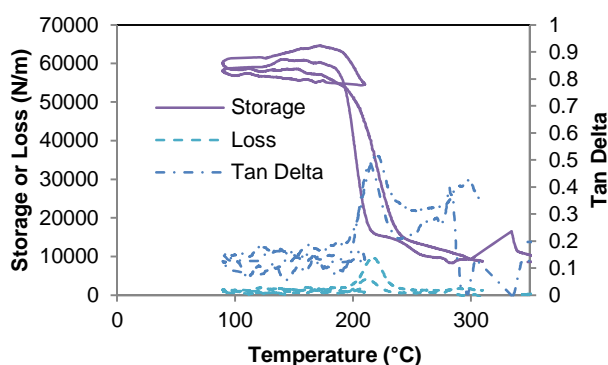

Figure S77. TMA (1st heating) of Cu-Acac catalyzed **1** (LECy) cured at 250 °C for 210 minutes, after 96 hours immersion in 85 °C water.
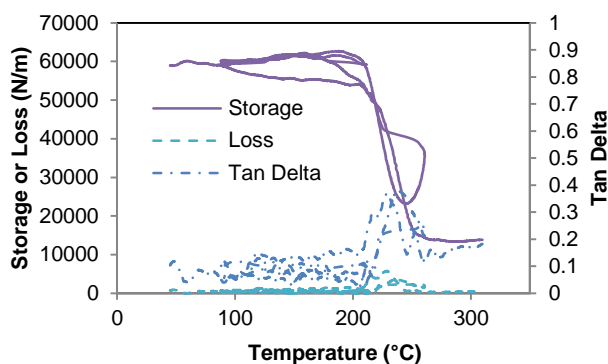
Figure S78. TMA (1st cooling and 2nd heating) of Cu-Acac catalyzed **1** (LECy) cured at 250 °C for 210 minutes, after 96 hours immersion in 85 °C water.
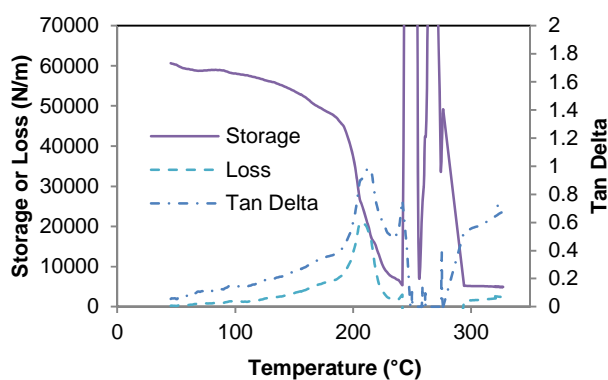
Figure S79. TMA (1st heating) of Cu-Acac catalyzed **2** (BADCy) cured at 210 °C for 30 minutes, after 96 hours immersion in 85 °C water. An instrument error prevented measurement of the cooled and re-heated sample.
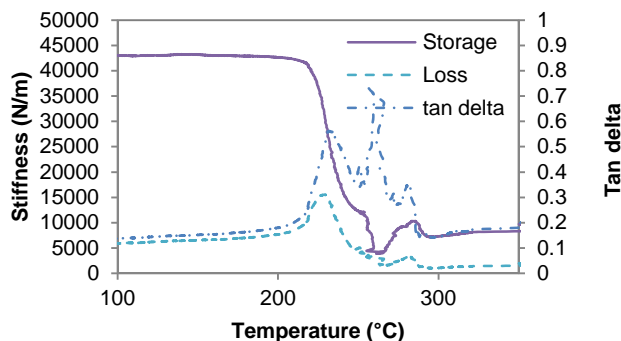
Figure S80. TMA (1st heating) of Cu-Acac catalyzed **2** (BADCy) cured at 210 °C for 24 hours, after 96 hours immersion in 85 °C water.
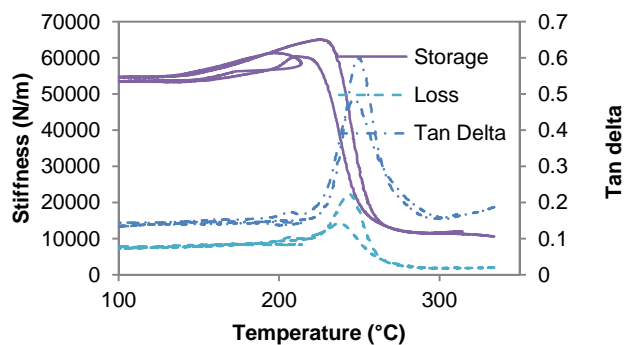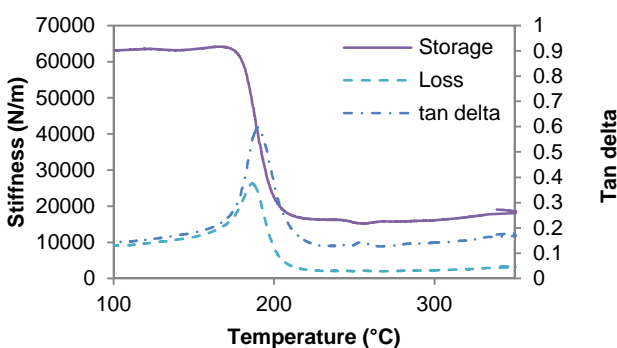
Figure S81. TMA (1st cooling and 2nd heating) of Cu-Acac catalyzed **2** (BADCy) cured at 210 °C for 24 hours, after 96 hours immersion in 85 °C water.
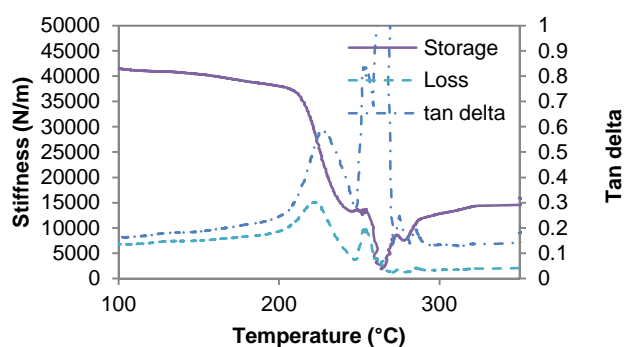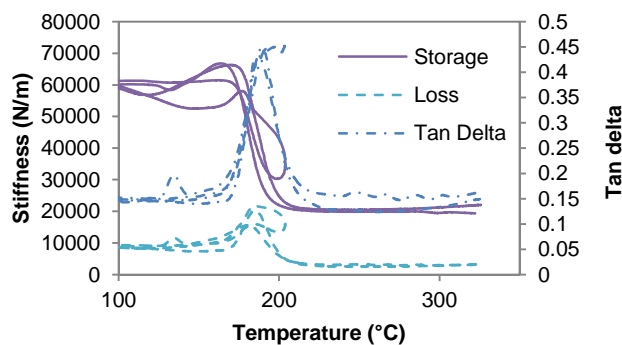

Figure S82. TMA (1st heating) of Cu-Acac catalyzed **2** (BADCy) cured at 250 °C for 5 minutes, after 96 hours immersion in 85 °C water.
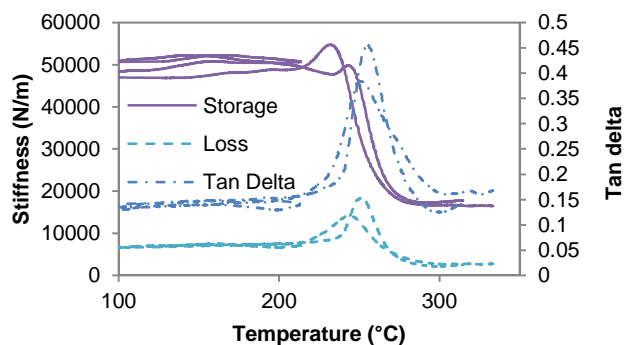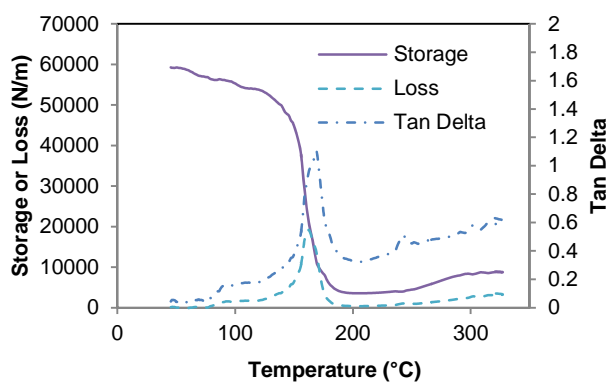

Figure S83. TMA (1st cooling and 2nd heating) of Cu-Acac catalyzed **2** (BADCy) cured at 250 °C for 5 minutes, after 96 hours immersion in 85 °C water.
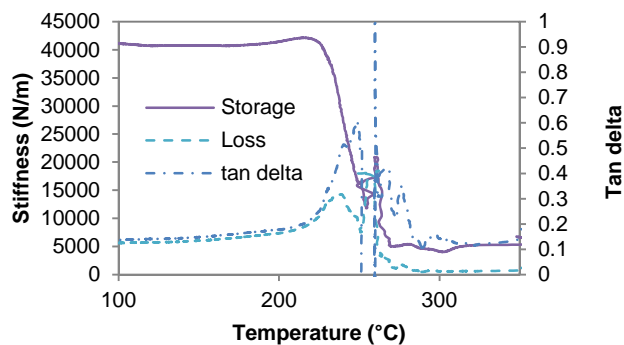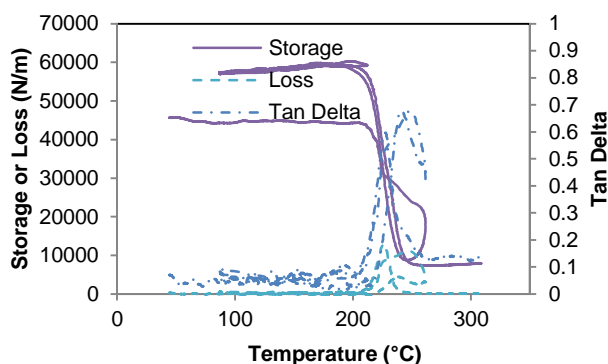
Figure S84. TMA (1st heating) of Cu-Acac catalyzed **2** (BADCy) cured at 250 °C for 210 minutes, after 96 hours immersion in 85 °C water.

Figure S85. TMA (1st cooling and 2nd heating) of Cu-Acac catalyzed **2** (BADCy) cured at 250 °C for 210 minutes, after 96 hours immersion in 85 °C water.

Figure S86. TMA (1st heating) of Cu-Acac catalyzed **3** cured at 170 °C for 210 minutes, after 96 hours immersion in 85 °C water.

Figure S87. TMA (1st cooling and 2nd heating) of Cu-Acac catalyzed **3** cured at 170 °C for 210 minutes, after 96 hours immersion in 85 °C water.

Figure S88. TMA (1st heating) of Cu-Acac catalyzed **3** cured at 170 °C for 24 hours, after 96 hours immersion in 85 °C water.
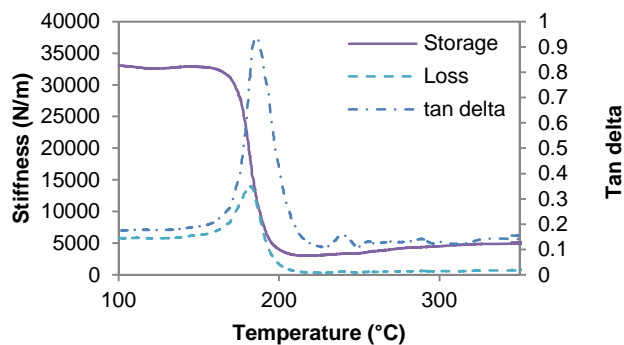

Figure S89. TMA (1st cooling and 2nd heating) of Cu-Acac catalyzed **3** cured at 170 °C for 24 hours, after 96 hours immersion in 85 °C water.
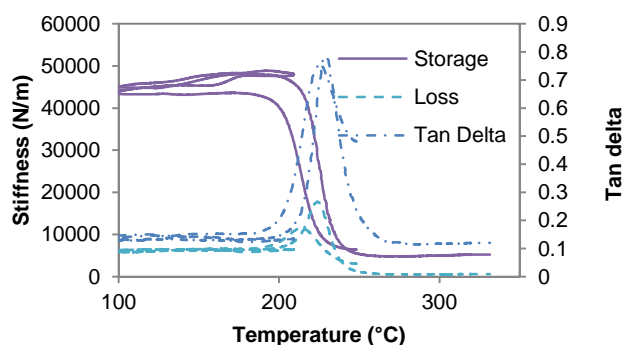
Figure S90. TMA (1st heating) of Cu-Acac catalyzed **3** cured at 210 °C for 30 minutes, after 96 hours immersion in 85 °C water.
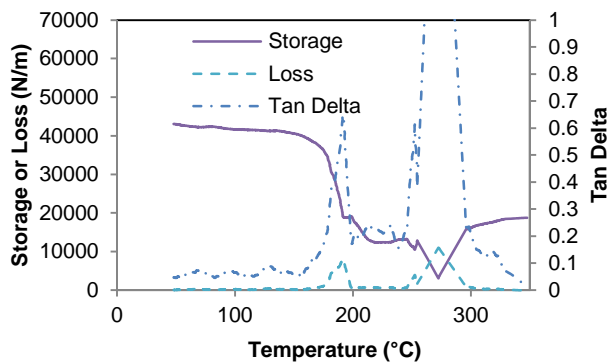

Figure S91. TMA (1st cooling and 2nd heating) of Cu-Acac catalyzed **3** cured at 210 °C for 30 minutes, after 96 hours immersion in 85 °C water.
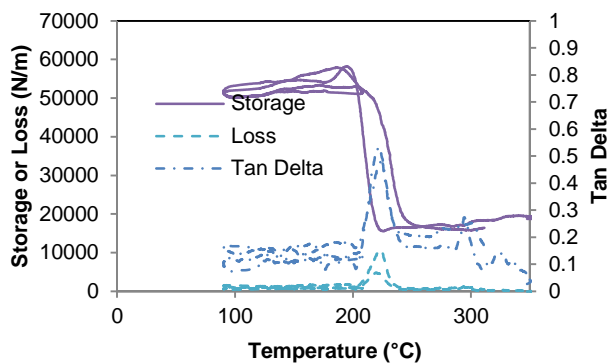

Figure S92. TMA (1st heating) of Cu-Acac catalyzed **3** cured at 210 °C for 24 hours, after 96 hours immersion in 85 °C water.

Figure S93. TMA (1st cooling and 2nd heating) of Cu-Acac catalyzed **3** cured at 210 °C for 24 hours, after 96 hours immersion in 85 °C water.

Figure S94. TMA (1st heating) of Cu-Acac catalyzed **4** cured at 170 °C for 210 minutes, after 96 hours immersion in 85 °C water.

Figure S95. TMA (1st cooling and 2nd heating) of Cu-Acac catalyzed **4** cured at 170 °C for 210 minutes, after 96 hours immersion in 85 °C water. Note: the run was re-started during the first cooling by re-heating to 250 °C after an unintended quench to room temperature.

Figure S96. TMA (1st heating) of Cu-Acac catalyzed **4** cured at 170 °C for 24 hours, after 96 hours immersion in 85 °C water.
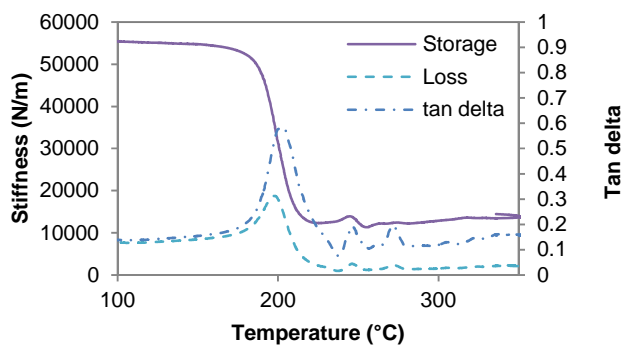

Figure S97. TMA (1st cooling and 2nd heating) of Cu-Acac catalyzed **4** cured at 170 °C for 24 hours, after 96 hours immersion in 85 °C water. Note: the run was re-started during the first cooling by re-heating to 250 °C after an unintended quench to room temperature.
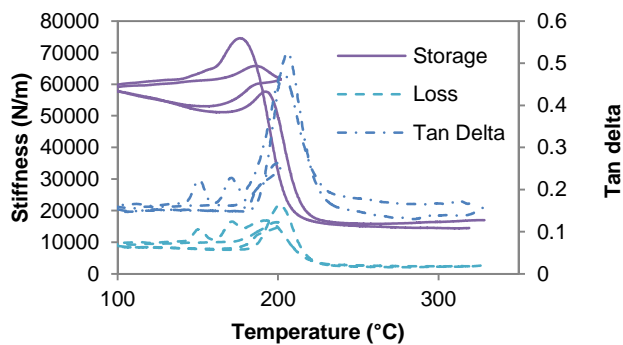

Figure S98. TMA (1st heating) of Cu-Acac catalyzed **4** cured at 210 °C for 30 minutes, after 96 hours immersion in 85 °C water.

Figure S99. TMA (1st cooling and 2nd heating) of Cu-Acac catalyzed **4** cured at 210 °C for 30 minutes, after 96 hours immersion in 85 °C water.

Figure S100. TMA (1st heating) of Cu-Acac catalyzed **4** cured at 210 °C for 24 hours, after 96 hours immersion in 85 °C water.

Figure S101. TMA (1st cooling and 2nd heating) of Cu-Acac catalyzed **4** cured at 210 °C for 24 hours, after 96 hours immersion in 85 °C water.

Table S10. Thermo-mechanical Data for Samples after 96 hrs of Water Immersion @ 85 °C in Cure Condition Experiments

| Mono-mer	Catalyst	T_{Cure}[a] (°C)	t_{cure}[b] (min)	T_G[a] (°C)	$T_{G\text{-fc}}$[b] (°C)	S'_r (N/m)[d]	$S'_{r\text{-fc}}$ (N/m)[d,b]
4	Cu-Acac	170	210	162	225 ± 14	3600	7500
4	Cu-Acac	170	1440	182	224 ± 10	3100	5200
4	Cu-Acac	210	30	191	224 ± 4	12000	17000
4	Cu-Acac	210	1440	198	201 ± 10	12000	17000
3	Cu-Acac	170	210	191	208 ± 6	8200	12000
3	Cu-Acac	170	1440	189	212 ± 1	8800	13000
3	Cu-Acac	210	30	189	216 ± 4	15000	14000
3	Cu-Acac	210	1440	186	185 ± 1	17000	21000
2	Cu-Acac	210	30	206	n/a	4300	n/a
2	Cu-Acac	210	1440	229	244 ± 6	7300	12000
2	Cu-Acac	250	5	222	251 ± 7	14000	18000
2	Cu-Acac	250	210	239	249 ± 19	5900	9500
1	Cu-Acac	210	30	204	229 ± 2	15000	16000
1	Cu-Acac	210	1440	220	225 ± 11	5100	14000
1	Cu-Acac	250	5	219	231 ± 8	9900	13000
1	Cu-Acac	250	210	219	229 ± 8	2700	13000

a. Peak temperature of loss component of stiffness.
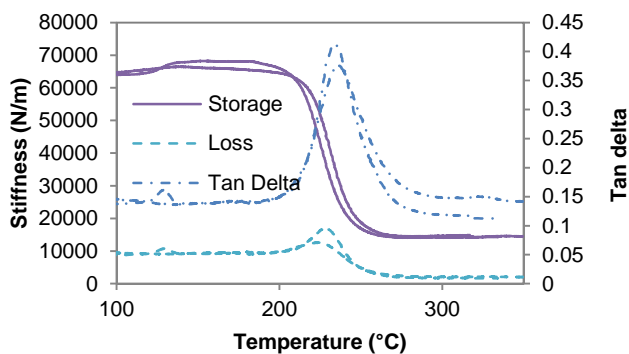b. The suffix "-fc" indicates measurement done at "full cure", that is, after heating to 350 °C.
c. Measured at 150 °C using a ± 5 °C window.
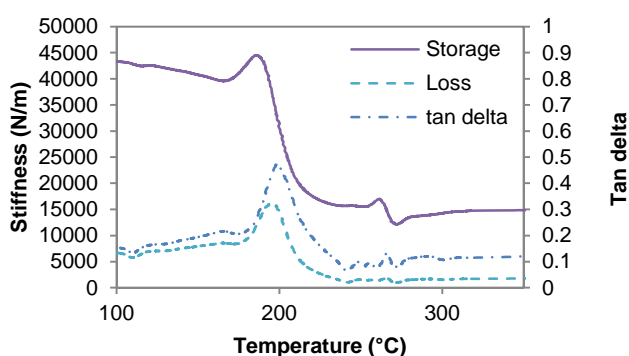d. Storage component of stiffness at T_G + 30 °C (T_G as defined in note a).
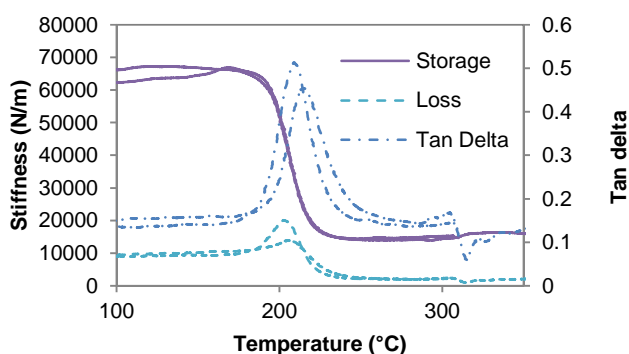
S5.3 "Wet" TMA Data (Catalyst Choice Experiments)
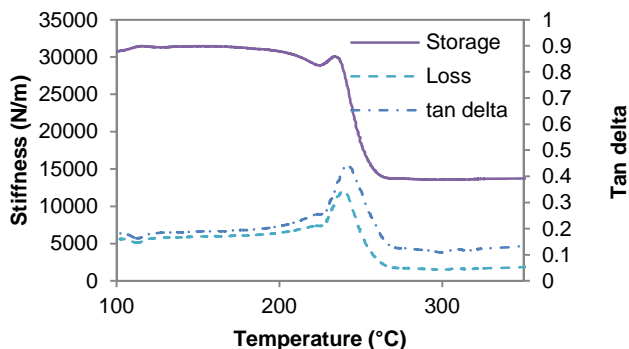
Figure S102. TMA (1st heating) of cured **3** (no catalyst) after exposure to 85 °C water for 96 hours.

Figure S103. TMA (cooling and 2nd heating) of cured **3** (no catalyst) after exposure to 85 °C water for 96 hours.
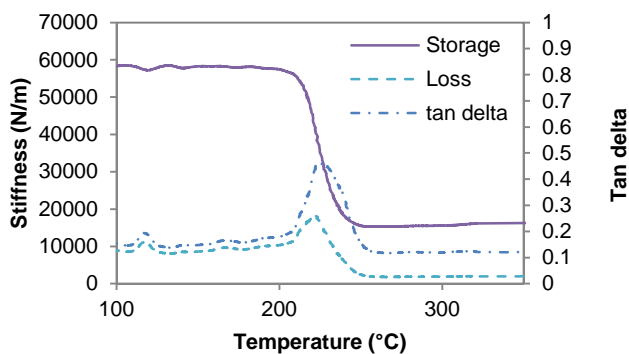

Figure S104. TMA (1st heating) of cured **3** (catalyzed with Cu-Acac) after exposure to 85 °C water for 96 hours.
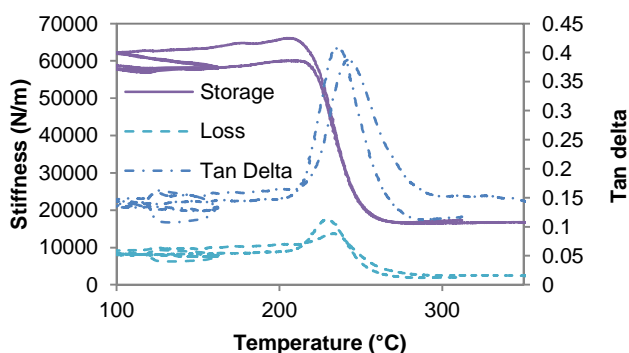

Figure S105. TMA (cooling and 2nd heating) of cured **3** (Cu-Acac catalyzed) after exposure to 85 °C water for 96 hours.

Note that exposure of cured **3** catalyzed with DBTDL to water resulted in destruction of samples, thus no wet TMA data are available.
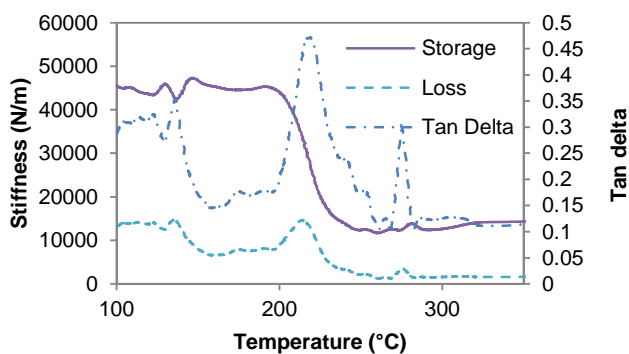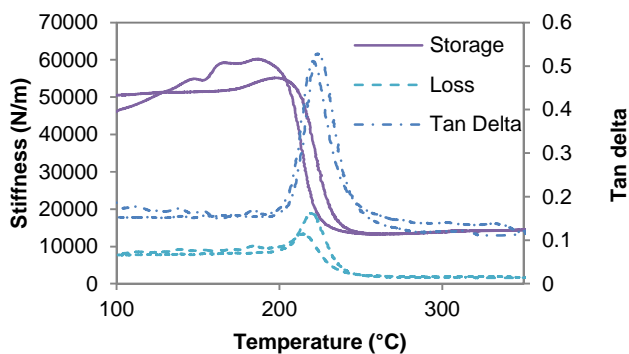
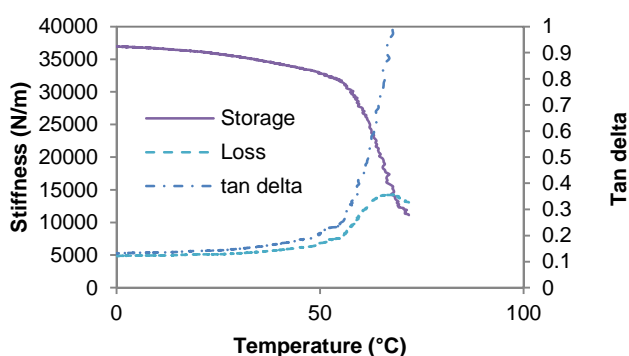**Figure S106**. TMA (1st heating) of cured **4** (no catalyst) after exposure to 85 °C water for 96 hours.

Figure S107. TMA (cooling and 2nd heating) of cured **4** (no catalyst) after exposure to 85 °C water for 96 hours.

Figure S108. TMA (1st heating) of cured **4** (Cu-Acac catalyzed) after exposure to 85 °C water for 96 hours.

Figure S109. TMA (cooling and 2nd heating) of cured **4** (Cu-Acac catalyzed) after exposure to 85 °C water for 96 hours.

Figure S110. TMA (1st heating) of cured **4** (DBTDL catalyst) after exposure to 85 °C water for 96 hours. Note that, due to the very low mechanical integrity of the sample, the scan was terminated early, and no subsequent cooling or re-heating was carried out.

Table S11. Thermo-mechanical Data for Samples after 96 hrs of Water Immersion @ 85 °C in Catalyst Choice Experiments

| Mono-mer	Catalyst	$T_G{}^a$ (°C)	$T_{G\text{-fc}}{}^b$ (°C)	CTE (µm / m °C)^c	CTE (µm / m °C$_{fc}$)^{b,c}	S'_r (N/m)^d	$S'_{r\text{-}fc}$ (N/m)^{d,b}
4	Not Added	222	229 ± 2	69 ± 3	75 ± 2	15000	17000
4	Cu-Acac	214	219 ± 2	82 ± 13	62 ± 1	13000	14000
4	DBTDL	68	n/a	n/a	n/a	n/a	n/a
3	Not Added	240	229 ± 2	58 ± 1	76 ± 2	14000	16000
3	Cu-Acac	195	203 ± 2	63 ± 1	74 ± 3	17000	15000
3	DBTDL	n/a	n/a	n/a	n/a	n/a	n/a

a. Peak temperature of loss component of stiffness.
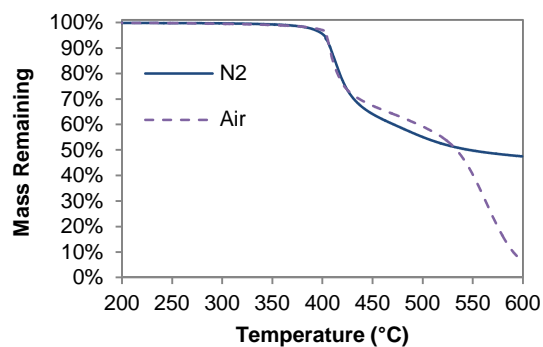b. The suffix "-fc" indicates measurement done at "full cure", that is, after heating to 350 °C.
c. Measured at 150 °C using a ± 5 °C window.
d. Storage component of stiffness at T_G + 30 °C (T_G as defined in note a).
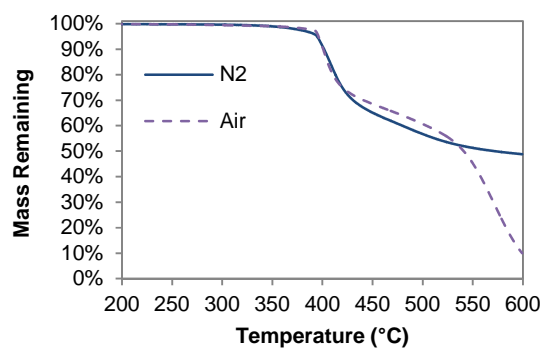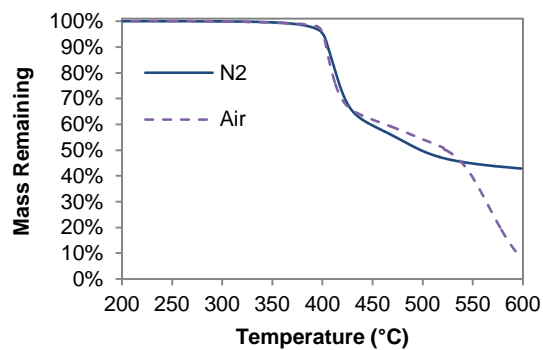
S6. Raw TGA Data
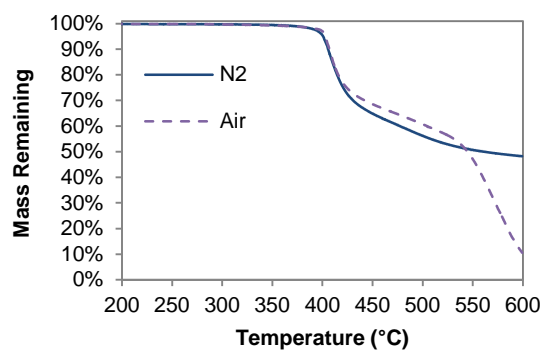
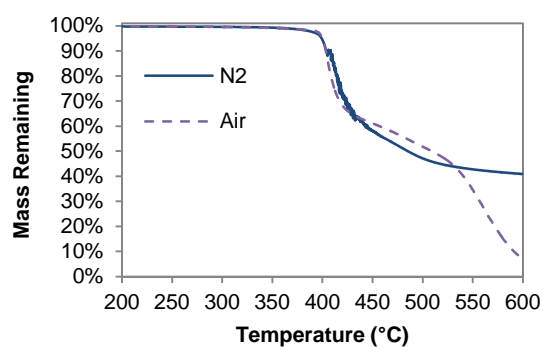**Figure S111**. TGA of cured **3** (no catalyst added).

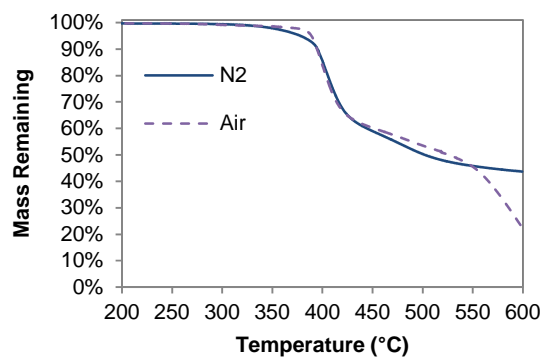**Figure S112**. TGA of cured **3** (Cu-Acac catalyzed).

Figure S113. TGA of cured **3** (DBTDL catalyzed).

Figure S114. TGA of cured **4** (no catalyst added).

Figure S115. TGA of cured **4** (Cu-Acac catalyzed).

Figure S116. TGA of cured **4** (DBTDL catalyzed).

Table S12. Thermogravimetric Data (Catalyst Choice Experiments)

Mono-mer	Catalyst	$T_{d-5\%}$ (°C)[a]	$T_{d-5\%}$ (°C)[a]	$T_{d,max}$ (°C)[b]	$T_{d,max}$ (°C)[b]	Char Yield (%)[c]	Char Yield (%)[c]
Atmosphere		N_2	Air	N_2	Air	N_2	Air
3	Not Added	401	403	405	408	48%	11%
3	Cu-Acac	402	404	413	406	48%	7%
3	DBTDL	395	396	408	402	49%	10%
4	Not Added	401	401	405	404	43%	8%
4	Cu-Acac	399	400	416	405	41%	7%
4	DBTDL	378	389	401	398	44%	23%

a. Temperature at which mass loss first equals or exceeds 5%.
b. Temperature at which the mass loss rate is maximum.
c. Mass fraction remaining after completion of heating run (10 °C/min. to 600 °C).

S7. Calculation of van der Waals volumes for networks 1 – 4.

The determination of van der Waals volumes for the networks consists of two parts, a first calculation of the van der Waals volume of each cyanate ester monomer, and then a correction for the conversion of cyanate ester to cyanurate. The correction is necessary because the conversion of cyanate ester to cyanurate involves the formation of chemical bonds, which of necessity brings together two atomic nuclei to a separation less than the sum of the van der Waals radii of the two corresponding atoms. The van der Waals volumes of the two atoms, which formerly do not overlap, must overlap significantly once a bond is formed, resulting in a significant reduction in van der Waals volume.

In order to estimate the van der Waals volume of the monomers, the correlation developed by Bicerano[S10] was utilized. This correlation has been shown to estimate van der Waals volumes with a standard deviation of 1.5 cc/mol (about 1% in the case of cyanate ester monomers). In the case of BADCy, the van der Waals volume was also computed by Georjon and Galy[S11] using the method of Bondi and the Sybyl software package from Tripos. The value

found by Georjon and Galy was 153.11 cc/mol, whereas the Bicerano correlation predicts a value of 153.00 cc/mol. Thus, the two methods agree quite closely. The advantage of the Bicerano method is that it works for any chemical structure that can be drawn using a specific set of elements (including H, C, N, O, and several others), and the calculations are simple enough to be performed by hand in a few minutes without the need for software.

The Bicerano correlation can also be utilized to calculate the van der Waals volumes of the cyanurate network. However, perhaps because triazine functionality is not specifically considered in the correlation, the predicted van der Waals volume for the fully cured BADCy network is slightly higher, at 153.2 cc/mol, then for BADCy. Thus, the correlation indicates an expansion of van der Waals volume on bonding, whereas the actual change must be negative for the reasons outlined above. Therefore, the Bicerano correlation was not used to determine the van der Waals volume of the cured network. Rather, the correction found by Georjon and Galy, which specifically indicates a reduction of 1.88 cc/mol for every bond formed by conversion of cyano groups to imine groups, was used. Since four such bonds are formed per monomer when di(cyanate esters) are converted to polycyanurates, complete conversion results in a loss of 9.52 cc/mol of van der Waals volume. The total van der Waals volume (V_w) was then determined by the formula $V_w = V_{w0} - 9.52\,\alpha$, where V_{w0} is the monomer van der Waals volume and α represents the conversion. The computed values for V_{w0} were 143.6 cc/mol for **1** (LECy), 153.0 cc/mol for **2** (BADCy), 163.2 cc/mol for **3**, and 172.6 cc/mol for **4**. These results are consistent with the addition of 9.4 cc/mol of van der Waals volume per bridge methyl group, and 9.8 cc/mol of van der Waals volume per methyl group *ortho-* to the cyanate ester. By comparison, using the tables provided by Bondi,[S12] substitution of a methyl group for a hydrogen adds 10.2 and 11.1 cc/mol of van der Waals volume per methyl group at the bridge and *ortho-* to the cyanate ester,

respectively. These differences among calculation methods are similar to the differences among

the more reliable methods as indicated by Bondi in Reference S12.

REFERENCES

S1. Pascault, J. P.; Williams, R. J. J. *J. Polym. Sci., Part B: Polym. Phys.* **1990**, *28*, 85-95.

S2. Hamerton, I.; Emsley, A. M.; Howlin, B. J.; Klewpatinond, P.; Takeda, S. *Polymer* **2003**, *44*, 4839-4852 (also see references therein).

S3. Sheng, X.; Akinc, M.; Kessler, M. R. *J. Therm. Anal. Calorim.* **2008**, *93*, 77-85.

S4. Guenthner, A. J.; Davis, M. C.; Ford, M. D.; Reams, J. T.; Groshens, T. J.; Baldwin, L. C.; Lubin, L. M.; Mabry, J. M. *Macromolecules* **2012**, *45*, 9707-9718.

S5. Guenthner, A. J.; Lamison, K. R.; Vij, V.; Reams, J. T.; Yandek, G. R.; Mabry, J. M. *Macromolecules* **2012**, *45*, 211-220.

S6. Reams, J. T.; Guenthner, A. J.; Lamison, K. R.; Vij, V.; Lubin, L. M.; Mabry, J. M. *ACS Appl. Mater. Interfaces* **2012**, *4*, 527-535.

S7. Guenthner, A. J.; Yandek, G. R.; Mabry, J., M; Lamison, K. R.; Vij, V.; Davis, M. C.; Cambrea, L. R. Insights into moisture uptake and processability from new cyanate ester monomer and blend studies. *SAMPE International Technical Conference*, SAMPE International Business Office: Covina, CA, **2010**; paper 42ISTC-119.

S8. Guenthner, A. J.; Vij, V.; Haddad, T. S.; Reams, J. T.; Lamison, K. R.; Sahagun, C. M.; Ramirez, S. M.; Yandek, G. R.; Suri, S. C.; Mabry, J. M. *J. Polym. Sci., Part A: Polym. Chem.* **2014**, *52*, 767-779.

S9. Snow, A. W. "The synthesis, manufacture and characterization of cyanate ester monomers" in Hamerton, I., *Chemistry and Technology of Cyanate Ester Resins*. Chapman & Hall: London, 1994, p. 35.

S10. Bicerano, J., *Prediction of Polymer Properties*. 3rd ed.; Marcel Dekker, Inc.: New York, 2002; pp. 66-78.

S11. Georjon, O.; Galy, J. *Polymer* **1998,** *39*, 339-345.

S12. Bondi, A. *J. Phys. Chem.* **1964**, *68*, 441-451.